UNIVERSIDADE FEDERAL DE SÃO CARLOS

Centro de Ciências Exatas e Tecnologia
Programa de Pós-Graduação em Física

Daniele de Souza

Propriedades ópticas de filmes semicondutores GaAsBi e GaSbBi
Optical properties of GaAsBi and GaSbBi semiconductor films

São Carlos-SP

2022

Daniele de Souza

Propriedades ópticas de filmes semicondutores GaAsBi e GaSbBi
Optical properties of GaAsBi and GaSbBi semiconductor films

Tese apresentada ao Programa de Pós-Graduação em Física da Universidade Federal de São Carlos para obtenção do título de Doutor em ciência.

Orientador Prof. Dra. Yara Galvão Gobato
Coorientador Prof. Dr. Helder Vinícius Avanço Galeti

São Carlos-SP

2022

Souza, Daniele de

Propriedades ópticas de filmes semicondutores GaAsBi e GaSbBi / Daniele de Souza -- 2022.
103f.

Tese de Doutorado - Universidade Federal de São Carlos, campus São Carlos, São Carlos
Orientador (a): Yara Galvão Gobato
Banca Examinadora: Yara Galvão Gobato, Helder Vinícius Avanço Galeti, Jorlandio Francisco Félix, Ingrid Barcelos, Paulo Sergio Pizani, Marcelo Barbosa de Andrade
Bibliografia

1. Fotoluminescência, Filmes finos, Bismuto. I. Souza, Daniele de. II. Título.

Ficha catalográfica desenvolvida pela Secretaria Geral de Informática (SIn)

DADOS FORNECIDOS PELO AUTOR

Bibliotecário responsável: Ronildo Santos Prado - CRB/8 7325

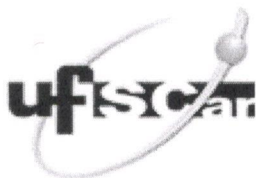

UNIVERSIDADE FEDERAL DE SÃO CARLOS

Centro de Ciências Exatas e de Tecnologia
Programa de Pós-Graduação em Física

Folha de Aprovação

Defesa de Tese de Doutorado da candidata Daniele de Souza, realizada em 02/05/2022.

Comissão Julgadora:

Profa. Dra. Yara Galvão Gobato (UFSCar)

Prof. Dr. Helder Vinicius Avanço Galeti (UFSCar)

Prof. Dr. Jorlandio Francisco Felix (UnB)

Prof. Dr. Ingrid Barcelos (CNPEM)

Prof. Dr. Paulo Sergio Pizani (UFSCar)

Prof. Dr. Marcelo Barbosa de Andrade (IFSC/USP)

O Relatório de Defesa assinado pelos membros da Comissão Julgadora encontra-se arquivado junto ao Programa de Pós-Graduação em Física.

Dedico este trabalho à minha família e aos meus amigos.

Agradecimentos

Ao longo dos 4 anos de doutorado, tive a colaboração de várias pessoas que foram fundamentais para a concretização deste trabalho e para as quais devo respeito e agradecimento.

Primeiramente, à Prof. Dra. Yara Galvão Gobato pela atenciosa orientação e por sempre estimular a estudar e entender as minhas limitações. Ao Prof. Dr Helder por todo os ensinamentos teóricos e práticos que foram fundamentais para a minha autonomia no laboratório. Ao professor Sérgio Souto pelos ensinamentos acerca de Raman que foram essenciais para escrever este trabalho.

Aos meus companheiros de laboratório Gabriela, Felipe e Caique, que foram pessoas especiais que me auxiliaram e pelo companheirismo ao longo deste trabalho.

Aos meus queridos amigos Ana Flávia, Lucas, Daniela e Paulo, que estiveram ao meu lado desde o mestrado. Aos meus novos amigos, Marcos, Renan, Carolina, Ricardo, Maju, que foram importantes nos momentos de dificuldades que enfrentei ao longo da pandemia.

Ao meu amigo querido Ricardo Soares Vieira (*in memoriam*), que foi meu mentor e me ensinou o quão bela a Física pode ser. E que infelizmente foi embora tão cedo, mas que deixou a lição de que o mais importante nessa vida é o amor.

À minha estimada amiga Maiza, que foi uma das pessoas importantes no processo de finalização desta tese, quero agradecer imensamente as palavras e o acolhimento nessa. Obrigada pelos 10 anos de amizades, seremos eternamente pés pretos.

À minha querida amiga Rejane, que foi importante no meu processo de recuperação de uma cirurgia de emergência, quando no processo de recuperação da COVID-19. Um imenso obrigada à minha amiga Thaís, que esteve ao meu lado enquanto estava hospitalizada sem poder receber visitas. À maravilhosa Nayara pelos momentos de conversa, acolhimento e comida de conforto. Ao meu querido amigo Célio, que sempre foi um refúgio quando eu estava mal.

À minha psicóloga, que foi uma pessoa extremamente importante no meu processo de melhora da minha saúde mental, fazendo com que eu conseguisse prosseguir com o meu trabalho, e, consequentemente, finalizar esta tese.

À minha família, que esteve sempre do meu lado apoiando as minhas escolhas, em especial a minha irmã Michelle, que me apoiou e cuidou de mim durante a minha recuperação. E aos meus queridos sobrinhos, que são os meus amores. Ao meu padrasto, que sempre me incentivou a estudar, principalmente comprando muitos livros.

O trabalho foi financiado pelas seguintes agências de fomento: Fundação de Amparo à Pesquisa do Estado de São Paulo (FAPESP), Coordenacão de Aperfeiçoamento de Pessoal de Nível Superior-Brasil (CAPES).

Irmão, você não percebeu

Que você é o único representante

Do seu sonho na face da terra
(Emicida)

Resumo

Os semicondutores III-V diluídos com bismuto têm apresentado um grande interesse tanto do ponto de visita de física fundamental como para possíveis aplicações em optoeletrônica e spintrônica. Quando adicionamos uma pequena quantidade de Bi nos materiais III-V, observamos uma redução importante na energia do band gap. Além disso, é esperada uma redução significativa na recombinação Auger para concentrações de Bi acima de 10%, tornando tais materiais promissores para possíveis aplicações em dispositivos optoeletrônicos na região do infravermelho próximo. Neste trabalho, realizamos um estudo sistemático das propriedades ópticas e estruturais de filme semicondutores contendo Bi, crescidos pela técnica de Epitaxia por Feixe Molecular (MBE). Em particular, investigamos: (i) filmes de $GaSb_{(1-x)}Bi_x$ crescidos em substratos GaSb (100) com diferentes concentrações de Bi e (ii) filmes de $GaAs_{(1-x)}Bi_x$ dopados tipo n e tipo p crescidos por substratos GaAs (100) e (311)B. Os filmes $GaSb_{(1-x)}Bi_x$ foram caracterizados por difração de raio X de alta resolução (HRXRD), microscopia de força atômica (AFM) e efeito Raman em temperatura ambiente e para lasers com diferentes comprimentos de onda. De forma geral, observamos que as amostras possuem uma alta qualidade cristalina. Observamos diversos modos Raman que foram associados aos modos Raman do GaSb, aglomerados de Bi e modos do GaBi. Dependendo da concentração de Bi e do comprimento de onda do laser, observamos que alguns picos Raman tiveram um aumento importante de intensidade do pico. Esse resultado foi atribuído ao efeito Raman ressonante. Os filmes de GaAsBi também foram investigados por diferentes técnicas experimentais tais como: HRXRD, micro-Raman à temperatura ambiente e fotoluminescência (PL) em baixa temperatura. Observamos que as amostras GaAsBi possuem concentração de Bi similares, mas com uma diferença importante na densidade de defeitos estruturais e de centros não radiativos. Este resultado indica que a densidade de defeitos depende consideravelmente do tipo de dopagem do $GaAs_{(1-x)}Bi_x$ e do tipo de orientação do substrato. Além disso, observamos que a amostra crescida no substrato GaAs (100) possui tensão mecânica compressiva 2.7 vezes maior do que as amostras crescidas no substrato GaAs (311)B. De forma geral, os resultados obtidos evidenciam que tanto presença de tensões compressivas como contribuições de defeitos associados com o Bi dependem do tipo de dopagem e orientação cristalina do substrato utilizado, afetando consideravelmente as propriedades ópticas dos filmes de GaAsBi.

Palavras-chave: Bismuto, filmes finos, MBE, PL, GaSbBi, GaAsBi.

Abstract

Bismuth-diluted III-V are interesting materials for possible applications in optoeletronic and spintronic devices. If we add a small amount of Bi in III-V materials, we observe a strong reduction in the band gap energy . In addition, it is expected that these materials present an important attenuation of Auger recombination for Bi concentrations higher than 10%. Therefore, these materials are good candidates for the development of optoelectronic devices in the near-infrared region. In this work , we have performed a systematic study of III-V materials with different Bi concentrations grown by molecular beam expitaxy (MBE) in different substrates. Particularly, we have investigated films of $GaSb_{(1-x)}Bi_x$ grown on (100) GaSb substrates and n- and p-doped $GaAs_{(1-x)}Bi_x$ films grown on (100) and (311)B GaAs substrates. The $GaSb_{(1-x)}Bi_x$ films were investigated using high resolution XRD (HRXRD), AFM and Raman spectroscopy. We have observed that the $GaSb_{(1-x)}Bi_x$ films have a good crystalline quality. In addition, we have observed several Raman modes associated with GaSb, Bi clusters and GaBi. We have observed an important increase of Raman intensity depending on the Bi concentration and laser wavelength. This result was attributed to the resonant Raman effect. We have also investigated the GaAsBi samples using different techniques such as: HRXRD, Raman and low temperature photoluminescence (PL). We have observed that the incorporation of Bi in the n- and p-type doped samples were similar. However, these samples have shown important difference in the density of structural defects and non-radiative centers. This result indicates that the density of defects depends on the type of doping in $GaAs_{(1-x)}Bi_x$ and on the substrate orientation. In addition, we have observed that the sample grown on the GaAs (100) substrate has a compressive strain 2.7 times higher than the samples grown on the substrate GaAs (311)B. In general, our results evidence that both the amount of compressive strain and the density of defects depend on the substrate orientation and type of doping, which affects considerable the optical properties of GaAsBi thin films.

Keywords:Bismuth, thin films, MBE, PL, GaSbBi, GaAsBi.

List of Figures

Figure 1 – (a) Conduction band splitting in the BAC model for GaNAs alloys and (b) Valence band splitting in the VBAC model for GaAsBi materials (LINHART; KUDRAWIEC, 2018). 23
Figure 2 – Anticrossing interaction model for the GaAsBi alloy (USMAN et al., 2011). 24

Contents

1 PUBLICATIONS 19

2 INTRODUCTION 21

3 PUBLISHED ARTICLES 27

4 CONCLUSION 99

BIBLIOGRAPHY 101

1 Publications

1. SOUTO, S. et al. Raman spectroscopy of $GaSb_{1\text{-}x}Bi_x$ alloys with high Bi content. **Applied Physics Letters**, v. 116, n. 20, p. 202103, 2020.

2. DE SOUZA, Daniele et al. Structural and optical properties of n-type and p-type $GaAs_{(1\text{-}x)}Bi_x$ thin films grown by molecular beam epitaxy on (311) B GaAs substrates. **Semiconductor Science and Technology**, v. 36, n. 7, p. 075018, 2021.

3. ALHASSAN, Sultan et al. Investigation of the effect of substrate orientation on the structural, electrical and optical properties of n-type $GaAs_{1\text{-}x}Bi_x$ layers grown by Molecular Beam Epitaxy. **Journal of Alloys and Compounds**, v. 885, p. 161019, 2021.

4.TORRES-MENDIETA, Rafael Omar et al. Toward Expanding the Optical Response of Ag2CrO4 and Bi2O3 by Their Laser-Mediated Heterojunction. **The Journal of Physical Chemistry C**, v. 124, n. 48, p. 26404-26414, 2020.

5. ASSIS, Marcelo et al. Revealing the nature of defects in α-Ag2WO4 by positron annihilation lifetime spectroscopy: A joint experimental and theoretical study. **Crystal Growth & Design**, v. 21, n. 2, p. 1093-1102, 2021.

6. GOUVEIA, Amanda Fernandes et al. Photoluminescence emissions of Ca1-xWO4: xEu3+: Bridging between experiment and DFT calculations. **Journal of Rare Earths**, 2021.

7. TRENCH, Aline B. et al. Interface matters: Design of an efficient α-Ag2WO4/Ag3PO4 photocatalyst. **Materials Chemistry and Physics**, v. 280, p. 125710, 2022.

2 Introduction

Bismuth-containing III–V semiconductor materials have had great attention in recent years for possible aplications in near-to-mid-infrared optoelectronic and spintronic devices (JUNG et al., 2017; MARKO et al., 2016). Yet, it is usually very difficult to incorporate Bi atoms into III–V alloys due to their large size atoms, making the growth of III–V bismides challenging and leading to specific requirements such as growth at low temperatures at near-stoichiometric conditions. Nevertheless, the growth of semiconductor materials at low temperatures usually results in the formation of various crystalline defects, which have an important impact on their optical properties (BEAUDOIN et al., 2015; LUO et al., 2017). Most of the previous studies of III–V bismides have been focused on undoped GaAsBi compounds (PAČEBUTAS et al., 2012; KINI et al., 2011; MAZZUCATO et al., 2014). Yet, it is also interesting to investigate n- or p- doped GaAsBi compounds for real applications in based devices (EROL et al., 2017; CETINKAYA et al., 2018). More recently, the successful incorporation of Bi into GaSb-based alloys has also attracted important attention for possible applications in optoeletronic devices in the mid-infrared region (RAJPALKE et al., 2013; DELORME et al., 2017). Yet, most of these previous studies have been focused only on the growth process, structural quality, and in optical properties such as absorption, photoreflectance, and photoluminescence. Actually,there are no previous studies on Raman spectroscopy of GaSbBi layers which report well-defined Bi-related vibrational modes. In this thesis, we have focused our attention on a systematic study of Raman spectroscopy of GaSbBi layers with different Bi contents and also on the optical properties of n- and p-doped GaAsBi layers on (100) GaAs and (311)B substrates.

The introduction of Bi in III–V materials have an important impact on their electronic properties as compared to III-V materials. Some examples are the significant bandgap energy reduction (∼84 meV/Bi%) (BRODERICK et al., 2011) and an important increase of the spin–orbit band splitting associated with the incorporation of a small amount of Bi into the host lattice of GaAs, which contributes to reduce the non-radiative Auger recombination (SIMMONS et al., 2015; PASHARTIS; RUBEL, 2017). On the other hand, their crystal quality is considerably affected by the affected by the low growth temperatures which are usually necessary to incorporate bismuth atoms into the GaAs host lattice (ALBERI et al., 2007). Actually, the alloys must be grown in the near-stoichiometric conditions and at much lower temperatures (below 400°C) as compared to the optimal growth conditions for the GaAs layers . Although, the requirement of growth at low temperature together with the large size of the Bi atoms and the strong tendency of Bi to segregate on the surface, make the growth of $GaAs_{(1\text{-}x)}$Bix really challenging (PTAK et al., 2012). Furthermore, most of the previous studies of $GaAs_{(1\text{-}x)}Bi_x$ films and heterostructures

were performed using the conventional (100) GaAs substrates (BASTIMAN et al., 2012) and there are few research works which have explored the growth of III–V bismides on high-index planes, which considerably influence the Bi incorporation and consequently their optical properties. In addition, the development of optoelectronic devices also require a controllable methodology for the doping of semiconductor alloys. However, there are very few investigations of the effect of doping on $GaAs_{(1-x)}Bi_x$ and most of these investigations were particularly focused on the effects of the doping on the structural and electrical properties. Nevertheless, it is interesting also to investigate the optical properties of n-type and p-type $GaAs_{(1-x)}Bi_x$ alloys.

As mentioned above, the growth of these materials is complex because Bi has a larger atomic radius than arsenic and gallium atoms, and for an effective incorporation of Bi to occur, it is necessary to follow some special growth conditions (FITOURI et al., 2011). One of the main conditions for the growth of these alloys is that it takes place at low temperature, to avoid the appearance of point defects. In the case of growth with a higher temperature than the ideal one, it is observed that these alloys present the segregation of Bi, Ga, and As atoms, thus forming islands full of these elements (known as droplets) on the surfaces of the samples, (TAIT; YAN; MILLUNCHICK, 2017; VARDAR et al., 2013) which can affect the optical quality of these materials. Another effect associated with the growth temperature is the appearance of Bi or As agglomerates along the thin film volume, called clusters (PUUSTINEN et al., 2013) that can effectively affect the optical quality of devices based on GaAs materials. In general, when these materials are grown above the ideal growth temperature, the absence of an atom can be observed at a certain point in the host lattice, which is called vacancies(PUUSTINEN et al., 2013).

On the other hand, there are several previous studies focused on GaAsN alloys. Their band structure and optical properties were explained by a simple theoretical model based on the interaction of the nitrogen (N) impurity level with the conduction band of GaAsN (BAC Model) (KUDRAWIEC et al., 2004; LINHART; KUDRAWIEC, 2018) which explains the changes of the band structure with the incorporation of nitrogen impurities. The BAC model is based on the interaction of nitrogen states with the GaAs matrix, which results in a change of the conduction band into two sub-bands (E_+ and E_-), which are illustrated in figure 1 (a).

A similar theoretical model was also developed to explain the interaction of Bi impurity states with valence band. When we add a small amount of Bi in the GaAs matrix, part of the Bi atoms will be incorporated via substitutional replacing the host matrix arsenic. However some the Bi atoms will not be incorporated and will act as an impurity. The bismuth is a p-type impurity and therefore induces states close to the valence band. These Bi levels interact with the valence band of the GaAs matrix, resulting in the change of this band into six E_+ and E_- sub-bands of the heavy hole (HH), E_+ and E_- light hole

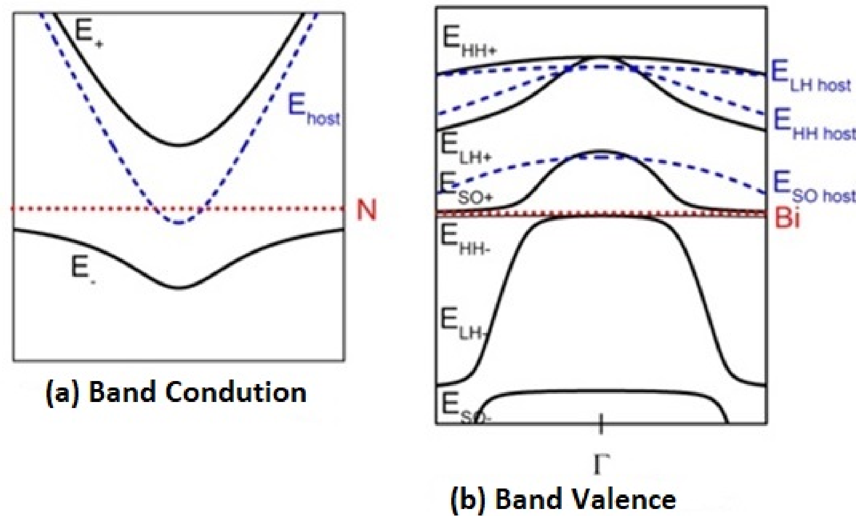

Figure 1 – (a) Conduction band splitting in the BAC model for GaNAs alloys and (b) Valence band splitting in the VBAC model for GaAsBi materials (LINHART; KUDRAWIEC, 2018).

(LH) and E_+ and E_- split-off (SO) which can be seen in figure 1 (b). This interaction of Bi impurity levels results in an important impact in the valence band of the GaAsBi alloys. The band gap energy reduction of these materials can be calculated through the following equation:

$$E_{\pm} = \frac{1}{2}\{E_k(k) + E_i \pm \sqrt{(E_m(k) - E_i)^2} + 4xV_{mi}^2\} \tag{2.1}$$

where E_k represents the maximum energy of the valence band of GaAs, E_i is the energy of the bismuth level, x is the concentration of Bi and V_{mi} is the coupling term between the impurity states with the valence band. However, a recent model proposed by Usmman et al. (USMAN et al., 2011), demonstrates that Bi impurities not only interact with the valence band but also interact with the conduction band illustrated in figure 2. As we increase the Bi concentration, we observe a strong reduction in both the conduction band (28 meV) and the valence band (55 meV). In addition to the strong reduction in the band gap energy of these materials (60-90 meV), another interesting modification due the incorporation of bismuth in the GaAs matrix is the increase in the spin-orbital band. III-V materials may exhibit non-radiative recombination, called Auger recombination, which affects the optical quality of devices based on these materials. We observed that as we increase the Bi concentration, we have a strong reduction in the band gap and a significant increase in the spin-orbital band, which significantly attenuates the Auger recombination for a concentration of 10% Bi. Usually, the n-type GaAsBi layers present levels of defects which are in the bandgap, which can affect considerable the performance of optoelectronic devices. These levels of defects act as traps for electrons, and consequently, the material

has a lower mobility of carriers and a lower optical efficiency (GELCZUK et al., 2017). These defects usually depend on the growth temperature which favors the appearance of point defects, such as the vacancy of Ga or arsenic. The incorporation of Bi usually suppresses the formation of carrier traps in the GaAs matrix, but at the same time may favor the appearance of defects related to Bi complexes. It was previously shown that the incorporation of Bi in n-type doped GaAs alloys (100) grown at 370° C with a low concentration of Bi ($0<x<0.023$) exhibits a reduction in carrier trap formation of two orders of magnitude when compared to the reference sample (GaAs) grown under the same conditions. However, these samples are usually susceptible to Bi-related defects such as, clusters and Bi pairs.

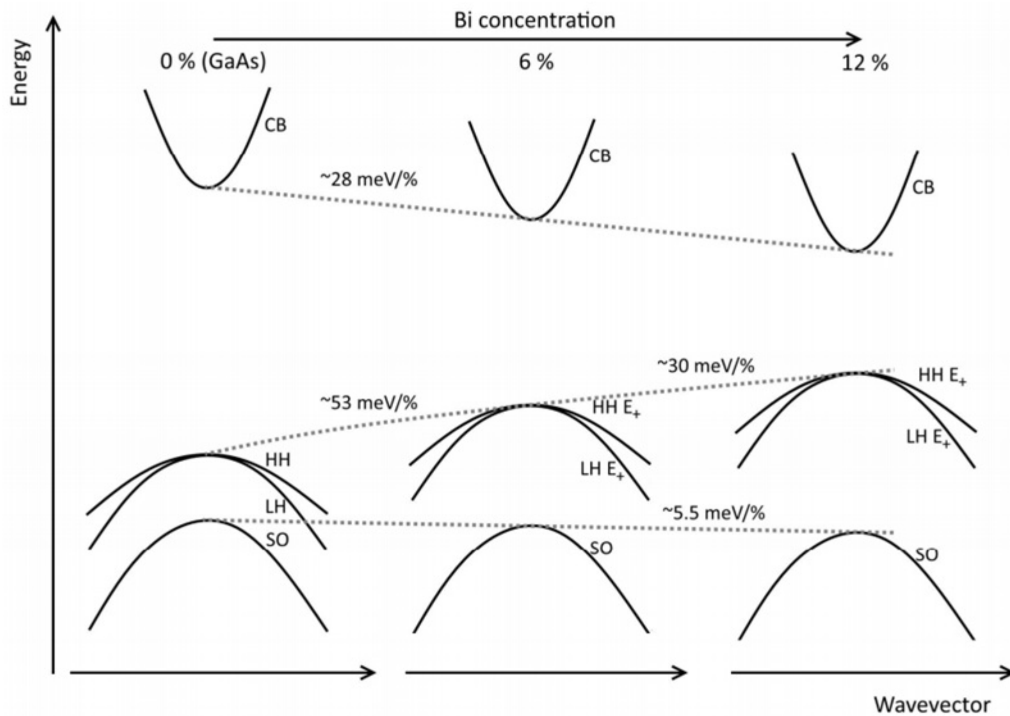

Figure 2 – Anticrossing interaction model for the GaAsBi alloy (USMAN et al., 2011).

Previous studies on p-type doped GaAsBi materials have shown that the levels induced by p-type doping modify the occupancy of localized Bi states, which affects the PL properties. A comparison between p-doped and non-doped GaAsBi alloys has shown the appearance of the S-curve behavior for the undoped material, while for p-type doped GaAsBi this behavior was not observed (YOSHIMOTO et al., 2013). However, there is still no previous study in the literature of optical properties of n- and p-type doped GaAsBi semiconductor materials grown on substrates of unconventional crystalline orientation. Recently, it was demonstrated that GaAsBi alloys grown on substrates oriented in high-index crystal directions exhibit an increase in the incorporation of Bi as compared to conventional substrates (100) (HENINI et al., 2007). Furthermore, the GaSbBi semiconductor has recently also become an interesting material, due to its gap reduction (40 meV/% Bi) (RA-

JPALKE et al., 2015), and due to the increase in the split-off band. Improvements in the optical properties of $GaSb_{(1-x)}Bi_x$ / GaSb heterostructures can be achieved by optimizing the growth conditions and by a better understanding of their electronic structure. These properties make this material an ideal candidate for optoelectronic applications since many of these devices work in the spectral range of 2 to 5μm (DELORME et al., 2017). However, this alloy also presents some important difficulties for the growth by molecular beam epitaxy (MBE) since the inclusion of Bi into GaSb alloys is complex, due to the enormous size difference between Sb and Bi and their electronegativity (LONGENBACH; WANG, 1991). As previously mentioned, bismuth has a strong tendency to segregate and form droplets on the surface of the material at low temperatures (300°C). To circumvent the problem, the growth temperature of these samples must be in the range of 330-390°C to effectively add bismuth in the alloy. However, compared to GaAsBi, the defects and crystal disorders may be smaller in GaSbBi due to the smaller difference between group V atoms in terms of their electronegativities and sizes (As and Sb). Additionally, the parameters of the BAC model determined for GaSbBi suggest that the band structure of this alloy is closer to conventional III-V alloys (such as GaAsSb or GaInSb) than those observed in high disorder alloys (such as GaNAs or InPBi) (POLAK; SCHAROCH; KUDRAWIEC, 2015).

In this thesis, we have investigated in detail the structural, electrical and optical properties of GaSbBi and n- and p-doped GaAsBi layers, although my main contribution is on optical properties of these materials. The other studies were performed in international collaborations. In chapter 3, we presented the complete work performed in this thesis, and in chapter 4 we present the conclusions.

3 PUBLISHED ARTICLES

Applied Physics Letters

Raman spectroscopy of $GaSb_{1-x}Bi_x$ alloys with high Bi content

S. Souto[1], Joonas Hilska[2], Y. Galvão Gobato[3, (a)], D. Souza [3], M. B. Andrade[4], Eero Koivusalo[2], Janne Puustinen[2], Mircea Guina[2]

[1]Departamento de Ciências Básicas – Faculdade de Zootecnia e Engenharia de Alimentos, Universidade de São Paulo, CEP 13635-900 Pirassununga, SP, Brazil

[2]Optoelectronics Research Centre, Physics Unit, Tampere University of Technology, Korkeakoulunkatu 3, 33720 Tampere, Finland

[3]Departamento de Física,Universidade Federal de São Carlos (UFSCAR)13560-905, São Carlos, SP, Brazil

[4]São Carlos Institute of Physics, University of São Paulo, PO Box 369, São Carlos, SP 13560-970, Brazil

Abstrat

We report on the crystal morphology and Raman scattering features of high structural quality $GaSb_{1-x}Bi_x$ alloys grown by molecular beam epitaxy with a high Bi content (x up to ∼0.10). The Raman spectra were measured at room temperature with different laser excitation wavelengths of 532 nm, 633 nm, and 785 nm. We observed well-defined Bi-induced Raman peaks associated with atomic Bi_n clusters and GaBi vibrational modes. Remarkably, some Bi-induced Raman modes were strongly enhanced when the laser energy was selected near an optical transition for the 5.8% Bi sample. This effect was attributed to a Raman resonant effect near an excited optical transition of the GaSbBi layer and has been used to identify the nature of the observed Raman peaks.

1. Introduction

Bismuth-containing III–V alloys have drawn considerable attention in recent years, owing to their potential for near-to-mid-infrared optoelectronics and spintronics applications [1–7]. Importantly, the introduction of Bi into III–V alloys results in a large bandgap reduction and spin–orbit splitting. However, Bi atoms are difficult to incorporate into III–V alloys due to their large size, making the growth of III–V bismides challenging and leading to strict requirements for growth at low temperatures at near-stoichiometric V/III flux ratios [2–4,8]. On the other hand, growth at low temperatures can trigger the formation of

various crystalline defects, which have a significant impact on the optical properties. While the majority of early studies have been focused on GaAsBi compounds, the incorporation of Bi into GaSb-based alloys has recently attracted much attention owing to possible applications in the mid-infrared region. So far, most studies concerning GaSbBi have focused on the growth process, structural quality, and optical properties, [2,4,9,10] such as absorption, photoreflectance, and photoluminescence. Yet, there are no reports on Raman spectroscopy for GaSbBi layers demonstrating well-defined Bi-related vibrational modes [1,10]. In fact, only a very weak shoulder around 213–215 cm^{-1} has been previously reported in the Raman spectra of dilute GaSbBi layers (0.4% Bi) associated with a GaBi vibrational Raman mode [10]. On the other hand, there are several reports on Raman spectroscopy of GaAsBi layers and other Bi-containing materials [11–19]. Despite these investigations, the interpretation of GaBi-related Raman peaks is still being unveiled. In fact, as the bulk GaBi crystal has not been synthesized, the identification of GaBi-related vibrational Raman modes is usually a difficult task. In general, two Bi-related Raman modes are usually observed around 185 and 210 cm^{-1} and are associated with TO(Γ) and LO(Γ) GaBi modes [15,17]. However, this interpretation is not in agreement with several predictions, [18,20,21] which have pointed out a separation of TO(Γ) and LO(ΓC) GaBi vibrational modes of less than 10 cm^{-1}. Moreover, atomic Bi_n clusters and disorder-activated modes have been suggested to further complicate the Raman spectra [18,19,22]. Resolving these issues calls for more extensive studies in order to understand the nature of Raman peaks in Bi-containing III–V alloys.

In this Letter, we have investigated the structural and Raman spectroscopic properties of high structural quality GaSbBi alloys grown by molecular beam epitaxy (MBE) with a high Bi content. We observed well-defined Bi-induced Raman peaks associated with atomic Bi_n clusters and GaBi vibrational modes. Remarkably, we have shown that by selecting the laser energy close to an excited transition of the GaSbBi semiconductor material, several Bi-induced Raman vibrational modes become clearly enhanced. We explain this effect via a resonant Raman effect near the E1 interband transition. In particular, we have used the resonant Raman effect and polarized Raman spectroscopy to identify the nature of the observed Raman peaks.

2. Experimental

Three GaSbBi samples (B1, B2, and B3) and a reference GaSb sample (R) were grown by MBE on n-GaSb(100) substrates. All samples were grown at a temperature of 350°C following the growth procedure described in our previous work [4], with the exception that the substrates were rotated during growth to produce uniform compositions across the wafers. The GaSbBi structures were grown under near-stoichiometric Sb/Ga flux ratios and different Bi/Ga beam equivalent pressure ratios of 0.08 (B1), 0.11 (B2),

and 0.14 (B3). The growth temperatures were measured using a thermocouple and are consistent with our previous work [4].

High-resolution x-ray diffraction (HR-XRD) ω-2θ scans from the (400) reflection were used to investigate the structural quality. The Bi contents were determined by fitting simulations based on the dynamical theory of x-ray diffraction to the HR-XRD data. Fully pseudomorphic layers and Vegard's law with a lattice constant of 6.27Å [9] for the GaBi binary were assumed in the simulations. The fully pseudomorphic growth was confirmed by reciprocal space mapping (RSM). The surfaces were characterized by atomic force microscopy (AFM), to exclude effects from surface imperfections.

Polarization-dependent Raman spectra were measured at room temperature using a Renishaw inVia Qontor Raman microscope with a 785 nm laser. The measurements were performed in quasibackscattering Porto geometry $\overline{Z}$(XX)Z and $\overline{Z}$(XY)Z with the basis X = [$\overline{0}$11], Y = [011], and Z = [100]. For non-polarized micro-Raman measurements, we used different laser wavelengths, i.e., 532 nm, 633 nm, and 785 nm, and a Horiba LabRAM HR Evolution system with a 1800 g/mm grating and a 50 $\times$ objective. In all Raman experiments, the spectral resolution was $\sim$ 1 cm^{-1} and the laser power densities were below $1W/cm^2$ to avoid sample heating.

3. Results and discussion

Figure 1 compiles the HR-XRD ω-2θ data (solid lines) overlaid by their respective simulations (dotted lines) for all the samples reported. The reference sample R exhibits a single intense and narrow peak corresponding to the GaSb(400) reflection, indicating that the grown epilayer is perfectly lattice-matched to the substrate. In fact, the FWHM of the diffraction peak is only $\sim$11.3 arcseconds and the data can be fitted with high accuracy by assuming an infinitely thick GaSb layer in the model. In contrast, all the Bi-containing samples (B1–B3) show clear intense secondary peaks corresponding to the GaSbBi epilayers, which are offset from the substrate peak by varying degrees based on the amount of compressive strain, which is proportional to the Bi content. In addition, the GaSbBi peaks are surrounded by clear Pendellösung oscillations, which indicates high interface quality and homogeneous Bi content. Based on the simulations, which follow the experimental data closely, the Bi contents are 5.8% (B1), 8.0% (B2), and 10.6% (B3). To confirm that no relaxation has occurred, a RSM from sample B3 was measured and is shown in the top-left inset of Figure 1. In the RSM, the substrate and epilayer peaks are aligned on the in-plane reciprocal space axis, indicating that no relaxation of the epilayer has occurred. Since samples B1 and B2 have the same thickness and lower strain, none of the samples are expected to be relaxed. To further exclude effects from structural imperfections, the surface quality was characterized by AFM. All the samples exhibited droplet-free smooth surfaces, with RMS roughnesses below 0.5 nm. A more detailed AFM

analysis can be found in the supplementary material (cf. Figure S1).

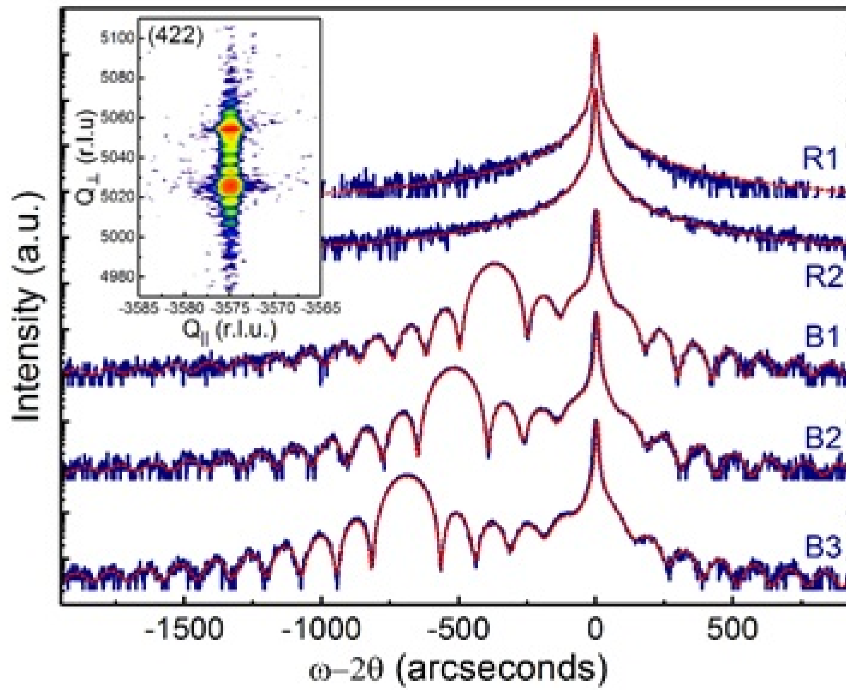

Figure 1. HR-XRD measurements (solid gray) and simulations (dotted red) from all the reported samples. The ω-2θ axis is centered to the GaSb(400) reflection, and the samples are labeled near the right-hand side axis. The inset shows the RSM from sample B3 corresponding to the (422) diffraction, with the substrate and epilayer peaks designated with S and L.

Figure 2 shows typical room temperature Raman spectra of samples with different Bi contents (B1–B3) and of the reference GaSb sample (R) measured with 785 nm excitation in the $\overline{Z}$(XX)Z configuration. The Raman spectra in the $\overline{Z}$(XY)Z configuration are shown in Figure S2 (see the supplementary material). Raman peaks around 114 cm^{-1}, 162 cm^{-1}, 235.5 cm^{-1}, and 269 cm^{-1} are observed for all samples, which is consistent with peaks observed in the literature for the bulk GaSb crystal.

These peaks are usually associated with the crystalline GaSb Zinc blende structure, point group T_d 43m, which shows second order: 2TA(X and Σ) (111±3 cm^{-1} and 117±3 cm^{-1}) and 2TA(W and Q) (160±65 cm^{-1}), first order: TO(Γ) (227.1±1.0 cm^{-1}) and LO(Γ) (237.1 ± 1.0 cm^{-1}), and second order: TO(X)+ TA(X) (272 ± 3 cm^{-1}) vibrational modes [23,24]. Particularly, the most intense Raman peak around 235.5 cm$_{-1}$ is associated with the LO(Γ) GaSb mode. We point out that this mode shows a clear red shift with increasing %Bi (Figure S3), indicating an increase in compressive strain, in agreement with the HR-XRD results. Moreover, the linewidth of the LO(Γ) GaSb mode increases as the Bi content is increased. These effects are associated with an increase in disorder with the increasing Bi content.

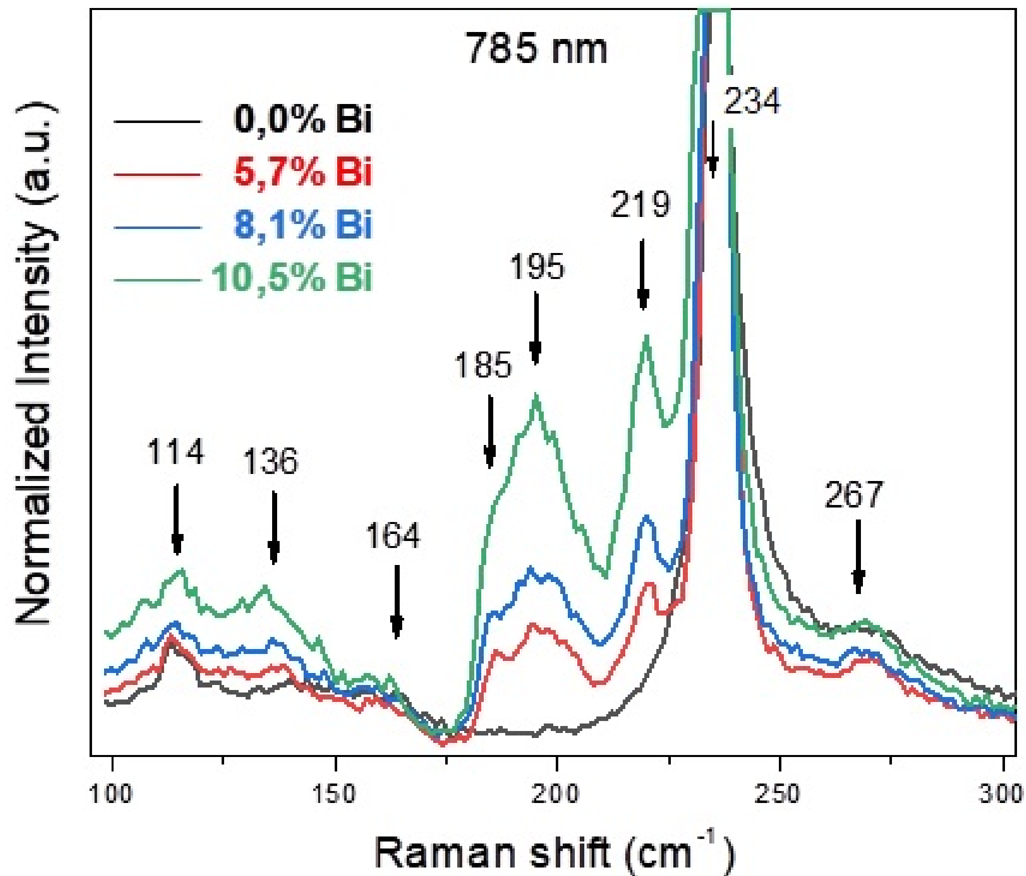

Figure 2. Raman spectra for different Bi contents using 785 nm laser excitation measured in the $\overline{Z}$ (XX)Z configuration.

In comparison to the Bi-free sample (R), the GaSbBi samples (B1-B3) show several additional Raman peaks around 136 cm^{-1}, 185 cm^{-1}, 195 cm^{-1}, and 219 cm^{-1}. Particularly, the peak at 219 cm^{-1} has a higher value than the peak usually associated with the LO(Γ) GaBi vibrational mode around 210 cm^{-1} in GaAsBi layers [15,17]. However, the polarized Raman results (Figure S2) show that this peak has different polarization behavior from the LO(C) GaSb vibrational mode, which makes this interpretation partially inconsistent. Moreover, this peak is at a much higher frequency than the theoretical value predicted for the LO(Γ) GaBi Raman mode [20,21]. Correspondingly, the Raman peak observed at 185 cm^{-1}, which has the same polarization as the LO(Γ) GaSb vibrational mode (Figure S2), was previously observed in several studies on GaAsBi [15,18,19,25,26] and was associated with the TO(Γ) GaBi vibrational mode, which is also inconsistent with our polarized Raman results. Particularly, this mode attribution implies a separation of 34 cm^{-1} between the LO(C) and TO(Γ) GaBi modes, which is much larger than the predicted separation of less than 10 cm^{-1} [18,20,21]. Therefore, we attribute the Raman peak observed around 185 cm^{-1} to be a convoluted LO(Γ)+TO(Γ) GaBi vibrational mode. This attribution is more consistent with the previous predictions [18,20,21] for the Raman peak positions as well as

for the frequency separation between the TO(Γ) and LO(Γ) GaBi modes. Moreover, instead of the LO(Γ) GaBi mode, the Raman peak around 219 cm^{-1} could be associated with GaSb Raman vibrational modes due to other zone boundaries, such as TO(X) and/or TO(L) [24], which are forbidden by the typical momentum conservation rules for first order Raman scattering in GaSb. Observation of the forbidden modes could be explained by Bi-induced disorder in the lattice, leading to the relaxation of Raman selection rules, as proposed in several previous works [24,27]. In the resonant condition (Figure 3), the appearance of the GaSb-like TO(X or L) phonon mode in the GaSbBi Raman spectra could be associated with Bi-induced mixing of the GaSb valence band. A similar effect was observed for the GaAsN semiconductor and attributed to the N-induced mixing of GaAs conduction bands [28,29]. However, a possible contribution of the longitudinal-optical-plasmoncoupled mode should also be considered. Therefore, further studies would be necessary for a complete understanding of the nature of this Raman peak.

At the other end of the spectrum, the Raman peak around 136 cm^{-1} has too low frequency to be associated with any LO or TO GaBi modes. In fact, this Raman peak is in the acoustic regime and is usually associated with disorder activated longitudinal acoustic (DALA) modes induced by Bi [27]. On the other hand, it could also be attributed to vibration modes of atomic Bi_n clusters, consistent with the fact that Bi atoms are not easily incorporated into the crystalline structure. The Bi incorporation into GaSbBi films has been generally reported to be over 97% substitutional in the group-V sublattice [9,30], translating to a low concentration of pure atomic Bi_n clusters, where some Bi atoms occupy other than substitutional sites. However, Punkkinen et al. [31] reported that Bi clustering in GaAsBi is driven by the existence of Ga vacancies in the lattice. Moreover, Ga vacancies in GaSbBi have been recently shown to contribute to large hole densities in GaSbBi [32]. Thus, there is a clear rationale for why such clusters would exist in these high Bi content GaSbBi materials. Therefore, these results lead us to tentatively attribute this peak to a combination of DALA and/or atomic Bi_4 cluster modes, which have shown Raman peaks near the observed peak around 136 cm^{-1} [22]. Finally, the peak at 195 cm^{-1} is not observed in the large majority of literature studies related to Bi-containing materials. However, a study on Bi-doped glasses [33] and a theoretical prediction [22] found a vibrational mode around 195 cm^{-1} related to the Bi_2 dimer. Therefore, we suggest this Bi_2 mode as the origin of the observed peak at 195 cm^{-1}. We do note that the higher Bi content as compared to previous studies of other III–V bismides could favor the formation of Bi_2 dimers and, thus, explain its absence in previous studies.

We have also measured Raman spectra using different excitation wavelengths of 532 and 633 nm. Figure 3 shows the Raman spectra of sample B1 (5.8%Bi) for all excitation wavelengths. Again, the most intense Raman peak around 235.5 cm^{-1} is the LO(Γ) GaSb mode and the small peak at 225 cm^{-1} is associated with the TO(Γ) GaSb mode [23]. The observation of the TO(Γ) GaSb mode evidences the presence of disorder induced by Bi

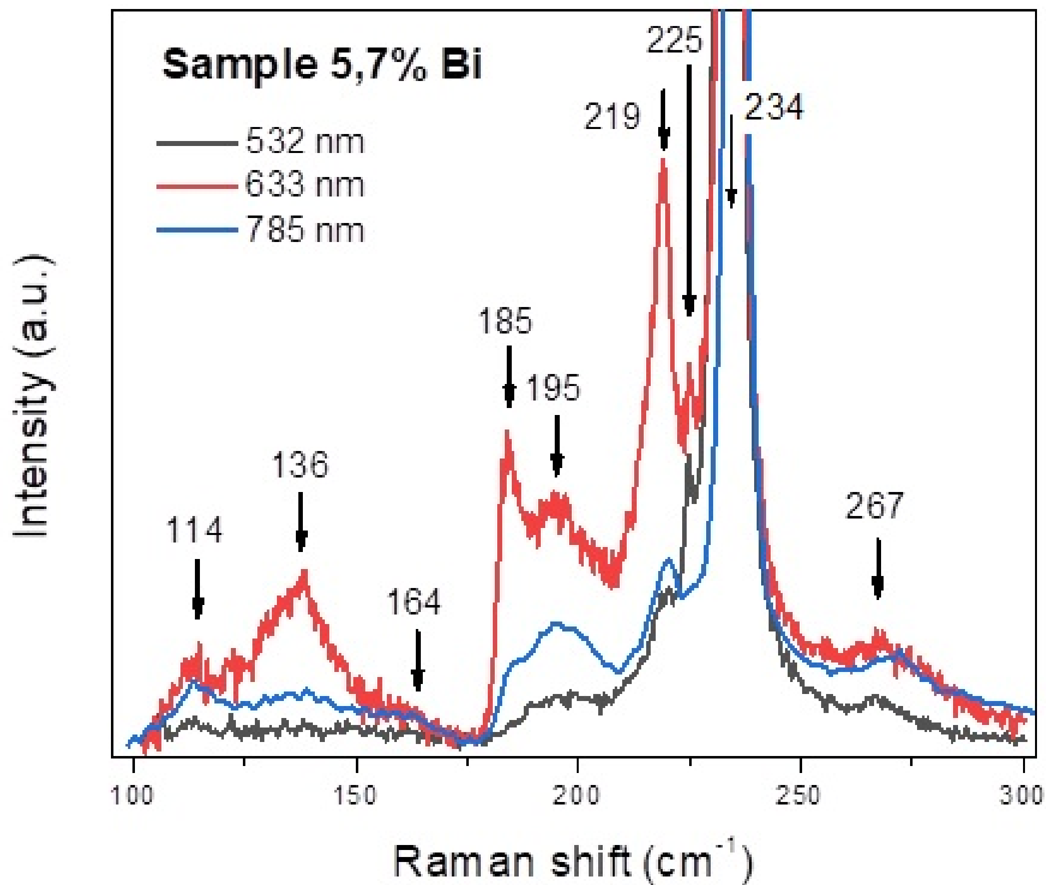

Figure 3. Non-polarized Raman spectra of sample B1 with different excitation wavelengths. The intensities have been normalized to the LO(Γ) GaSb mode.

atoms as the TO(Γ) peak is forbidden by the selection rules. The spectrum measured using 532 nm excitation shows the same features as those observed for the 785 nm excitation, but with less distinct peaks and lower signal-to-noise ratios in the region of Bi-induced modes. Conversely, the Raman spectrum for 633 nm excitation shows particularly distinct peaks related to the Bi-induced modes.

Remarkably, the Raman peaks at 219, 185, and 136 cm^{-1} are strongly enhanced under 633 nm excitation. This can be explained by the resonant Raman effect as the laser excitation at 1.96 eV (633 nm) is near an excited optical transition of the GaSbBi material. Some theoretical studies on the band structure of GaSbBi [34–36] have used the popular valence band anti-crossing model (VBAC) and have shown a transition between the LH/HH- valence sub-band and the conduction band, which would be around the 633 nm laser excitation energy for 5.8%Bi. However, Polak et al. [37] showed that the VBAC model is less valid for GaSbBi alloys, owing to the weaker chemical dissimilarity between Sb and Bi, than, for example, As or P and Bi. In fact, theoretical calculations based on the density functional theory show that an interband transition on the K-line has an energy gap near the 633 nm laser energy (i.e., the E1 transition), particularly for a Bi content

TABLE I. Summary of the observed Raman peaks and their properties.

Wavenumber	Assignment	Selection rule[a]		Order		Bi induced
(cm^{-1})		$\overline{Z}$(XX)Z	$\overline{Z}$(XY)Z	1st	2nd	
114	2TA(X + Σ)	Allowed	Forbidden		x	
136	DALA	Forbidden	Forbidden	x		x
162	2TA(W + Q)	Allowed	Forbidden		x	
185	LO(Γ) + TO(Γ) GaBi	Allowed	Forbidden	x		x
195	Bi2 dimer	Allowed	Forbidden	x		x
219	TO(X)/TO(L) GaSb	Forbidden	Forbidden	x		x
225	TO(Γ) GaSb	Forbidden	Forbidden	x		
235.5	LO(Γ) GaSb	Allowed	Forbidden	x		
269	TO(X) + TA(X) GaSb	Allowed	Forbidden		x	

[a]For a perfect bulk crystal. Note that many forbidden modes are observed in the Raman spectra by Bi-induced disorder and relaxation of the selection rules.

close to 5.8%Bi [38,39], which is more likely the resonant transition.

We find the resonant Raman results to be fully consistent with the above discussion on the nature of observed peaks. Namely, the 136 cm^{-1} and 185 cm^{-1} Raman peaks are extremely sensitive to the resonant condition, have the same polarization as the GaSb LO mode, and are also observed in GaAsBi layers. Previously, we tentatively ascribed the 136 cm^{-1} mode to DALA and/or Bi_4 clusters based on earlier reports [22,27]. Considering that this mode is sensitive to the resonant condition, we can now rule out the contribution of atomic Bi_4 clusters, as they are not expected to have a resonant optical transition at the wavelength of 633 nm. Conversely, the modes at 185 cm^{-1}, TO(Γ) and LO(Γ) of GaBi in the GaSbBi alloy, are resonant due to the E1 gap as expected. Interestingly, the 219 cm^{-1} peak is also sensitive to the resonant condition, but has different polarization from the LO(Γ) GaSb mode. Therefore, we suggest that the 219 cm^{-1} Raman peak is associated with other zone boundaries of GaSb Raman vibrational modes, such as TO(X) and TO(L) [27], which could be allowed by increased disorder due to Bi incorporation. Again, this interpretation is consistent with the polarized Raman spectra. Furthermore, it is expected that this GaSb vibrational mode could be resonant to the E1 gap absorption of the GaSbBi crystal. Finally, the 195 cm^{-1} peak is not sensitive to the resonant condition. In fact, our results indicate that the 195 cm^{-1} peak has a different nature and could indeed be associated with the vibration of the dimer Bi_2, which is not coupled to vibrational modes related to GaSb [22,33]. As a summary of the above discussion, all the observed Raman peaks are compiled in Table I.

4. Conclusion

In conclusion, we have observed several distinct peaks in the Raman spectra (non-polarized and polarized) of GaSbBi layers, which are not visible in GaSb grown under

similar conditions. We have observed a resonant Raman effect in a GaSbBi layer with 5.8%Bi using 633 nm excitation, which enhanced some of the Bi-induced Raman peaks. The resonant Raman effect and polarized Raman results were used to investigate and characterize the nature of the observed Raman peaks. Particularly, the Raman peak observed at 185 cm^{-1} was associated with a convoluted LO(Γ) + TO(Γ) GaBi mode. The Raman peaks observed at 136 cm^{-1}, 195 cm^{-1}, and 219 cm^{-1} were associated with DALA, atomic Bi_2 cluster, and TO(X)/TO(L) GaSb phonon modes, respectively.

Reference

[1] S. Wang and P. Lu, Bismuth-Containing Alloys and Nanostructures (Springer, 2019).

[2] O. Delorme, L. Cerutti, E. Tournie, and J.-B. Rodriguez, "Molecular beam epitaxy and characterization of high Bi content GaSbBi alloys," J. Cryst. Growth 477, 144–148 (2017).

[3] X. Lu, D. A. Beaton, R. B. Lewis, T. Tiedje, and M. B. Whitwick, "Effect of molecular beam epitaxy growth conditions on the Bi content of GaAsBi," Appl. Phys. Lett. 92, 192110 (2008).

[4] J. Hilska, E. Koivusalo, J. Puustinen, S. Suomalainen, and M. Guina, "Epitaxial phases of high Bi content GaSbBi alloys," J. Cryst. Growth 516, 67–71 (2019). 5 A. R. H. Carvalho, V. Orsi Gordo, H. V. A. Galeti, Y. Galv ao Gobato, M. P. F. de Godoy, R. Kudrawiec, O. M. Lemine, and M. Henini, "Magneto-optical properties of GaBiAs layers," J. Phys. D: Appl. Phys. 47, 075103 (2014).

[6] O. Delorme, L. Cerutti, E. Luna, G. Narcy, A. Trampert, E. Tournie, and J.-B. Rodriguez, "GaSbBi/GaSb quantum well laser diodes," Appl. Phys. Lett. 110, 222106 (2017).

[7] M. Gladysiewicz, R. Kudrawiec, and M. S. Wartak, "Electronic band structure and material gain of III-V-Bi quantum wells grown on GaSb substrate and dedicated for mid-infrared spectral range," J. Appl. Phys. 119, 075701 (2016).

[8] J. Puustinen, J. Hilska, and M. Guina, "Analysis of GaAsBi growth regimes in high resolution with respect to As/Ga ratio using stationary MBE growth," J. Cryst. Growth 511, 33–41 (2019).

[9] M. K. Rajpalke, W. M. Linhart, M. Birkett, K. M. Yu, J. Alaria, J. Kopaczek, R. Kudrawiec, T. S. Jones, M. J. Ashwin, and T. D. Veal, "High Bi content GaSbBi alloys," J. Appl. Phys. 116, 043511 (2014).

[10] S. Das, T. Das, S. Dhar, M. de la Mare, and A. Krier, "Near infrared photoluminescence observed in dilute GaSbBi alloys grown by," Infrared Phys. Technol. 55, 156–160 (2012).

[11] R. S. Joshya, V. Rajaji, C. Narayana, A. Mascarenhas, and R. Kini, "Anharmonicity in light scattering by optical phonons in GaAs1-xBix," J. Appl. Phys. 119, 205706 (2016).

[12] F. Sarcan, O. Dönmez,Ömer and Kara, A. Erol, E. Akalın, M. C¸. Arıkan, H. Makhloufi, A. Arnoult, and C. Fontaine, “Bismuth-induced effects on optical, lattice vibrational, and structural properties of bulk GaAsBi alloys,” Nanoscale Res. Lett. 9, 119 (2014).

[13] T. M. Christian, B. Fluegel, D. A. Beaton, A. Kirstin, and A. Mascarenhas, “Bismuth-induced Raman modes in GaP1xBix,” Jpn. J. Appl. Phys., Part 1 55, 108002 (2016).

[14] S. Yoon, M. J. Seong, B. Fluegel, and A. Mascarenhas, “Photogenerated plasmons in GaAs1xBix,” Appl. Phys. Lett. 91, 082101 (2007).

[15] J. A. Steele, R. A. Lewis, M. Henini, O. M. Lemine, D. Fan, Y. Mazur, V. G. Dorogan, P. C. Grant, S.-Q. Yu, and G. J. Salamo, “Raman scattering reveals strong LO-phonon-hole-plasmon coupling in nominally undoped GaAsBi: Optical determination of carrier concentration,” Opt. Express 22, 11680 (2014).

[16] W. Pan, J. A. Steele, P. Wang, K. Wang, Y. Song, L. Yue, X. Wu, H. Xu, Z. Zhang, S. Xu, P. Lu, L. Wu, Q. Gong, and S. Wang, “Raman scattering studies of dilute InP1xBix alloys reveal unusually strong oscillator strength for Bi nduced modes,” Semicond. Sci. Technol. 30, 094003 (2015).

[17] J. A. Steele, R. A. Lewis, M. Henini, O. M. Lemine, and A. Alkaoud, “Raman scattering studies of strain effects in (100) and (311)B GaAs1-xBix epitaxial layers,” J. Appl. Phys. 114, 193516 (2013).

[18] P. Verma, K. Oe, M. Yamada, H. Harima, M. Herms, and G. Irmer, “Raman studies on GaAs1xBix and InAs1xBix,” J. Appl. Phys. 89, 1657–1663 (2001).

[19] M. Seong, S. Francoeur, S. Yoon, A. Mascarenhas, S. Tixier, M. Adamcyk, and T. Tiedje, “Bi-induced vibrational modes in GaAsBi,” Superlattices Microstruct. 37, 394 (2005).

[20] R. Pilevar Shahri and A. Akhtar, “First principles study and comparison of vibrational and thermodynamic properties of XBi (X = In, Ga, B, Al),” Chin. Phys. B 26, 093107 (2017).

[21] A. Belabbes, A. A. Zaoui, and M. Ferhat, “Lattice dynamics study of bismuth III–V compounds,” J. Phys.: Condens. Matter 20, 415221 (2008).

[22] D. Liang, W. Shen, C. Zhangy, P. Lu, and S. Wang, “Structural, electronic, vibrational and optical properties of Bin clusters,” Mod. Phys. Lett. B 31, 1750260 (2017).

Supplementary Material

Raman spectroscopy of $GaSb_{1-x}Bi_x$ alloys with high Bi content

S. Souto[1], Joonas Hilska[2], Y. Galvão Gobato[3, (a)], D. Souza [3], M. B. Andrade[4], Eero Koivusalo[2], Janne Puustinen[2], Mircea Guina[2]

[1]Departamento de Ciências Básicas – Faculdade de Zootecnia e Engenharia de Alimentos, Universidade de São Paulo, CEP 13635-900 Pirassununga, SP, Brazil

[2]Optoelectronics Research Centre, Physics Unit, Tampere University of Technology, Korkeakoulunkatu 3, 33720 Tampere, Finland

[3]Departamento de Física,Universidade Federal de São Carlos (UFSCAR)13560-905, São Carlos, SP, Brazil

[4]São Carlos Institute of Physics, University of São Paulo, PO Box 369, São Carlos, SP 13560-970, Brazil

In this section, we present supplementary characterization results supporting the analysis made in the manuscript. First, since the growth of III-V bismide materials are highly susceptible to surface defects, such as the formation of droplets of different chemical composition [1-3], that could influence the analysis of the Raman spectra, the sample surfaces were characterized by atomic force microscopy (AFM). Fig. S1 shows a compilation of the AFM micrographs, where all the samples exhibit droplet-free and smooth surfaces, with root-mean-square roughnesses below 0.5 nm. Still, a clear distinction is seen in the surface microstructure between the reference sample (Fig. S1 a) and the Bi containing samples (Fig. S1 c-d). Namely, the Bi containing samples all share a similar surface mounding pattern, which is consistent with earlier reports on GaSbBi [1, 3-5] and GaAsBi [2, 6, 7], while the Bi-free sample shows a less distinct nm-scale islanding pattern. This mounding pattern is commonly thought to arise from Ehrlich-Schwoebel (ES) barriers on the step-edges in conjunction with anisotropic surface diffusion of the adatoms [8-10]. The mechanism for forming such clear mounds only on the Bi containing samples could be explained by increased surface diffusion rates induced by Bi [11], which can enhance the effects of the ES barriers. A side effect from the mounding are the slightly increased surface roughness values in comparison to the Bi-free sample, although it has recently been shown that by precise control of the V/III ratio the mounding amplitude can be controlled and thus minimized for optimal surface quality [2].

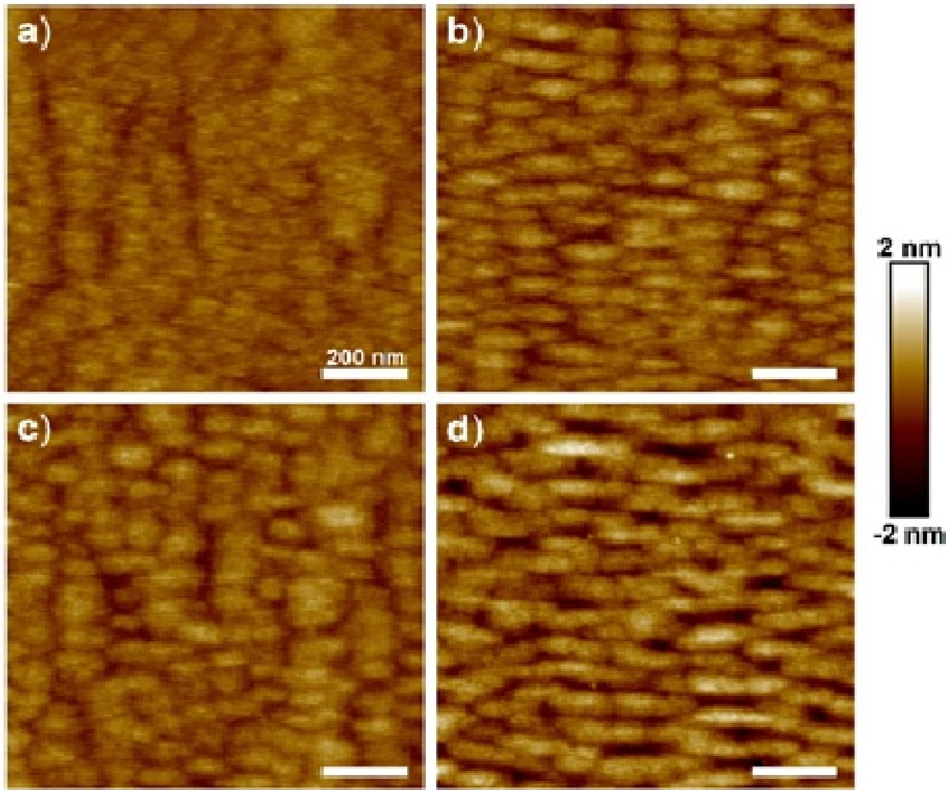

FIG. S1. AFM micrographs from samples R (a) and B1-B3 (b-d), respectively. The white scale bars are 200 nm for all images and the vertical scale on the right-hand side is shared by the images.

Fig. S2 shows the polarization dependent Raman spectra for all reported samples in the study. They were measured using 785 nm excitation in quasi-backscattering Porto geometries $\overline{Z}$(XX)Z and $\overline{Z}$(XY)Z with the basis X=[0$\overline{1}$1], Y=[011] and Z=[100]. For all samples, the Raman intensity is very low for the $\overline{Z}$(XY)Z configuration as expected by Raman selection rules. Particularly, the GaSb LO mode at 235.5 cm^{-1} is not observed for the reference sample in the $\overline{Z}$(XY)Z configuration. On the other hand, it is clearly observed in the aforementioned configuration for the Bi-containing samples, which clearly indicates Bi-induced disorder. Moreover, additional Bi-related Raman features are clearly observed for the B1-B3 samples. Their Raman intensity follows the expected trend of increasing intensity as a function of Bi content as discussed in the manuscript.

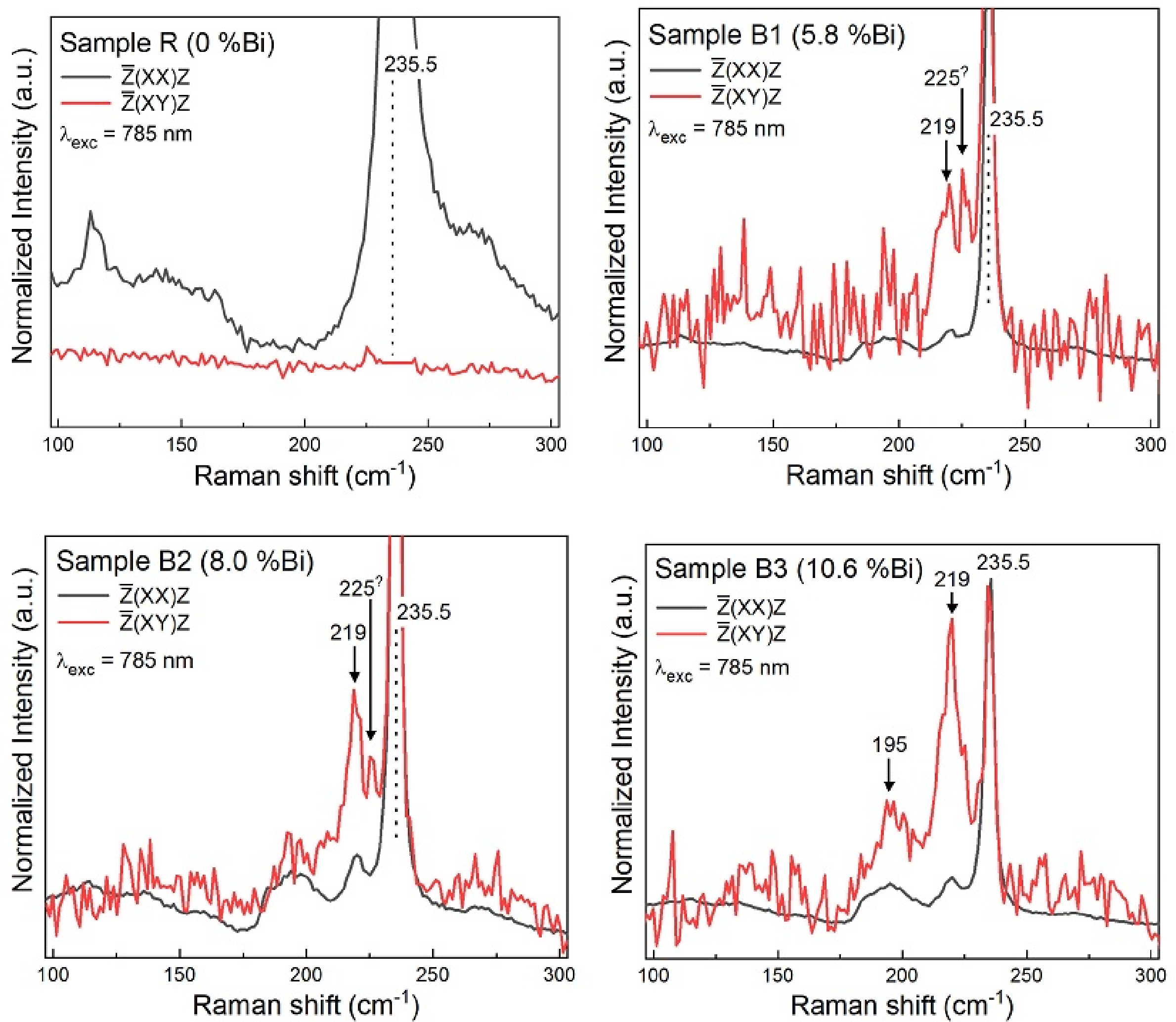

FIG. S2. Polarized room temperature Raman spectra for the reference sample R and for samples with different Bi contents (B1-B3). The intensities are normalized to the GaSb LO peak.

We also remark that all Raman peaks at the acoustic range and longer wavenumber range features are consistent with previous results reported in literature for GaSb crystal. Particularly, the Raman peaks at around 265-276 and ~440 cm^{-1} range are ascribed to second order Raman scattering and/or combinations of different Raman peaks as discussed in the manuscript. In addition, a slight shift for GaSb LO Raman peak with increasing Bi content, as shown in Fig. S3, was associated with an increase of strain, which is consistent with our HR-XRD results.

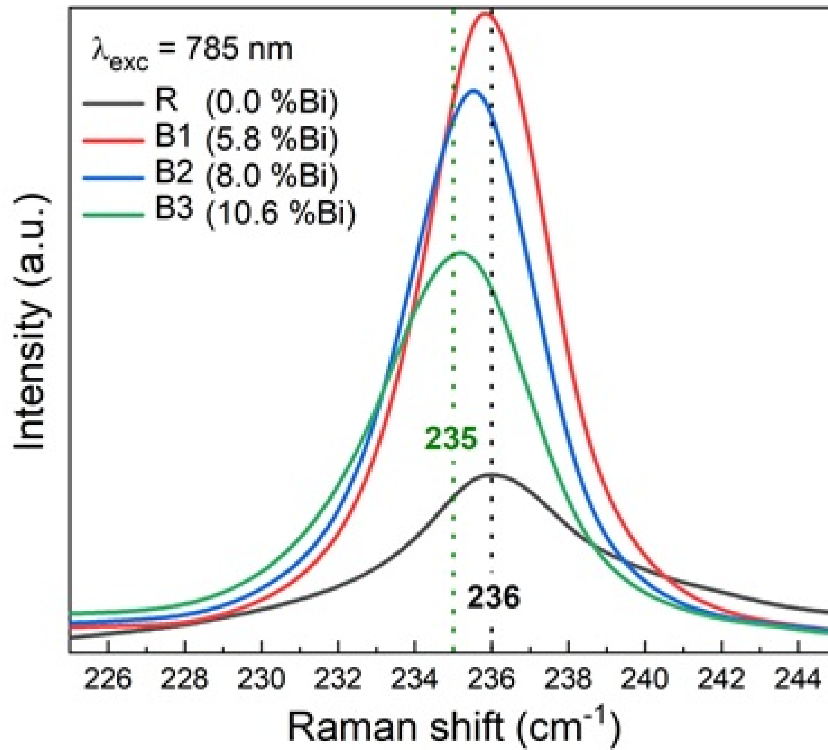

FIG. S3. Raman spectra for all samples in the region of GaSb LO mode using 785 nm excitation. The data is interpolated by B-spline for clarity.

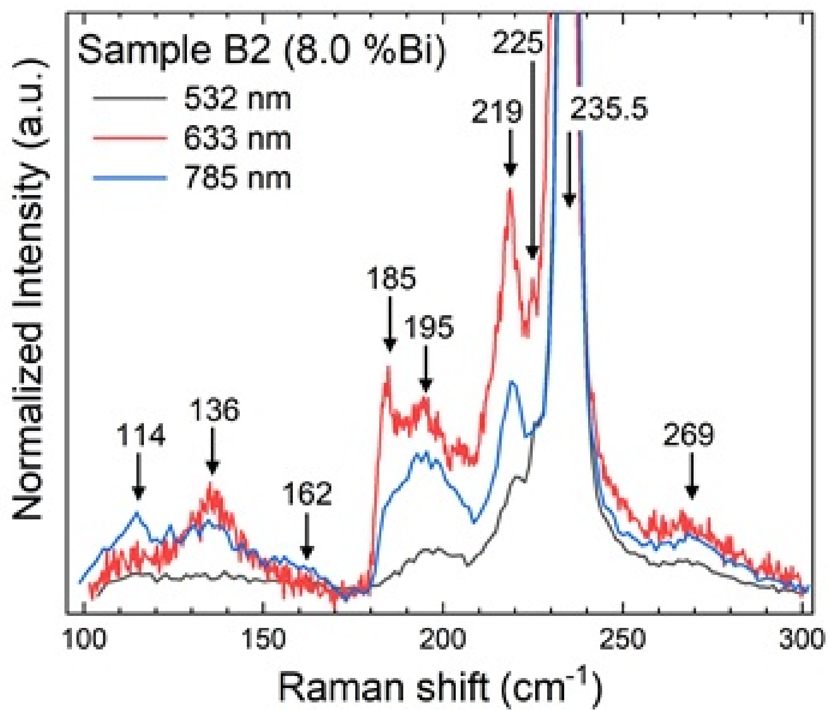

FIG. S4. Raman spectra of R2 sample for different laser wavelengths.

Figs. S4 and S5 show the Raman spectra for samples B2 and B3 respectively using different laser wavelengths. We observed that the Raman resonant effect is less important than for sample B3 because the excitation wavelength is far from the resonant condition.

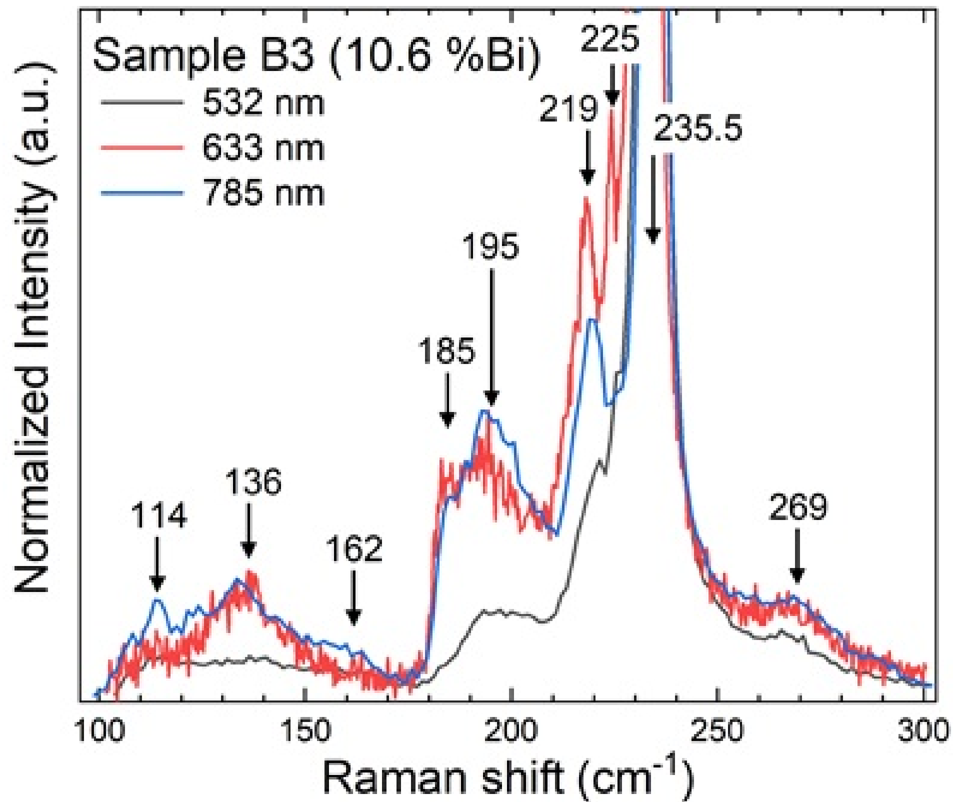

FIG. S5. Raman spectra for sample B3 using different laser wavelengths.

Reference

[1] J. Hilska, E. Koivusalo, J. Puustinen, S. Suomalainen and M. Guina, "Epitaxial phases of high Bi content GaSbBi alloys," Journal of Crystal Growth, vol. 516, pp. 67-71, 2019.

[2] J. Puustinen, J. Hilska and M. Guina, "Analysis of GaAsBi growth regimes in high resolution with respect to As/Ga ratio using stationary MBE growth," Journal of Crystal Growth, vol. 511, pp. 33-41, 2019.

[3] M. K. Rajpalke, W. M. Linhart, K. M. Yu, T. S. Jones, M. J. Ashwin and T. D. Veal, "Bi flux-dependent MBE growth of GaSbBi alloys," Journal of Crystal Growth, vol. 425, pp. 241-244, 2015.

[4] O. Delorme, L. Cerutti, E. Tournié and J.-B. Rodriguez, "Molecular beam epitaxy and characterization of high Bi content GaSbBi alloys," Journal of Crystal Growth, vol. 477, pp. 144-148, 2017.

[5] M. K. Rajpalke, W. M. Linhart, M. Birkett, K. M. Yu, J. Alaria, J. Kopaczek, R.

Kudrawiec, T. S. Jones, M. J. Ashwin and T. D. Veal, "High Bi content GaSbBi alloys," Journal of Applied Physics, vol. 116, p. 043511, 2014.

[6] X. Lu, D. A. Beaton, R. B. Lewis, T. Tiedje and M. B. Whitwick, "Effect of molecular beam epitaxy growth conditions on the Bi content of GaAsBi," Applied Physics Letters, vol. 92, p. 192110, 2008.

[7] F. Bastiman, A. R. B. Mhomad, J. S. Ng, J. P. R. David and S. J. Sweeney, "Non-stoichiometric GaAsBi/GaAs (100) molecular beam epitaxy growth," Journal of Crystal Growth, vol. 338, pp. 57-61, 2012.

[8] M. D. Johnson, C. Orme, A. W. Hunt, D. Graff, J. Sudijono, L. M. Sander and B. G. Orr, "Stable and unstable growth in molecular beam epitaxy," Physical Review Letters, vol. 72, p. 116, 1994.

[9] G. Apostolopoulos, N. Boukos, J. Herfort, A. Travlos and K. H. Ploog, "Surface morphology of low temperature grown GaAs on singular and vicinal substrates," Materials Sceince and Engineering, vol. B88, pp. 205-208, 2002.

[10] B. Z. Nosho, B. R. Bennett, E. H. Aifer and M. Goldenberg, "Surface morphology of homoepitaxial GaSb films grown on flat and vicinal substrates," Journal of Crystal Growth, vol. 236, pp. 155-164, 2002.

[11] R. R. Wixom, L. W. Rieth and G. B. Stringfellow, "Sb and Bi surfactant effects on homo-epitaxy of GaAs on (001) patterned substrates," Journal of Crystal Growth, vol. 265, p. 367, 2004.

PUBLISHED ARTICLE

IOP Publishing

Structural and optical properties of n-type and p-type $GaAs_{(1-x)}Bi_x$ thin films grown by molecular beam epitaxy on (311)B GaAs substrates

Daniele De Souza[1], Sultan Alhassan[2,3], Saud Alotaibi[2], Amra Alhassni[2], Amjad Almunyif[2,4], Hind Albalawi[4], Igor P Kazakov[5], Alexey V Klekovkin[5], Sergey A ZinovEv[5], Igor A Likhachev[6], Elkhan M Pashaev[6], Sergio Souto[7], Yara Galv~ao Gobato[1], Helder Vinicius Avanço Galeti[8], and Mohamed Henini[2]

[1] Physics Department, Federal University of São Carlos, São Carlos-SP, Brazil

[2] School of Physics and Astronomy, University of Nottingham, Nottingham NG7 2RD, United Kingdom

[3] School of Physics, College of Science, Jouf University, Skaka 74631-7365, Saudi Arabia

[4] Physics Department, Faculty of Science, Princess Nourah Bint Abdulrahman University, Riyadh, Saudi Arabia

[5] P.N.Lebedev Physical Institute, Russian Academy of Science, 119991, GSP-1 Moscow, Russia

[6] National Research Center 'Kurchatov Institute', 123182 Moscow, Russia

[7] FZEA/ZAB, University of São Paulo, Pirassununga-SP, Brazil

[8] Electrical Engineering Department, Federal University of São Carlos, São Carlos-SP, Brazil

Abstract

In this paper, we report on the structural and optical properties of n-type Si-doped and p-type Be-doped $GaAs_{(1-x)}Bi_x$ thin films grown by molecular beam epitaxy on (311)B GaAs substrates with nominal Bi content x = 5.4%. Similar samples without Bi were also grown for comparison purposes (n-type GaAs and p-type GaAs). X-ray diffraction (XRD), micro-Raman at room temperature, and photoluminescence measurements as a function of temperature and laser excitation power (P_{EXC}) were performed to investigate their structural and optical properties. XRD results revealed that the Bi incorporation in both n-type and p-type doped GaAsBi was similar, despite that the samples present remarkable differences in the number of Bi related defects, non-radiative centers and alloy

disorder. Particularly, our results evidence that the Bi-related defects in n- and p-doped GaAsBi alloys have important impact on the differences of their optical properties.

Keywords: exciton localization, structural disorder, optical properties, doped semiconductor,dilute bismides

1. Introduction

It is well known that dilute bismides materials such as $GaAs_{(1-x)}Bi_x$ alloys are of great interest due to the fact that they can extend the application of standard III–V semiconductor devices to operate in the mid-infrared spectrum [1, 2]. The main features for this interest are due to the important changes to the electronic properties such as significant bandgap energy reduction (∼84 meV/Bi%) [3] and an increase of the spin–orbit band splitting associated with the incorporation of a small amount of Bi into the host lattice of GaAs, which help reduce the non-radiative Auger recombination [4–6]. However, the crystal quality of III-V alloys is profoundly affected by the growth temperature in order to incorporate bismuth atoms into GaAs host lattice. The alloy must be grown near-stoichiometric conditions and at much lower temperatures (below 400°C) as compared to GaAs optimal growth conditions [7, 8]. The low growth temperature requirement together with the large size of the Bi atom and thestrong tendency of Bi to surface segregate, make the growth of $GaAs_{(1-x)}Bix$ challenging. In addition, although most investigations of $GaAs_{(1-x)}Bi_x$ films and heterostructures were performed using the conventional (100) GaAs substrates, there are few studies exploring the growth on high-index planes, which can considerably influence the Bi incorporation and consequently their electrical and optical properties [9–13]. Remarkably, it has been shown that enhancement of Bi incorporation in $GaAs_{(1-x)}Bi_x$ thin films could be obtained by using (311)B orientation [9]. On the other hand, while optoelectronic devices require a controllable methodology for the doping of alloys, there are relatively a very few studies addressing the doping process of only (100) $GaAs_{(1-x)}Bi_x$ [14–21]. These investigations have particularly concentrated on the effects the doping has on the structural, electrical and optical properties. Therefore, it is worth noting that the structural and optical properties of n-type and p-type $GaAs_{(1-x)}Bi_x$ alloys and heterostructures using non-(100) GaAs substrates have not been investigated yet.

In this paper, we present a detailed study on the structural and optical properties of n-type and p-type doped $GaAs_{(1-x)}Bi_x$ layers grown on high index (311)B oriented GaAs substrates. n-type and p-type GaAs control samples were also grown for comparison purposed. The samples were grown by molecular beam epitaxy (MBE), and Bi compositions were determined by high resolution x-ray diffraction (HR-XRD) measurements. Both n-doped and pdoped $GaAs_{(1-x)}Bi_x$ samples were found to have the same Bi composition, meaning that the substitutional incorporation of Bi does not depend on the type of doping. The optical properties were investigated using photoluminescence (PL) and micro-Raman

spectroscopy. The obtained results, which revealed that the n and p $GaAs_{(1-x)}Bi_x$ samples have remarkable differences in terms of the density of structural defects and non-radiative centers, indicate that the density of Bi-related defects depend on the type of doping in $GaAs_{(1-x)}Bi_x$.

2. Experimental details

The samples investigated in this work were grown in an MBE system (CNA, Russia) equipped with standard effusion cells. For the evaporation of Bi a standard Ga furnace with reduced screen insulation was used to improve temperature control. The samples consisted of a 100 nm thick doped GaAs buffer layer (n and p = ~2-3 × 10^{18} cm^{-3}) followed by 1 μm thick doped $GaAs_{(1-x)}Bi_x$ layer (Si-doped n-type = 2 × 10^{16} cm^{-3}; and Be-doped p-type = 2 × 10^{16} cm^{-3}) grown on (311)B oriented GaAs substrates. The respective control samples do not contain Bi and are just doped GaAs with similar layer structures grown in the same technological modes. For simplicity, the samples are labeled as n-GaAs, n-$GaAs_{0.94}Bi_{0.06}$, p-GaAs and p-$GaAs_{0.94}Bi_{0.06}$. Doping of n- or p-type conductivity was carried out during the growth of $GaAs_{(1-x)}Bi_x$ layers from standard molecular sources, which contained Si and Be dopants at temperatures of 850°C or 652°C, respectively. The Si (n-type dopant) and Be (p-type dopant) sources were calibrated by growing Si-doped and Be-doped GaAs control samples and using Hall measurements to determine the free electron and hole concentrations, respectively. In addition, secondary ion mass spectrometry depth profiling measurements were carried out on p-i-n samples in order to obtain information about the in-depth distribution of Si and Be elements.

$GaAs_{(1-x)}Bi_x$ layer was grown at a growth rate of 0.1 nm s^{-1} and substrate temperature of 280°C. Calibration of the substrate temperature at low temperature was carried out using temperature reference points of the arsenic desorption and transition of surface reconstruction on the (100) from (4 × 4) to (2 × 3) [22]. In the process of growing the GaAs(Bi) layer, the Ga, Bi and As beam equivalent pressures as measured by an ion gauge were 1.5 × 10^{-7} Torr, 6.4 × 10^{-8} Torr, and 1.3 × 10^{-6} Torr, respectively. It is worth mentioning that when growing a $GaAs_{(1-x)}Bi_x$ layer on (100) GaAs substrate, a (1 × 3) or (4 × 3) reconstruction was observed.

X-ray diffraction (XRD) measurements were carried out in a Rigaku Smartlab diffractometer using Cu Kα1 radiation [23, 24]. High quality double-crystal Ge (220) was used as collimator. The XRD rocking curves were measured using 2θ-ω scans with a horizontal slit positioned in front of the detector in order to minimize diffuse and background scattering. The x-ray spot on the sample's surface was about 5 × 0.4 mm^2. For each sample symmetrical and two asymmetrical reflections were measured (with large and small angles of incidence of x-ray beam). Asymmetrical (400) reflections were chosen for the considered samples. Analysis of the symmetrical XRD curve allowed us to estimate

the average lattice parameters of the Bi-containing layer in the vertical direction [25]. From the calculated lattice parameters and the Vegard's law [26], an average concentration of Bi atoms incorporated into the epilayers was determined. The lattice parameter in lateral direction with respect to the direction of the layer's growth averaged over the x-ray spot was obtained using a detailed analysis of the asymmetric reflections [25]. By using the calculated lattice parameters, the tetragonal strain of the lattice of Ga(As,Bi) layers can be reconstructed. In addition to HRXRD, the EDS method was used to control the Bi concentration in the $GaAs_{(1-x)}Bi_x$ layers, which is described in more detail in [27].

The optical properties of $GaAs_{(1-x)}Bi_x$ samples were investigated using PL and micro-Raman techniques. PL measurements were performed as a function of temperature, between 15 and 200 K using a Janis closed-loop helium cryostat, and excitation power, ranging from 0.5 mW to 50 mW. A 532 nm Nd:YAG solid state laser was used as an excitation power (P_{EXC}) source and a 0.5 m Spex monochromator with a nitrogen-cooled Ge detector and lock-in amplifier. Micro-Raman measurements were carried out using a Lab RAM HR Horiba Jobin Yvon system having a 50× objective, a spectral resolution of about 1 cm^{-1} and a 633 nm laser excitation with laser power in the range from 0.3 mW to 30 mW.

3. Results and discussion

3.1. High-resolution x-ray diffraction (HR-XRD)

In order to determine the Bi content in the $GaAs_{1-x}Bi_x$ epilayers, the experimental XRD curves were simulated and are shown in figure 1. From the calculated lattice parameters and the Vegard's law, an average concentration of Bi atoms incorporated into the epilayers' lattice was determined. The simulations show that the lattice parameter of $GaAs_{(1-x)}Bi_x$ is equal to 5.684 Å and the Bi concentrations in both n-type and p-type samples grown on (311)B substrates are 5.4%. The distortion of the lattice of the strained $GaAs_{(1-x)}Bi_x$ layers was determined by analyzing the asymmetric reflections. The biaxial elastic strains of the lattice cell were estimated assuming a cubic lattice of Bi-containing layer. The value of the lattice parameter of $GaAs_{(1-x)}Bi_x$ layer was calculated using the Vegard law and lattice parameters of GaAs and GaBi [28]. For the present work it was considered that GaBi has a zinc-blende cubic lattice with a lattice parameter a = 6.178 Å.

The strain in the vertical (ϵ_{zz}) and lateral (ϵ_{xx}) directions are given by equations $\epsilon_{zz} = \frac{a_{\perp} - A_{FR}}{a_{FR}}$ and $\epsilon_{xx} = \frac{a_{\parallel} - A_{FR}}{a_{FR}}$, respectively, where $a_{\perp}$ is the lattice parameter in vertical direction, $a_{\parallel}$ -lattice parameter in the lateral direction and a_{FR}-lattice parameter of fully relaxed GaAs lattice.

Using the above equations, ϵ_{zz} and ϵ_{xx} of both samples are found to be the same and have values of 0.00035 and -0.018, respectively. One can therefore conclude that there

is some residual strain in $GaAs_{(1-x)}Bi_x$ layers [29]. It is important to point out that due to the large size of the spot of x-rays impinging on the samples, the data presented here represent only averaged values of strain. Particular features of the layer's strains need detailed analysis which is out of the scope of this paper. For the reference doped GaAs samples no biaxial strain was found indicating that there is no second lattice parameter.

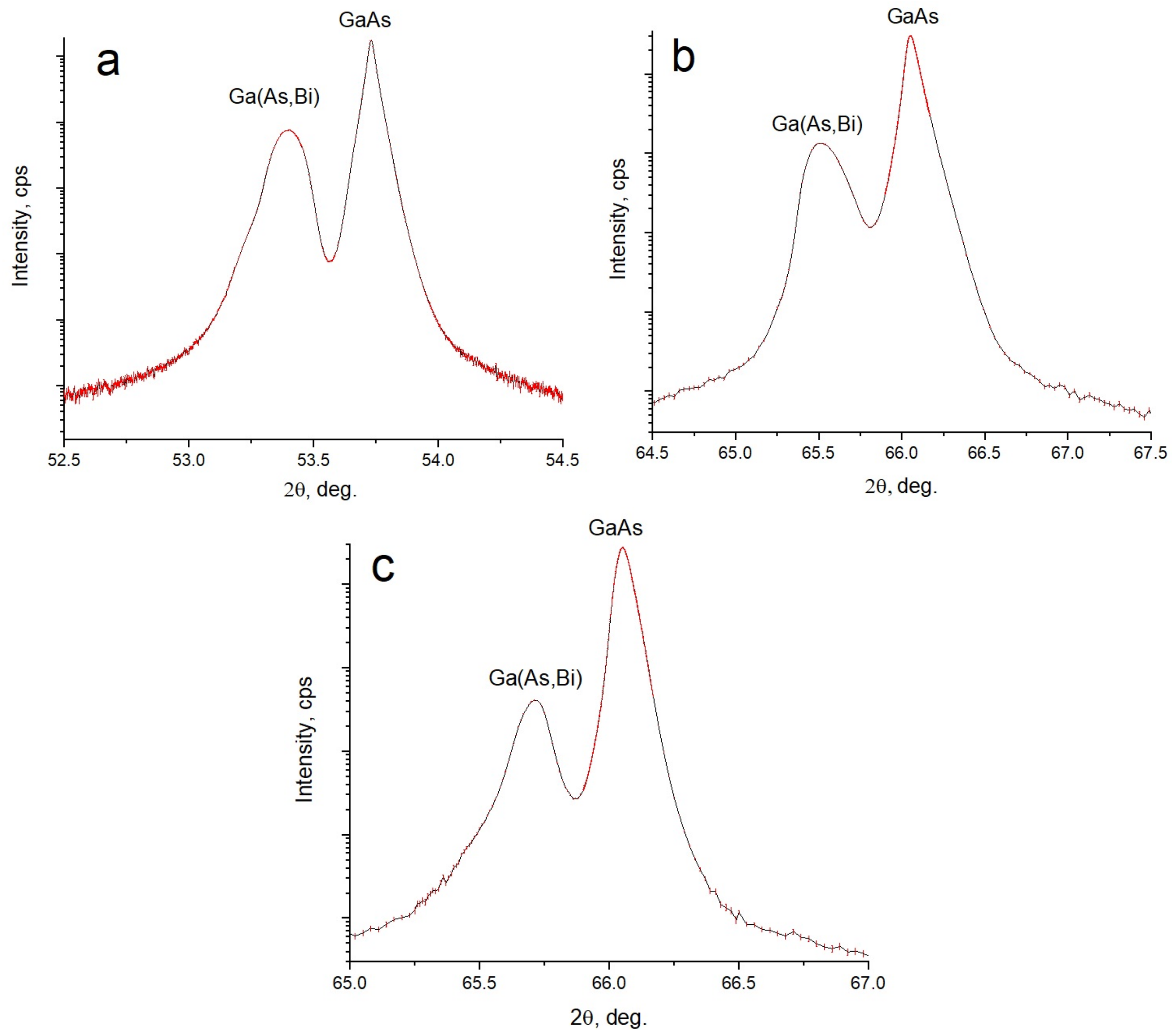

Figure 1.Experimental symmetrical (311) (a) and two asymmetrical (400) (b), (c) XRD curves from the p-$GaAs_{0.94}Bi_{0.06}$ sample. The n-$GaAs_{0.94}Bi_{0.06}$ sample demonstrates similar XRD curves. The asymmetrical XRD curves correspond to small (b) and large (c) incidence angles of the x-rays.

3.2. Raman spectroscopy

Figure 2 shows typical room temperature Raman spectra for 3 mW laser power of p-GaAs, n-GaAs, p-$GaAs_{0.94}Bi_{0.06}$ and n-$GaAs_{0.94}Bi_{0.06}$ samples. We have observed two Raman peaks at around 289 cm^{-1} and 266 cm^{-1} for all samples. These peaks are associated with the well-established longitudinal and transversal-optics phonons at the center of the Brillouin zone, LO (Γ) and TO (Γ), respectively. The Raman spectrum of crystalline zinc

blende structure of GaAs (T_d symmetry) present only two first order peaks around 292 cm^{-1} LO (Γ) and 267 cm^{-1} TO (Γ) [30–33] . We remark that these modes show a clear redshift, which is associated with sample growth conditions, carriers–plasmons–phonons coupling, and an increase of compressive strain with increased Bi content. The existence of compressive strain in these samples is in agreement with the HR-XRD results. For backscattering Raman configuration of (311)B face, both Raman LO (Γ) and TO (Γ) modes are allowed by selection rules.

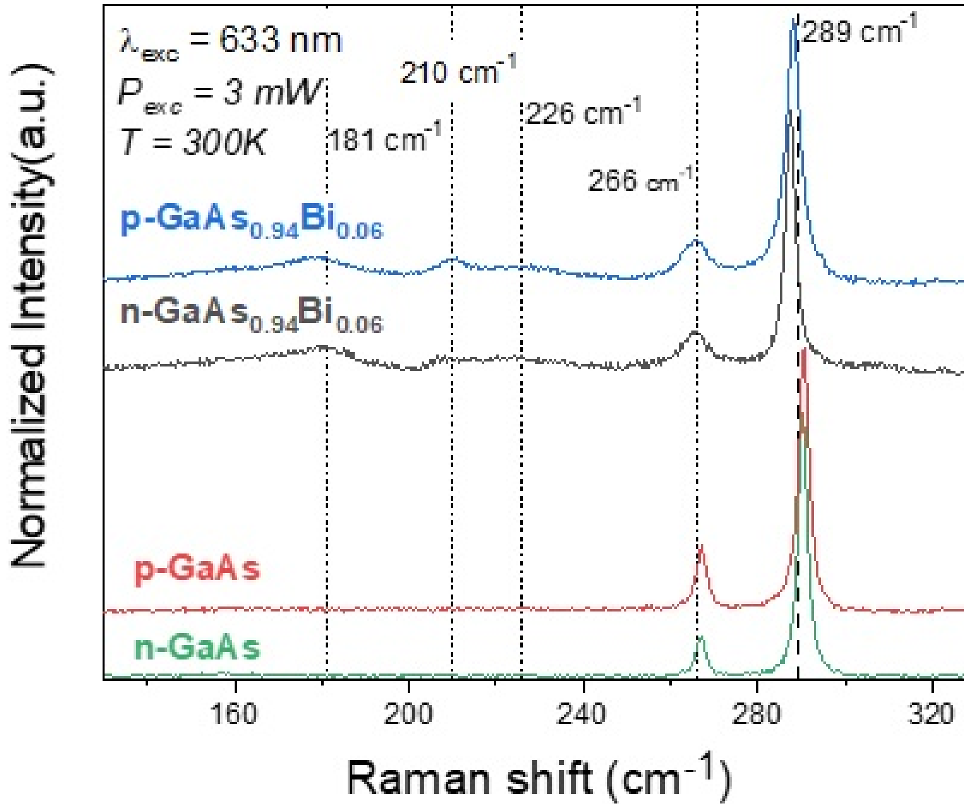

Figure 2. Room temperature Raman spectra of n-GaAs, p-GaAs, and n-$GaAs_{0.94}Bi_{0.06}$, and p-$GaAs_{0.94}Bi_{0.06}$ (311)B samples obtained with a laser excitation and power of 633 nm and 3 mW, respectively.

The observed Bi related Raman peaks, around 181, 210, and 226 cm^{-1}, were previously reported in the literature [13, 29, 34–43]. However, the interpretation of these peaks is controversial [37, 40–43]. Usually, the 181 cm^{-1} and 210 cm^{-1} Raman peaks are associated with the GaBi TO (Γ) mode and GaBi LO (Γ) mode, respectively. On the other hand, the Raman mode around 226 cm^{-1} could be due to other zone boundaries such as longitudinal-acoustics phonons: LA (X) and LA (L), which are not allowed due to momentum conservation. These Raman modes can be induced by the increase of disorder due to Bi incorporation in $GaAs_{1-x}Bi_x$ samples. Other possible interpretations for these observed peaks were also reported in the literature. For example, the peak at around 181 cm^{-1} could not only be a TO (Γ) mode but it could be associated with the convoluted LO (Γ) + TO (Γ) GaBi vibrational mode [41, 44]. However, it is well established that the

181 cm^{-1} peak is related to the GaBi Raman mode. In the following, we will focus our discussion on the two different ranges of the Raman spectra: range I where we observe the TO (Γ) and LO (Γ) GaAs modes (240-310 cm^{-1}) and range II where Bi induced Raman modes (140-240 cm^{-1}) were observed.

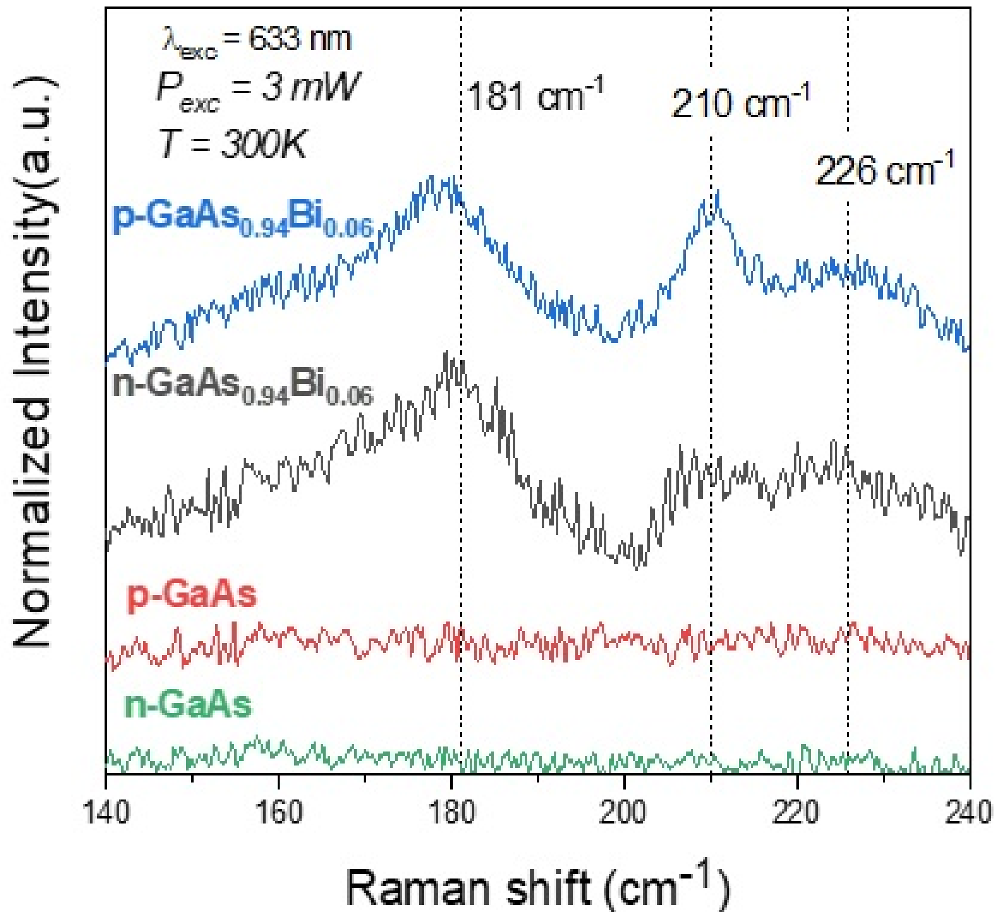

Figure 3. Raman spectra of n-GaAs, p-GaAs, n-$GaAs_{0.94}Bi_{0.06}$, and p-$GaAs_{0.94}Bi_{0.06}$ (311)B samples in the range of Bi-related Raman modes (range I). The laser excitation and power were 633 nm and 3 mW, respectively.

Figure 3 shows the Raman spectra for all samples in the range 140-240 cm^{-1}. It is worth pointing out that no Raman peak was detected in this range for n-GaAs and p-GaAs samples. On the other hand, the n-$GaAs_{0.94}Bi_{0.06}$ and p-$GaAs_{0.94}Bi_{0.06}$ samples show clearly Raman peaks. These Bi induced peaks are associated with GaBi Raman modes and Bi-disorder-induced breakdown selection rules in the crystal structure. The observation of Bi-induced peaks confirms that the Bi atom is incorporated in the GaAs (311)B host lattice resulting in $GaAs_{(1-x)}Bi_x$ crystal.

For doped samples, it is necessary to consider the contribution of the longitudinal optical phonon-plasmon coupled (LOPC) Raman modes, which usually change the shape of the spectrum in the LO (Γ) and TO (Γ) region [45–51]. Actually, in doped samples the carriers plasmons couple with LO phonon and result in L^+ and L^- Raman peaks, which

depend on effective mass, mobility, and carrier concentration. Usually, the L^- peak is broader and has a frequency lower than TO (Γ) Raman mode. As the carrier concentration increases, the L^- peak becomes sharper and closer to the TO (Γ) Raman frequency. On the other hand, the L^+ peak is usually sharp and close to the LO (Γ) Raman frequency, presents a blueshift, and a broadening with increasing carrier concentration. For samples with low mobility, usually only one LOPC Raman mode is observed, between LO (Γ) and TO (Γ) frequencies, due to the strong plasmon damping. For low carrier concentration, LOCP is close to LO (Γ) Raman frequency. If the carrier concentration is increased, the LOPC has an initial blueshift, followed by a redshift up to the TO (Γ) Raman frequency, with increase broadening. Usually, for GaAs, except for the L^+ for $n > 10^{18}$ cm^{-3}, the LOPC Raman peaks are not well resolved in the range of LO (Γ) and TO (Γ). The LO (Γ) and TO (Γ) Raman peaks are due to regions with reduced density of carriers (depletion regions) where there is no effect of phonon-plasmon coupling.

We have also measured the effect of laser power on the LOPC modes. It is not our intention to investigate the effect of photon-generated carriers. The main aim was to determine the limit of laser power that does not introduce important changes due to the photo-generated carriers. Depending on the laser power, the Raman spectra can have a significant contribution from photo-generated carriers [52-58], which can modify the LOPC modes due to intrinsic doping. Figure 4 shows typical Raman spectra of p-$GaAs_{0.94}Bi_{0.06}$ and n-GaAs samples, and in figure S3 (see supplementary material) spectra of p-GaAs and n-$GaAs_{0.94}Bi_{0.06}$ samples for different laser powers. We observed marked changes for laser power in the range of 3 mW to 30 mW.

On the other hand, there is no significant change in Raman spectra for 0.3 mW and 3 mW powers. The fitting of the spectra with two Lorentz functions shows that the variations of parameters in this laser power range are less than 8%. However, we remark that the LOCP modes induced by photongenerated carriers are dependent on the type of intrinsic doping and it is different for n-GaAs, p-GaAs, n-$GaAs_{0.94}Bi_{0.06}$, and p-$GaAs_{0.94}Bi_{0.06}$ samples. We conclude that the contribution of photon-generated carriers can be disregarded for laser power less than 3 mW. Therefore, we have used 3 mW of laser power for our Raman measurements.

Figure 5 shows the Raman spectra for all samples in the range 240-310 cm^{-1} (range II). We have observed two sharp Raman peaks related to TO (Γ) and LO (Γ) GaAs Raman modes for GaAs samples. We have not seen an evident effect of doping, probably due to the low doping concentration of these samples: 2×10^{16} cm^{-3}, for n and p-doped. Notably, the peak L^+ was not observed in the range 290-1500 cm^{-1} (not shown here), which is usually expected for n-type samples. The Raman spectrum is well fitted with two Lorentz functions. There is no clear contribution of LOCP modes in the range 260-300 cm^{-1} (fitting parameters shown in table 1). In addition, the obtained full width at half

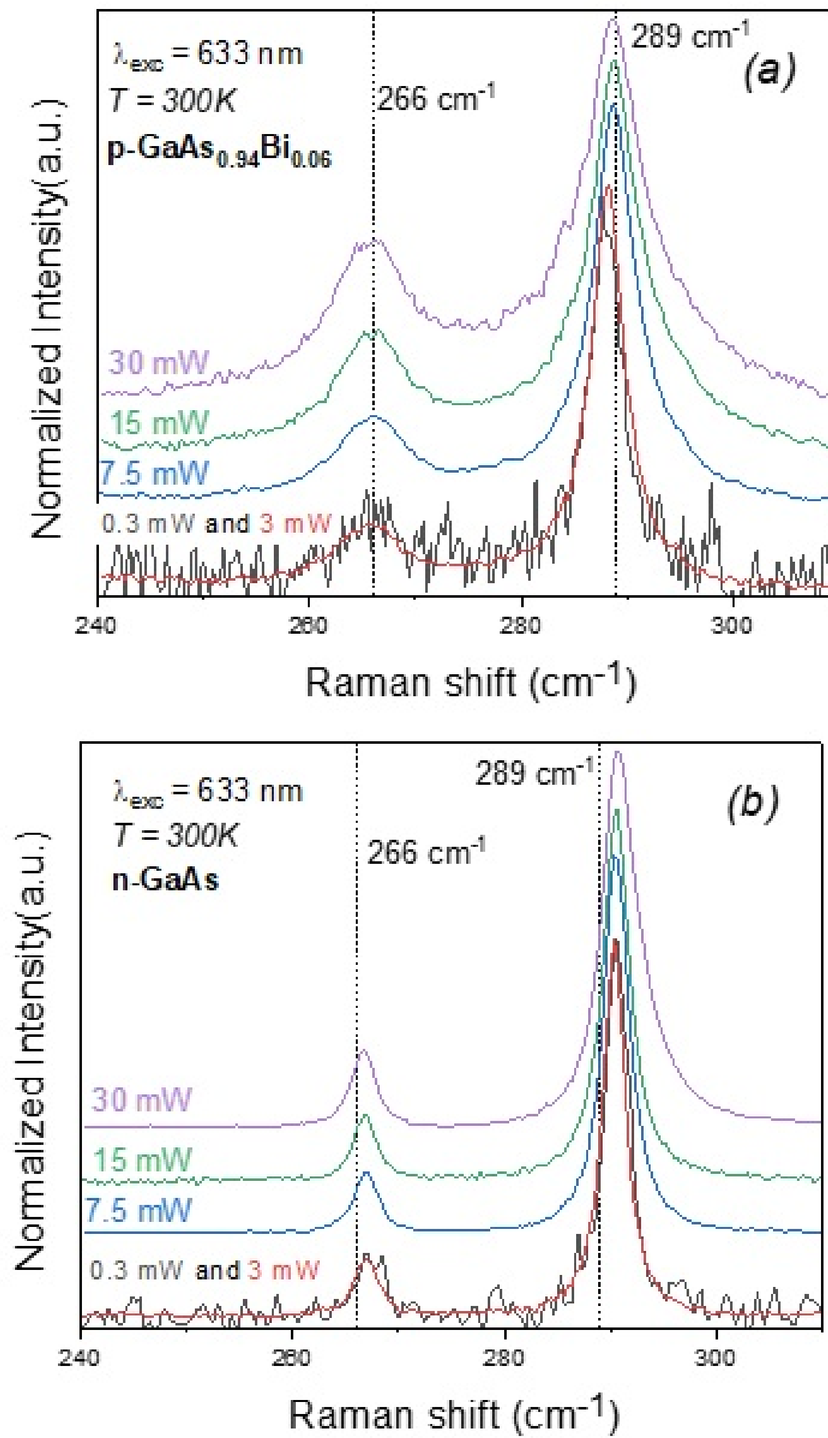

Figure 4. Laser power dependence of Raman spectra for (a) p-$GaAs_{0.94}Bi_{0.06}$ and (b) n-GaAs (311)B samples using a laser excitation of 633 nm.

maximum (FWHM) of about 3 cm^{-1} which is a typical value obtained for GaAs bulk crystals also shows that there is no evidence of an important contribution of LOCP modes. For the p-GaAs sample, a small effect in the width of LO (Γ) Raman mode was observed, probably related to the small increased crystal disorder.

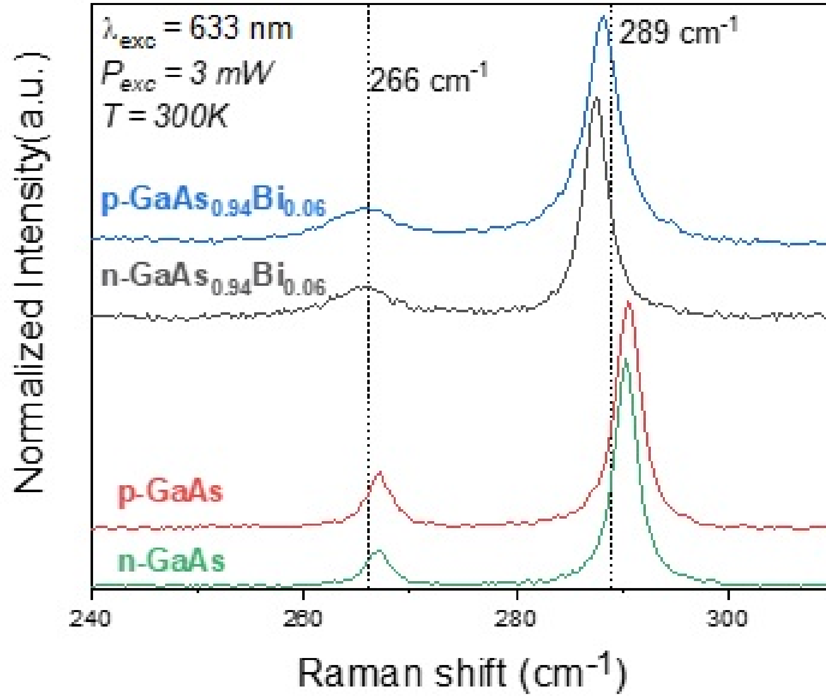

Figure 5. Raman spectra of n-GaAs, p-GaAs, n-$GaAs_{0.94}Bi_{0.06}$, and p-$GaAs_{0.94}Bi_{0.06}$ (311)B samples for laser excitation and power of 633 nm and 3 mW, respectively, in the range of GaAs Raman modes (range II).

Furthermore, for the n-$GaAs_{0.94}Bi_{0.06}$ samples, we have also not observed the L^{+} Raman mode. There is no evidence of a third peak in the range of 260-300 cm^{-1}, like for the p-$GaAs_{0.94}Bi_{0.06}$ sample. These spectra can also be fitted by two Lorentz functions centered at 265.4 and 265.6 cm^{-1} next to the TO peak (266 cm^{-1} TO(Γ) GaAs), and 287.5cm^{-1} and 288.2 cm^{-1} next to LO peak (292 cm^{-1} LO(Γ) GaAs) (see table 1). It was also observed a clear redshift and a broadening for Raman modes of n-$GaAs_{0.94}Bi_{0.06}$ and p-$GaAs_{0.94}Bi_{0.06}$ samples as compared to n-GaAs and p-GaAs. The redshift due to bismuth is different for LO (Γ) modes (for n-type $\Delta\omega$ = 3.0 cm^{-1} and for p-type $\Delta\omega$ = 2.3 cm^{-1}) and TO (Γ) modes (for ntype $\Delta\omega$ = 1.6 cm^{-1} and for p-type $\Delta\omega$ = 1.4 cm^{-1}). This redshift, which is usually associated with strain and the Bi incorporation, is given by $\Delta\omega$LO or TO = $\Delta\omega$alloy + $\Delta\omega$strain [13, 59]. Similar behavior was reported previously in the literature for undoped (100) and (311)B $GaAs_{(1-x)}Bi_x$ samples [13, 29, 34, 36, 39, 40, 59]. Taking LO(Γ) of bulk GaAs crystal at 292 cm^{-1} as reference, the experimental value obtained for the ratio $\Delta\omega$/Bi% for LO(Γ) GaAs mode, -86.5 (n-type) and -70.4 (p-type), and TO(Γ) GaAs mode, -26.6 (n-type) and -5.9 (p-type), are consistent with values obtained in literature, i.e. -68 to -120 and -20 to -30, respectively [13, 29,35, 37, 41].

Table 1. Raman parameters for n-GaAs and p-GaAs reference samples, and n-$GaAs_{0.94}Bi_{0.06}$ and p-$GaAs_{0.94}Bi_{0.06}$ samples

Sample	n-GaAs		n-$GaAs_{0.94}$ $Bi_{0.06}$		p-GaAs		n-$GaAs_{0.94}$ $Bi_{0.06}$	
Mode	TO	LO	TO	LO	TO	LO	TO	LO
ω_{peak}(cm^{-1})	290.4	267.0	287.5	265.4	290.6	267.1	288.2	265.6
FWHM	2.7	3.0	2.8	7.0	3.0	3.0	3.8	8.3
I_{peak}	1	0.15	1	0.15	1	0.25	1	0.16

It is well known that the crystal structure is affected by the incorporation of Bi atom, which substitutes an As atom and, therefore, introduces strain and crystal disorder [13, 29, 34, 36, 37, 39–41, 59]. The increase of disorder could explain the observed broadening of the LO (Γ) GaAs mode, in the p-$GaAs_{0.94}Bi_{0.06}$ sample, and TO (Γ) GaAs Raman modes. On the other hand, the incorporation of Bi atom could also contribute to intrinsic p-doping, which increases with increasing Bi concentration with doping in the range p = 10^{17}–10^{18} cm^{-3} and could possibly play a part in the broadening of the peaks. The observation of similar linewidth of LO (Γ) peaks for n-$GaAs_{0.94}Bi_{0.06}$ as compared to n-GaAs or p-GaAs, indicates a compensation effect of n-doping with the intrinsic p-doping due to Bi incorporation in GaAs [37].

The LOCP for undoped $GaAs_{(1-x)}Bi_x$ samples is due to hole plasmons, which usually contribute to the changes observed in the Raman spectra, particularly for $x >$ 1% [13, 35, 40, 41, 59]. However, the observed differences between n-$GaAs_{0.94}Bi_{0.06}$ and p-$GaAs_{0.94}Bi_{0.06}$ samples are not related to Bi concentrations which are 5.4% for both samples, or to the effect of strain, also the same for the two samples, as the XRD results indicate. The broadening and little blueshift of LO peak observed in the p-$GaA_{0.94}Bi_{0.06}$ sample as compared to n-$GaAs_{0.94}Bi_{0.06}$ sample could be associated with the convoluted LOCP and LO (Γ) Raman peaks. Other effects, such as increasing in disorder and defects density could also contribute to these differences of Raman spectra for these samples. These effects could also manifest themselves in the PL spectra as will be discussed below.

3.3. Photoluminescence

Figure 6 shows low-temperature (15 K) PL spectra for doped $GaAs_{0.94}Bi_{0.06}$ and GaAs samples. The PL peaks observed in doped GaAs samples at around 1.52 eV and between 1.3 and 1.5 eV are associated with free exciton (FE) recombination (peaks with high intensity and sharp profile), and impurities (n or p dopant) recombination, respectively. The PL peaks of $GaAs_{0.94}Bi_{0.06}$ samples show a strong redshift as compared to GaAs samples, as expected due to Bi incorporation and consequent reduction of the band-gap energy and formation of localized states [3, 60-63]. We observed that the redshift of the PL

emission increases from n-$GaAs_{0.94}Bi_{0.06}$ (1.152 eV) to p-$GaAs_{0.94}Bi_{0.06}$ (1.027 eV) samples, which could indicate a higher Bi incorporation for p-doped samples. If we assume that the substitutional Bi causes a band-gap reduction of 84 meV per % of Bi and compare with the FE band-gap of GaAs, one could estimate the amount of effective substitutional Bi incorporated in each GaAs(1-x)Bix sample (x = 5.8% for pdoped and x = 4.4% for n-doped). On the other hand, both $GaAs_{0.94}Bi_{0.06}$ samples present the same estimated value of Bi content (x = 5.4%) and similar residual strain values as estimated by HR-XRD data. However, as mentioned above the PL emissions at low temperatures are observed in an energy range distinct of the expected band-gap reduction. Therefore, other contributions such as strain or Bi-defect level-band related transition could also contribute to explain the observed differences in PL peak position for n- and p-doped GaAsBi samples. As discussed previously, the giant reduction in the bandgap energy of $GaAs_{(1-x)}Bi_x$ alloys has been described using a valence band (VB) anti-crossing interaction between the Bi level and the host GaAs VB. Additionally, the lowtemperature PL peak is also expected to present an energy shift for samples under different strain conditions (compressive versus tensile), due to changes in the structure of the band. In samples with compressive strain usually the PL peak is redshifted with respect to the expected FE [6, 63] and, therefore, this effect should happen with similar magnitude in both $GaAs_{0.94}Bi_{0.06}$ samples as pointed by HR-XRD strain estimation. On the other hand, the presence of Bi-related localized states close to the VB edge also cause a redshift in the PL peak since the exciton localized recombination changes the PL line shapes to exhibit an asymmetric characteristic with a low energy tail, which usually dominates the excitonic recombination processes at low temperatures. The origin of these localized states is attributed to the formation of Bi-related complexes and to alloy disorder in Ga(As, Bi).

As pointed previously, there are few studies on optical and electrical properties of n- and p-doped $GaAs_{(1-x)}Bi_x$ alloys [14-21]. Particularly, it was shown that the incorporation of Bi suppresses the formation of GaAs-like electron traps, thus reducing the total trap concentration in dilute $GaAs_{(1-x)}Bi_x$ layers as compared to GaAs grown under the same growth conditions [18]. However, the Bi incorporation can also introduce Bi-related defects which can be acceptor and donor levels [18]. For n-doped $GaAs_{(1-x)}Bi_x$ samples it was previously shown that the Bi-induced levels are mainly electron traps [18] while for p-doped samples they are mainly hole traps [15]. These Biinduced traps can affect considerably the optical properties of $GaAs_{(1-x)}Bi_x$ layers [18]. In addition, the presence of different Bi induced traps for n- or p-doped samples can affect differently the optical properties of n- and p-doped GaAsBi layers with the same Bi-concentration. For n-doped $GaAs_{0.94}Bi_{0.06}$ layers it was previously shown that both band to band (B-B) and donor to VB (D-B) optical recombination, can contribute to the PL spectrum [18]. The D-B emission was attributed to the recombination of carriers from Bi-induced donor traps and VB [18]. The contribution of this D-B transition explains the observed lower red-shift of the PL

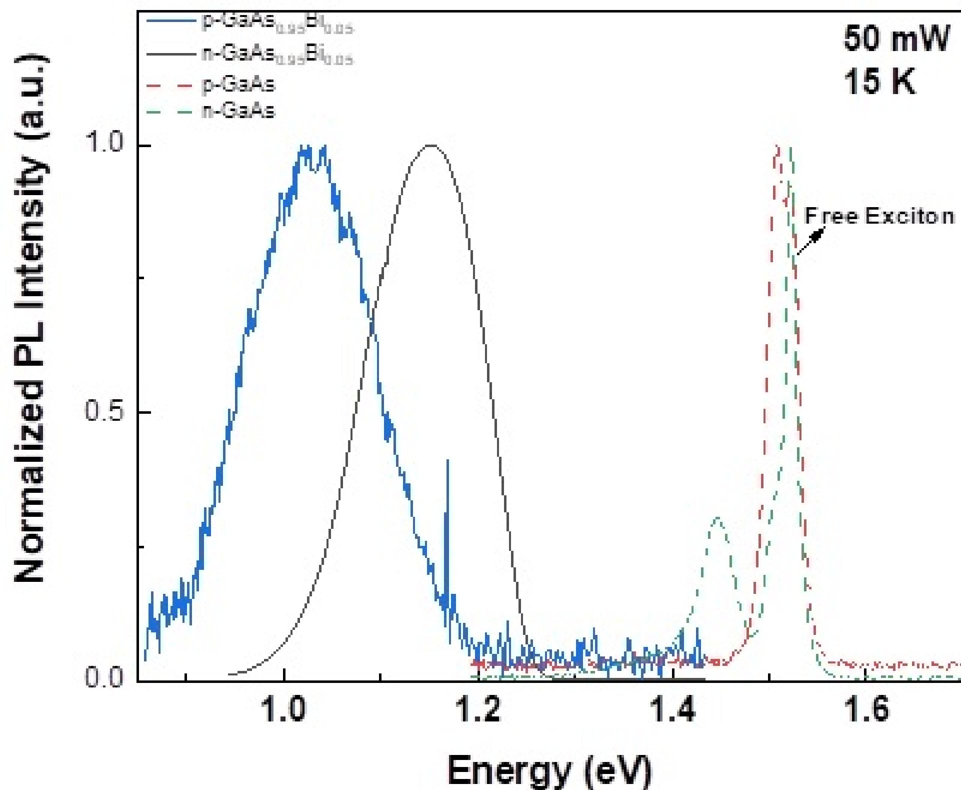

Figure 6. Typical normalized PL spectra for n-$GaAs_{0.94}Bi_{0.06}$, p-$GaAs_{0.94}Bi_{0.06}$, n-GaAs, and p-GaAs samples at 15 K.

peak energy observed in our n-doped $GaAs_{0.94}Bi_{0.06}$ samples as compared to the standard band-gap reduction (i.e. 84 meV per % of Bi). Actually, it is well known that the energy position of Bi-induced donor trap level does change with the Bi incorporation while the Birelated shift of the VB is typically 51 meV/%Bi [18]. As both emissions are not well resolved at low temperature, the total PL peak energy has a smaller red shift than the expected bandgap reduction for 5.4% Bi. A similar contribution of the D–B emission in the PL spectra was previously observed for GaAsN layers [64].

On the other hand, for p-doped samples it was previously shown that the energy red-shift of the PL peak as compared to p-GaAs sample could be associated with the following optical transition: (a) conduction band (CB) to Bi-induced states and (b) CB to shallow Be acceptor states (B-A) [19]. These contributions explain the temperature and laser power dependence of our results. In addition, we observed that the PL spectrum of our p-$GaAs_{0.94}Bi_{0.06}$ sample has much smaller optical efficiency (lower PL intensity and higher signal-tonoise ratio) as compared to the n-$GaAs_{0.94}Bi_{0.06}$ sample. This behavior is also consistent with the observed broadening of the LO Raman peak sample. This indicates that higher density of non-radiative centers is present in p-$GaAs_{0.94}Bi_{0.06}$ as compared to n-GaAs0.94Bi0.06 sample. The non-radiative centers do not contribute to effectively change the band-gap energy in the electronic structure of the host lattice [65–67] but affects the optical efficiency.

In general, our results indicate that the density of nonradiative Bi related defects are higher for the p-doped $GaAs_{(1-x)}Bi_x$ than for the n-doped $GaAs_{(1-x)}Bi_x$. Particularly, the contribution of different Bi-related traps in n- an p-type samples seems to have important role on optical properties of these (311)B oriented alloys.

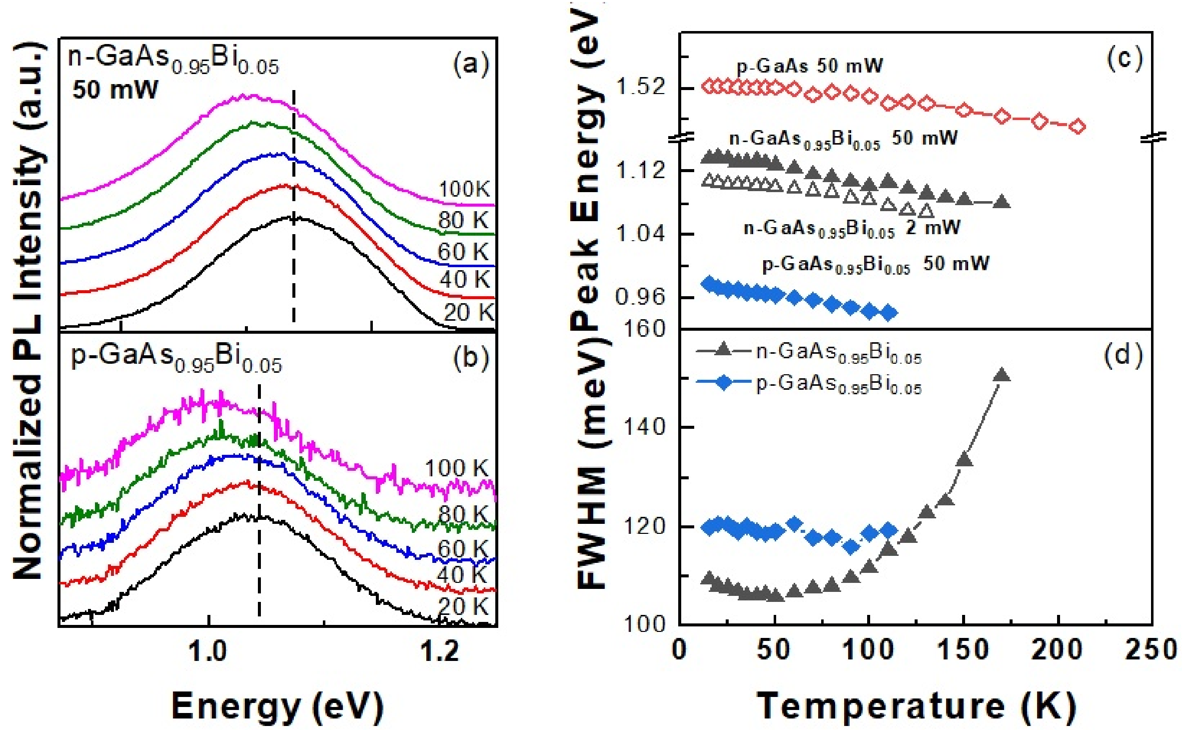

Figure 7. Typical normalized PL spectra as a function of temperature for (a) n-type and (b) p-type under 50 mW laser excitation power. (c) PL energy peak and (d) PL FWHM temperature dependences.

Figures 7(a) and (b) presents the temperature dependence of the PL spectra of doped $GaAs_{(1-x)}Bi_x$ samples. The PL energy peaks exhibit a monotonic redshift with increasing temperature due to the decrease of the band-gap energy, and follow the Varshni empirical dependence formalism [61, 65, 68]. The latter observation indicates the apparent absence of the Bi localization effect which manifests itself as an S-shape profile typically observed in N and Bi diluted III-V alloys. The temperature dependence of the PL peak position and FWHM does not evidence an S-shape profile, which is usually observed for $GaAs_{(1-x)}Bi_x$ samples [69-71]. This S-shape behavior could probably occur in our samples at higher temperatures. However, for our samples the PL signal is only detected in the range of 15-100 K, which is probably not enough to observe the S-shape behavior. On the other hand, the laser excitation power of 50 mW could also be high enough to observe the S-shape, since at this condition, the exciton localization regime can be lost already and the radiative recombination are dominated by the FE regime. In order to avoid a misinterpretation due to the saturation effect of the localized states at high power excitation, PL measurements using lower laser power excitation (2 mW) were performed for n-type samples (figure 7(c)). As clearly seen in figure 7(c) the temperature dependence

of the PL peak shows the same trend for both laser excitation powers of 2 mW and 50 mW. On the other hand, the p-$GaAs_{0.94}Bi_{0.06}$ sample has no significant PL intensity at low laser power excitation of 2 mW (not shown here). In addition, the PL signal is observed only at higher laser excitation powers because its optical efficiency is lower than that of the n-$GaAs_{0.94}Bi_{0.06}$ sample. Moreover, the important PL quenching observed for the p-doped sample with increasing temperature could be due to a higher density of non-radiative Bi complexes and native defects related to GaAs host lattice. A similar effect has been observed in nitrogen diluted III-V alloys [72].

As reported previously in the literature for p-doped (100) $GaAs_{(1-x)}Bi_x$ samples [19], this monotonic PL energy dependence as a function of temperature indicates a downward shift of the Fermi level induced by p-type doping that modifies carrier occupation at the localized states. As previously discussed, the incorporation of Bi atom could also contribute to intrinsic p-doping, which increases the overall doping with increasing Bi concentration [18]. Bi complexes or clusters involving two or more Bi atoms have been experimentally evidenced as the most likely candidates to form such acceptor levels [21,73] and can contribute to the B-A recombination.

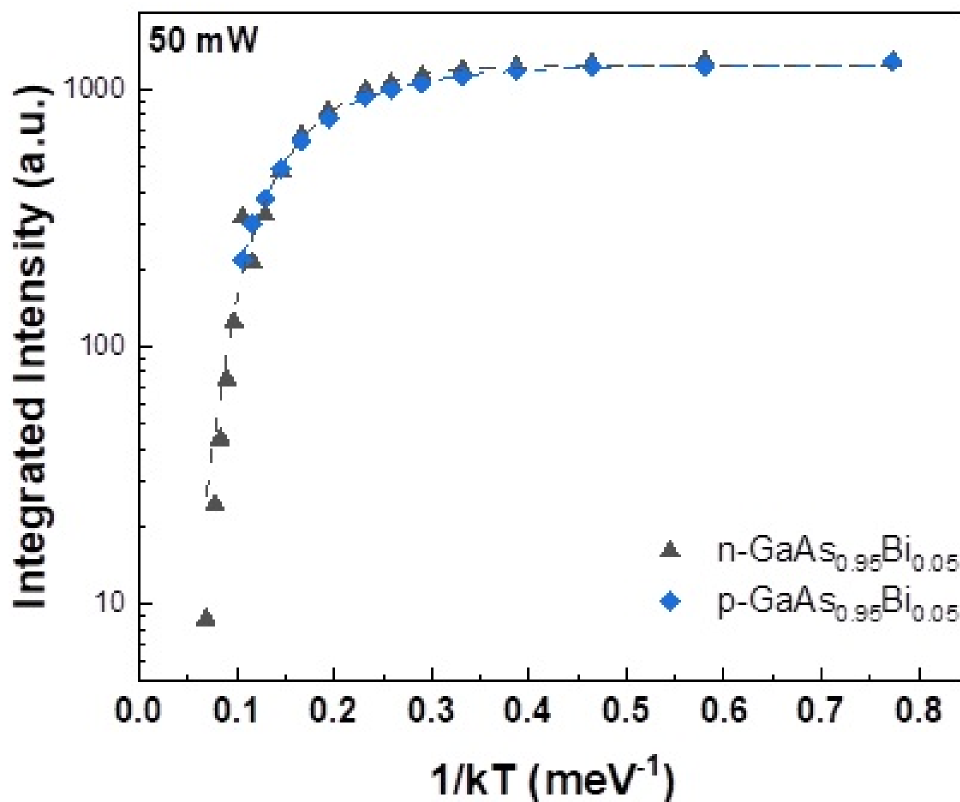

Figure 8. Arrhenius plot of PL intensity for p-$GaAs_{0.94}Bi_{0.06}$ and n-$GaAs_{0.94}Bi_{0.06}$ samples. Dashed lines illustrate the fitted lines using equation (1).

In order to further investigate the temperature dependence of PL intensity and

activation energies of carriers involved in the radiative recombination, the PL data was first fitted using a simple Arrhenius equation (not shown here). However, the fitting was not satisfactory as two distinct exponential trends were observed, indicating two activation energies,which describe the thermal activation of carriers in two temperature regimes. Therefore, an additional energy term was included in the Arrhenius equation [12, 71, 73] and was found to fit the data better, resulting in the below expression used to fit the data:

$$\frac{I_{PL}(T)}{I_0} = \frac{1}{1 + A_1 e^{\frac{-E_1}{\kappa_B T}} + A_2 e^{\frac{-E_2}{\kappa_B T}}} \tag{3.1}$$

Table 2. Arrhenius fitting parameters for n-$GaAs_{0.94}Bi_{0.06}$ and p-$GaAs_{0.94}Bi_{0.06}$ samples.

Samples	**Activation energy (meV)**		**Parameter A**	
$n-GaAs_{0.94}Bi_{0.06}$	E_1	19.89±3	A_1	3.30±1
	E_2	73.85±3	A_2	39.92±12
$p-GaAs_{0.94}Bi_{0.06}$	E_1	11.74±6	A_1	243.8±16
	E_2	41.32±1	A_2	5.03±2

where I_{PL} is the integrated PL intensity, A_1 and A_2 are constants related to the density of non-radiative recombination centers, E_1 and E_2 are activation energies of these centers, k_B is the Boltzmann constant, T the temperature and I_0 the approximate PL intensity when $T \rightarrow 0$ [71, 74, 75].

As discussed previously, $GaAs_{(1-x)}Bi_x$ alloys tend to form localized pairs and clusters, which have different configurations and binding energies [3, 6, 66, 76], alloy disorder, and potential fluctuation. These states are usually associated with two groups with different activation energies in undoped $GaAs_{(1-x)}Bi_x$ samples: one ranges from 8 to 17 meV and is related to Bi clusters and Bi pairs [3, 71, 74, 75], and the other energy around 50 meV is related to alloy disorder [69, 75, 77, 78]. For samples shown in figure 8(a), E_1 energies ranging between 11 meV and 20 meV are attributed to Bi clusters and Bi pairs, while E_2 values ranging from 41 to 73 meV are associated with alloy disorder (around 50 meV). While Bi clusters and alloy disorder are present in both n- and p-doped GaAsBi samples, the fitting results (table 2) indicate higher contribution of E_1 centers for p-$GaAs_{0.94}Bi_{0.06}$ ($A_1 \gg A_2$) and higher contribution of E_2 centers for n-$GaAs_{0.94}Bi_{0.06}$ ($A_1 \ll A_2$). This results indicate that the density of Bi related defects is higher for p-doped $GaAs_{(1-x)}Bi_x$ than for n-doped $GaAs_{(1-x)}Bi_x$.

Figure 9 shows the PL spectra, PL peak energy and PL intensity as a function of PEXC for both doped samples. As the excitation power increases the PL peak blueshifts as shown in figure 9(c), which evidences the filing of localized states. The lowest PL peak energy observed at 5 mW excitation is attributed to localized exciton (LE) recombination,

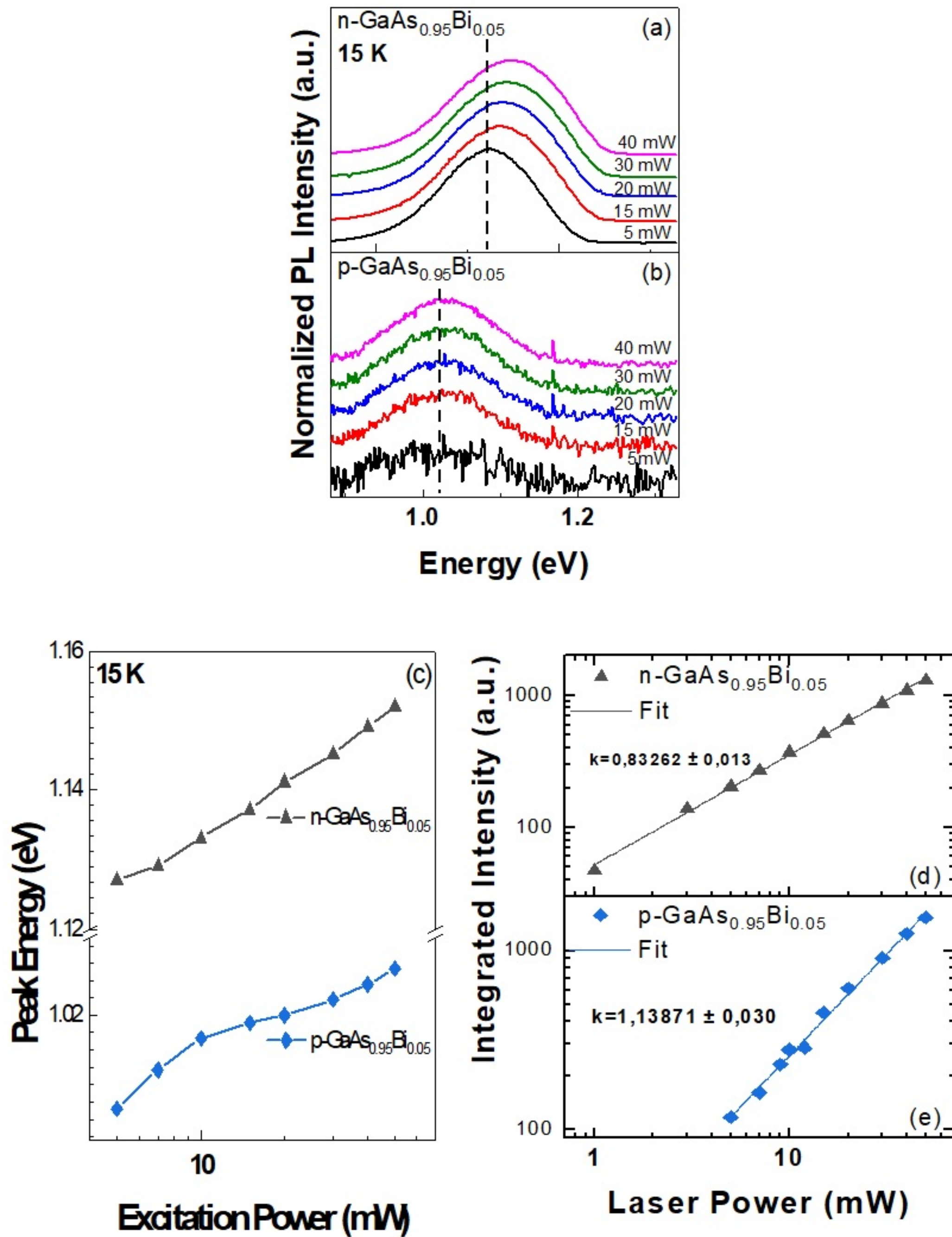

Figure 9. (a) PL peak energy as a function of P_{EXC} and (b), (c) integrated PL intensity (I_{PL}) at 15 K as function of P_{EXC} for p-$GaAs_{0.94}Bi_{0.06}$ and n-$GaAs_{0.94}Bi_{0.06}$ samples. The dashed lines illustrate the fitting using equation: $I_{PL} = \beta(P_{EXC})^{k}$.

while the highest energy emission observed at 40 mW excitation is assigned to FE. On the other hand, it is expected that PL peak energy for the impurity related recombination remains constant irrespective of the laser excitation intensity. We have observed that the PL spectra of n- and p-doped $GaAs_{0.94}Bi_{0.06}$ samples are relatively less sensitive to laser power excitation, i.e. show a relatively small appreciable energy shift as a function of excitation power. This effect is particularly more important in p-doped GaAsBi sample. These results can be attributed to the contribution of different recombination mechanisms for both samples, as reported previously [18, 19].

The integrated PL intensity (I_{PL}) as a function of laser excitation power (P_{EXC}) is shown in figures 9(d) and (e) and their respective fitting curves using the power-law $I_{PL} = \beta(P_{EXC})^k$ [79], where β and k are fitting parameters. The exponent k = 1 for excitonic recombination (whether radiative or nonradiative recombination dominates) and k = 2 for free carrier recombination, assuming that non-radiative recombination dominates. The value of k is approximately unity at 15 K for both samples, which indicates the dominance of excitonic recombination. However, $k > 1$ for p-doped sample, indicating that FEs and free carriers (as B-A recombination) contribute to the recombination, and it is limited by non-radiative centers, while $k < 1$ for n-doped sample indicate that the emission is governed by LEs.

4.Conclusion

Structural and optical properties of n- and p-doped $GaAs_{(1-x)}Bi_x$ thin films grown by MBE on (311)B GaAs substrates reveal the same effective amount of Bi incorporation and strain in both types of doped $GaAs_{(1-x)}Bi_x$ samples. However, the samples present remarkable differences in terms of density of Bi-related defects. Particularly, these defects have important contribution in the presence of non-radiative centers and also contribute to different radiative recombination such as acceptor (donor) to band transition. Our results also indicate that the density of Bi related defects depend on the type of doping (n-or p-doping) of $GaAs_{(1-x)}Bi_x$ and have different effects on the PL properties of n- and p-doped GaBiAs layers grown on (311)B substrate orientation.

Reference

[1] D. Jung, S. Bank, M. L. Lee, and D. Wasserman, Next-Generation Mid-Infrared Sources, J. Opt. 19, 123001 (2017).

[2] I. P. Marko, C. A. Broderick, S. Jin, P. Ludewig, W. Stolz, K. Volz, J. M. Rorison, E. P. O'Reilly, and S. J. Sweeney, Optical Gain in GaAsBi/GaAs Quantum Well Diode Lasers, Sci. Rep. 6, 28863 (2016).

[3] M. Usman, C. A. Broderick, A. Lindsay, and E. P. O'Reilly, Tight-Binding Analysis

of the Electronic Structure of Dilute Bismide Alloys of GaP and GaAs, Phys. Rev. B - Condens. Matter Mater. Phys. 84, 245202 (2011).

[4] R. A. Simmons, S. R. Jin, S. J. Sweeney, and S. K. Clowes, Enhancement of Rashba Interaction in GaAs/AlGaAs Quantum Wells Due to the Incorporation of Bismuth, Appl. Phys. Lett. 107, 142401 (2015).

[5] C. Pashartis and O. Rubel, Localization of Electronic States in III-V Semiconductor Alloys: A Comparative Study, Phys. Rev. Appl. 7, 064011 (2017).

[6] Z. Batool, K. Hild, T. J. C. Hosea, X. Lu, T. Tiedje, and S. J. Sweeney, The Electronic Band Structure of GaBiAs/GaAs Layers: Influence of Strain and Band Anti-Crossing, J. Appl. Phys. 111, 113108 (2012).

[7] Z. Batool, S. Chatterjee, A. Chernikov, A. Duzik, R. Fritz, C. Gogineni, K. Hild, T. J. C. Hosea, S. Imhof, S. R. Johnson, Z. Jiang, S. Jin, M. Koch, S. W. Koch, K. Kolata, R. B. Lewis, X. Lu, M. Masnadi-Shirazi, J. M. Millunchick, P. M. Mooney, N. A. Riordan, O. Rubel, S. J. Sweeney, J. C. Thomas, A. Thränhardt, T. Tiedje, and K. Volz, Chapter 7 - Bismuth-Containing III–V Semiconductors: Epitaxial Growth and Physical Properties, in edited by M. B. T.-M. B. E. Henini (Elsevier, Oxford, 2013), pp. 139–158.

[8] X. Lu, D. A. Beaton, R. B. Lewis, T. Tiedje, and M. B. Whitwick, Effect of Molecular Beam Epitaxy Growth Conditions on the Bi Content of GaAs1-x Bix, Appl. Phys. Lett. 92, 192110 (2008).

[9] M. Henini, J. Ibáñez, M. Schmidbauer, M. Shafi, S. V. Novikov, L. Turyanska, S. I. Molina, D. L. Sales, M. F. Chisholm, and J. Misiewicz, Molecular Beam Epitaxy of GaBiAs on (311) B GaAs Substrates, Appl. Phys. Lett. 91, 350 (2007).

[10] J. F. Rodrigo, D. L. Sales, M. Shafi, M. Henini, L. Turyanska, S. Novikov, and S. I. Molina, Effect of Annealing on the Structural and Optical Properties of (3 1 1)B GaAsBi Layers, Appl. Surf. Sci. 256, 5688 (2010).

[11] P. K. Patil, F. Ishikawa, and S. Shimomura, GaAsBi/GaAs MQWs MBE Growth on (411) GaAs Substrate, Superlattices Microstruct. 100, 1205 (2016).

[12] G. A. Prando, V. Orsi Gordo, J. Puustinen, J. Hilska, H. M. Alghamdi, G. Som, M. Gunes, M. Akyol, S. Souto, A. D. Rodrigues, H. V. A. Galeti, M. Henini, Y. G. Gobato, and M. Guina, Exciton Localization and Structural Disorder of GaAs1-XBix/GaAs Quantum Wells Grown by Molecular Beam Epitaxy on (311)B GaAs Substrates, Semicond. Sci. Technol. 33, 084002 (2018).

[13] F. S. Al mashary, S. de Castro, A. F. da Silva, J. F. Felix, M. R. Piton, H. V. A. Galeti, A. De Giovanni Rodrigues, Y. G. Gobato, N. Al Saqri, M. Henini, M. M. Al huwayz, A. M. Albadri, A. Y. Alyamani, H. A. Albrathen, S. A. Alhusaini, K. M. Aljaber, A. Z. Alanazi, and F. S. Alghamdi, Effect of Growth Techniques on the Structural, Optical and Electrical

Properties of Indium Doped TiO2 Thin Films, J. Alloys Compd. 766, 194 (2018).

[14] J. A. Steele, R. A. Lewis, M. Henini, O. M. Lemine, and A. Alkaoud, Raman Scattering Studies of Strain Effects in (100) and (311)B GaAs 1-XBix Epitaxial Layers, J. Appl. Phys. 114, 193516 (2013).

[15] R. N. Kini, L. Bhusal, A. J. Ptak, R. France, and A. Mascarenhas, Electron Hall Mobility in GaAsBi, J. Appl. Phys. 106, 043705 (2009).

[16] P. M. Mooney, M. C. Tarun, V. Bahrami-Yekta, T. Tiedje, R. B. Lewis, and M. Masnadi-Shirazi, Defect Energy Levels in P-Type GaAsBi and GaAs Grown by MBE at Low Temperatures, Semicond. Sci. Technol. 31, 065007 (2016).

[17] P. M. Mooney, K. P. Watkins, Z. Jiang, A. F. Basile, R. B. Lewis, V. Bahrami-Yekta, M. Masnadi-Shirazi, D. A. Beaton, and T. Tiedje, Deep Level Defects in N-Type GaAsBi and GaAs Grown at Low Temperatures, J. Appl. Phys. 113, 133708 (2013).

[18] R. L. Field, J. Occena, T. Jen, D. Del Gaudio, B. Yarlagadda, C. Kurdak, and R. S. Goldman, Influence of Surface Reconstruction on Dopant Incorporation and Transport Properties of GaAs(Bi) Alloys, Appl. Phys. Lett. 109, 252105 (2016).

[19] Ł. Gelczuk, J. Kopaczek, T. B. O. Rockett, R. D. Richards, and R. Kudrawiec, Deep-Level Defects in n-Type GaAsBi Alloys Grown by Molecular Beam Epitaxy at Low Temperature and Their Influence on Optical Properties, Sci. Rep. 7, 12824 (2017).

[20] M. Yoshimoto, M. Itoh, Y. Tominaga, and K. Oe, Quantitative Estimation of Density of Bi-Induced Localized States in GaAs1-XBix Grown by Molecular Beam Epitaxy, J. Cryst. Growth 378, 73 (2013).

[21] M. A. Stevens, S. Lenney, J. McElearney, K. A. Grossklaus, and T. E. Vandervelde, Characterization of Tellurium and Silicon as N-Type Dopants for GaAsBi, Semicond. Sci. Technol. 35, 105006 (2020).

[22] P. V.V., P. M.A., and S. B.R., Control of Parameters during GaAs Molecular Beam Epitaxy at Low Growth Temperature, Semiconductors 36, 837 (2002).

[23] M. A. Chuev, B. A. Aronzon, E. M. Pashaev, M. V. Koval'Chuk, I. A. Subbotin, V. V. Rylkov, V. V. Kvardakov, P. G. Medvedev, B. N. Zvonkov, and O. V. Vikhrova, Diluted Magnetic Semiconductors: Actual Structure and Magnetic and Transport Properties, Russ. Microelectron. 37, 73 (2008).

[24] B. A. Aronzon, M. V. Kovalchuk, E. M. Pashaev, M. A. Chuev, V. V. Kvardakov, I. A. Subbotin, V. V. Rylkov, M. A. Pankov, I. A. Likhachev, B. N. Zvonkov, Y. A. Danilov, O. V. Vihrova, A. V. Lashkul, and R. Laiho, Structural and Transport Properties of GaAs/δ-Mn/GaAs/In xGa1-xAs/GaAs Quantum Wells, J. Phys. Condens. Matter 20, 145207 (2008). [25] D. Keith Bowen and B. K. Tanner, High Resolution X-Ray Diffractometry And Topography (CRC Press, 2005). [26] L. Vegard, Die Konstitution Der Mischkristalle

Und Die Raumfüllung Der Atome, Zeitschrift Für Phys. 5, 17 (1921).

[27] M. Ferhat and A. Zaoui, Structural and Electronic Properties of III-V Bismuth Compounds, Phys. Rev. B 73, 115107 (2006).

[28] E. Tisbi, E. Placidi, R. Magri, P. Prosposito, R. Francini, A. Zaganelli, S. Cecchi, E. Zallo, R. Calarco, E. Luna, J. Honolka, M. Vondráček, S. Colonna, and F. Arciprete, Increasing Optical Efficiency in the Telecommunication Bands of Strain-Engineered Ga(As,Bi) Alloys, Phys. Rev. Appl. 14, 014028 (2020).

[29] R. Loudon, The Raman Effect in Crystals, Adv. Phys. 13, 423 (1964).

[30] R. A. Muñoz-Hernández, S. Jiménez-Sandoval, G. Torres-Delgado, C. Roch, X. K. Chen, and J. C. Irwin, Light Scattering in P-type GaAs:Ge, J. Appl. Phys. 80, 2388 (1996).

[31] J. Menendez, Characterization of Bulk Semiconductors Using Raman Spectroscopy, in Raman Scattering in Materials Science, edited by W. H. Weber and R. Merlin (Springer, New York, 2000).

[32] R. Merlin, A. Pinczuk, and W. H. Weber, Overview of Phonon Raman Scattering in Solids, in Raman Scattering in Materials Science, edited by R. Merlin and W. H. Weber (Springer, New York, 2000).

[33] J. A. Steele, R. A. Lewis, M. Henini, O. M. Lemine, D. Fan, Y. I. Mazur, V. G. Dorogan, P. C. Grant, S.-Q. Yu, and G. J. Salamo, Raman Scattering Reveals Strong LO-Phonon-Hole-Plasmon Coupling in Nominally Undoped GaAsBi: Optical Determination of Carrier Concentration, Opt. Express 22, 11680 (2014).

[34] J. Li, K. Forghani, Y. Guan, W. Jiao, W. Kong, K. Collar, T. H. Kim, T. F. Kuech, and A. S. Brown, GaAs1-YBiy Raman Signatures: Illuminating Relationships between the Electrical and Optical Properties of GaAs1-YBiy and Bi Incorporation, AIP Adv. 5, 067103 (2015).

[35] P. Wang, W. Pan, X. Wu, C. Cao, S. Wang, and Q. Gong, Heteroepitaxy Growth of GaAsBi on Ge(100) Substrate by Gas Source Molecular Beam Epitaxy, Appl. Phys. Express 9, 045502 (2016).

[36] A. Erol, E. Akalin, K. Kara, M. Aslan, V. Bahrami-Yekta, R. B. Lewis, and T. Tiedje, Raman and AFM Studies on Nominally Undoped, p- and n-Type GaAsBi Alloys, J. Alloys Compd. 722, 339 (2017).

[37] R. Butkutė, G. Niaura, E. Pozingytė, B. Čechavičius, A. Selskis, M. Skapas, V. Karpus, and A. Krotkus, Bismuth Quantum Dots in Annealed GaAsBi/AlAs Quantum Wells, Nanoscale Res. Lett. 12, 436 (2017).

[38] A. S. Pashchenko, L. S. Lunin, S. N. Chebotarev, and M. L. Lunina, Study of the Structural and Luminescence Properties of InAs/GaAs Heterostructures with Bi-Doped

Potential Barriers, Semiconductors 52, 729 (2018).

[39] R. S. Joshya, V. Rajaji, C. Narayana, A. Mascarenhas, and R. N. Kini, Anharmonicity in Light Scattering by Optical Phonons in GaAs1-xBix, J. Appl. Phys. 119, 205706 (2016).

[40] P. Verma, K. Oe, M. Yamada, H. Harima, M. Herms, and G. Irmer, Raman Studies on $GaAs_{1-x}Bi_x$ and $InAs_{1-x}Bi_x$, J. Appl. Phys. 89, 1657 (2001).

[41] M. J. Seong, S. Francoeur, S. Yoon, A. Mascarenhas, S. Tixier, M. Adamcyk, and T. Tiedje, Bi-Induced Vibrational Modes in GaAsBi, Superlattices Microstruct. 37, 394 (2005).

[42] F. Sarcan, Ö. Dönmez, K. Kara, A. Erol, E. Akalın, M. Çetin Arıkan, H. Makhloufi, A. Arnoult, and C. Fontaine, Bismuth-Induced Effects on Optical, Lattice Vibrational, and Structural Properties of Bulk GaAsBi Alloys, Nanoscale Res. Lett. 9, 119 (2014).

[43] S. Souto, J. Hilska, Y. Galvão Gobato, D. Souza, M. B. Andrade, E. Koivusalo, J. Puustinen, and M. Guina, Raman Spectroscopy of GaSb1-xBix Alloys with High Bi Content, Appl. Phys. Lett. 116, 202103 (2020).

[44] A. Mooradian and A. L. McWhorter, Polarization and Intensity of Raman Scattering from Plasmons and Phonons in Gallium Arsenide, Phys. Rev. Lett. 19, 849 (1967).

[45] A. Mooradian and G. B. Wright, Observation of the Interaction of Plasmons with Longitudinal Optical Phonons in GaAs, Phys. Rev. Lett. 16, 999 (1966).

[46] M. Cardona, Proceedings of the 15th International Conference on the Physics of Semiconductors, Kyoto, Sept. 1st-5th, 1980, in Journal of the Physical Society of Japan, v.49(1980) Suppl. A., edited by S. Tanaka and Y. Toyozawa (Physical Society of Japan, Kyoto, 1980), p. 23.

[47] D. Olego and M. Cardona, Raman Scattering by Coupled LO-Phononplasmon Modes and Forbidden TO-Phonon Raman Scattering in Heavily Doped p-Type GaAs, Phys. Rev. B 24, 7217 (1981).

[48] G. Abstreiter, M. Cardona, and A. Pinczuk, Light Scattering by Free Carrier Excitations in Semiconductors, in Light Scattering in Solids IV. Topics in Applied Physics, Vol 54, edited by M. Cardona and G. Güntherodt (Springer, Berlin, 1984), pp. 5–150.

[49] R. Fukasawa and S. Perkowitz, Raman-Scattering Spectra of Coupled LO-Phonon–Hole-Plasmon Modes in p -Type GaAs, Phys. Rev. B 50, 14119 (1994).

[50] G. Irmer, M. Wenzel, and J. Monecke, Light Scattering by a Multicomponent Plasma Coupled with Longitudinal-Optical Phonons: Raman Spectra of-Type GaAs:Zn, Phys. Rev. B - Condens. Matter Mater. Phys. 56, 9524 (1997).

[51] J. Hu, O. V. Misochko, A. Goto, and K. G. Nakamura, Delayed Formation of Coherent LO Phonon-Plasmon Coupled Modes in n- and p-Type GaAs Measured Using a

Femtosecond Coherent Control Technique, Phys. Rev. B - Condens. Matter Mater. Phys. 86, 235145 (2012).

[52] R. Srnanek, G. Irmer, J. Geurts, M. Lentze, D. Donoval, B. Sciana, D. Radziewicz, M. Tlaczala, M. Florovic, and I. Novotny, Micro-Raman Study of Photoexcited Plasma in GaAs Bevelled Structures, Appl. Surf. Sci. 243, 96 (2005).

[53] J. E. Kardontchik and E. Cohen, Raman Scattering from Plasmons in Photoexcited GaP, Phys. Rev. Lett. 42, 669 (1979).

[54] A. Pinczuk, J. Shah, and P. A. Wolff, Collective Modes of Photoexcited Electron-Hole Plasmas in GaAs, Phys. Rev. Lett. 47, 1487 (1981).

[55] S. Yoon, M. J. Seong, B. Fluegel, A. Mascarenhas, S. Tixier, and T. Tiedje, Photogenerated Plasmons in GaAs1-XBix, Appl. Phys. Lett. 91, 082101 (2007).

[56] H. Talaat, T. A. El-Brolossy, S. Negm, and S. Abdalla, Photomodulation of the Coupled Plasmon-LO Phonon of GaAs Surfaces, J. Phys. Condens. Matter 15, 5829 (2003).

[57] S. Zhu, W. Qiu, H. Wang, T. Lin, P. Chen, and X. Wang, Raman Spectroscopic Determination of Hole Concentration in Undoped GaAsBi, Semicond. Sci. Technol. 34, 015008 (2019).

[58] J. A. Steele, Structural and Optical Studies of GaAs1-XBix and p-Bi203 for Optoelectronic Devices, University of Wollongong, 2015.

[59] J. Li, K. Forghani, Y. Guan, W. Jiao, W. Kong, K. Collar, T. H. Kim, T. F. Kuech, and A. S. Brown, GaAs1-yBiy Raman Signatures: Illuminating Relationships between the Electrical and Optical Properties of GaAs1-yBiy and Bi Incorporation, AIP Adv. 5, 067103 (2015).

[60] X. Lu, D. A. Beaton, R. B. Lewis, T. Tiedje, and Y. Zhang, Composition Dependence of Photoluminescence of GaAs1-x Bi x Alloys, Appl. Phys. Lett. 95, 041903 (2009).

[61] R. Kudrawiec, M. Syperek, P. Poloczek, J. Misiewicz, R. H. Mari, M. Shafi, M. Henini, Y. G. Gobato, S. V. Novikov, J. Ibáñez, M. Schmidbauer, and S. I. Molina, Carrier Localization in GaBiAs Probed by Photomodulated Transmittance and Photoluminescence, J. Appl. Phys. 106, 023518 (2009).

[62] K. Alberi, O. D. Dubon, W. Walukiewicz, K. M. Yu, K. Bertulis, and A. Krotkus, Valence Band Anticrossing in GaBi XAs 1-X, Appl. Phys. Lett. 91, 051909 (2007).

[63] M. Usman, C. A. Broderick, Z. Batool, K. Hild, T. J. C. Hosea, S. J. Sweeney, and E. P. O'Reilly, Impact of Alloy Disorder on the Band Structure of Compressively Strained GaBixAs1-x, Phys. Rev. B - Condens. Matter Mater. Phys. 87, 115104 (2013).

[64] T. Wilson, N. P. Hylton, Y. Harada, P. Pearce, D. Alonso-Álvarez, A. Mellor, R. D. Richards, J. P. R. David, and N. J. Ekins-Daukes, Assessing the Nature of the Distribution

of Localised States in Bulk GaAsBi, Sci. Rep. 8, 6457 (2018).

[65] K. Alberi, T. M. Christian, B. Fluegel, S. A. Crooker, D. A. Beaton, and A. Mascarenhas, Localization Behavior at Bound Bi Complex States in GaA S1-x B Ix, Phys. Rev. Mater. 1, 024605 (2017).

[66] K. Alberi, B. Fluegel, D. A. Beaton, M. Steger, S. A. Crooker, and A. Mascarenhas, Origin of Deep Localization in GaA s 1-x B Ix and Its Consequences for Alloy Properties, Phys. Rev. Mater. 2, 114603 (2018).

[67] A. R. Mohmad, F. Bastiman, J. S. Ng, S. J. Sweeney, and J. P. R. David, Photoluminescence Investigation of High Quality GaAs1-x Bi x on GaAs, Appl. Phys. Lett. 98, 122107 (2011).

[68] S. Imhof, A. Thränhardt, A. Chernikov, M. Koch, N. S. Köster, K. Kolata, S. Chatterjee, S. W. Koch, X. Lu, S. R. Johnson, D. A. Beaton, T. Tiedje, and O. Rubel, Clustering Effects in Ga(AsBi), Appl. Phys. Lett. 96, 131115 (2010).

[69] M. K. Shakfa, D. Kalincev, X. Lu, S. R. Johnson, D. A. Beaton, T. Tiedje, A. Chernikov, S. Chatterjee, and M. Koch, Quantitative Study of Localization Effects and Recombination Dynamics in GaAsBi/GaAs Single Quantum Wells, J. Appl. Phys. 114, 164306 (2013).

[70] O. Donmez, A. Erol, M. C. Arikan, H. Makhloufi, A. Arnoult, and C. Fontaine, Optical Properties of GaBiAs Single Quantum Well Structures Grown by MBE, Semicond. Sci. Technol. 30, 094016 (2015).

[71] S. Mazzucato, H. Lehec, H. Carrère, H. Makhloufi, A. Arnoult, C. Fontaine, T. Amand, and X. Marie, Low-Temperature Photoluminescence Study of Exciton Recombination in Bulk Gaasbi, Nanoscale Res. Lett. 9, 19 (2014).

[72] S. Mazzucato, P. Boonpeng, H. Carrère, D. Lagarde, A. Arnoult, G. Lacoste, T. Zhang, A. Balocchi, T. Amand, X. Marie, and C. Fontaine, Reduction of Defect Density by Rapid Thermal Annealing in GaAsBi Studied by Time-Resolved Photoluminescence, Semicond. Sci. Technol. 28, 022001 (2013).

[73] Y. Zhang, A. Mascarenhas, and L. W. Wang, Similar and Dissimilar Aspects of III-V Semiconductors Containing Bi versus N, Phys. Rev. B - Condens. Matter Mater. Phys. 71, 155201 (2005).

[74] S. Imhof, C. Wagner, A. Thränhardt, A. Chernikov, M. Koch, N. S. Köster, S. Chatterjee, S. W. Koch, O. Rubel, X. Lu, S. R. Johnson, D. A. Beaton, and T. Tiedje, Luminescence Dynamics in Ga(AsBi), Appl. Phys. Lett. 98, 161104 (2011).

[75] M. Yoshimoto and K. Oe, Present Status and Future Prospects of Bi-Containing Semiconductors, 1st Int. Work. Bismuth Contain. Semicond. (2010).

[76] T. Schmidt, K. Lischka, and W. Zulehner, Excitation-Power Dependence of the near-Band-Edge Photoluminescence of Semiconductors, Phys. Rev. B 45, 8989 (1992).

Supporting Information

Structural and optical properties of n-type and p-type $GaAs_{(1-x)}Bi_x$ thin films grown by molecular beam epitaxy on (311)B GaAs substrates

Daniele De Souza[1], Sultan Alhassan[2,3], Saud Alotaibi[2], Amra Alhassni[2], Amjad Almunyif[2,4], Hind Albalawi[4], Igor P Kazakov[5], Alexey V Klekovkin[5], Sergey A ZinovEv[5], Igor A Likhachev[6], Elkhan M Pashaev[6], Sergio Souto[7], Yara Galv~ao Gobato[1], Helder Vinicius Avanço Galeti[8], and Mohamed Henini[2]

[1] Physics Department, Federal University of São Carlos, São Carlos-SP, Brazil

[2] School of Physics and Astronomy, University of Nottingham, Nottingham NG7 2RD, United Kingdom

[3] School of Physics, College of Science, Jouf University, Skaka 74631-7365, Saudi Arabia

[4] Physics Department, Faculty of Science, Princess Nourah Bint Abdulrahman University, Riyadh, Saudi Arabia

[5] P.N.Lebedev Physical Institute, Russian Academy of Science, 119991, GSP-1 Moscow, Russia

[6] National Research Center 'Kurchatov Institute', 123182 Moscow, Russia

[7] FZEA/ZAB, University of São Paulo, Pirassununga-SP, Brazil

[8] Electrical Engineering Department, Federal University of São Carlos, São Carlos-SP, Brazil

Experimental Results

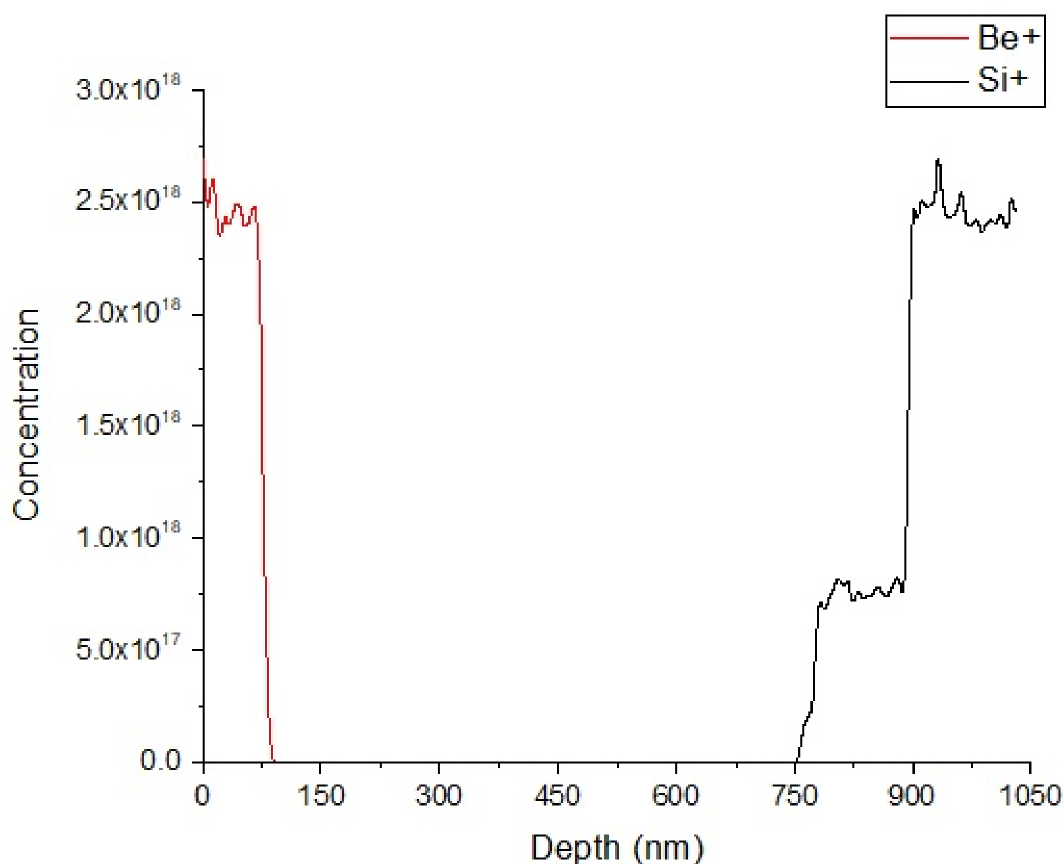

Figure S1. SIMS concentration profile of a GaAs calibration sample (p-i-n structure).

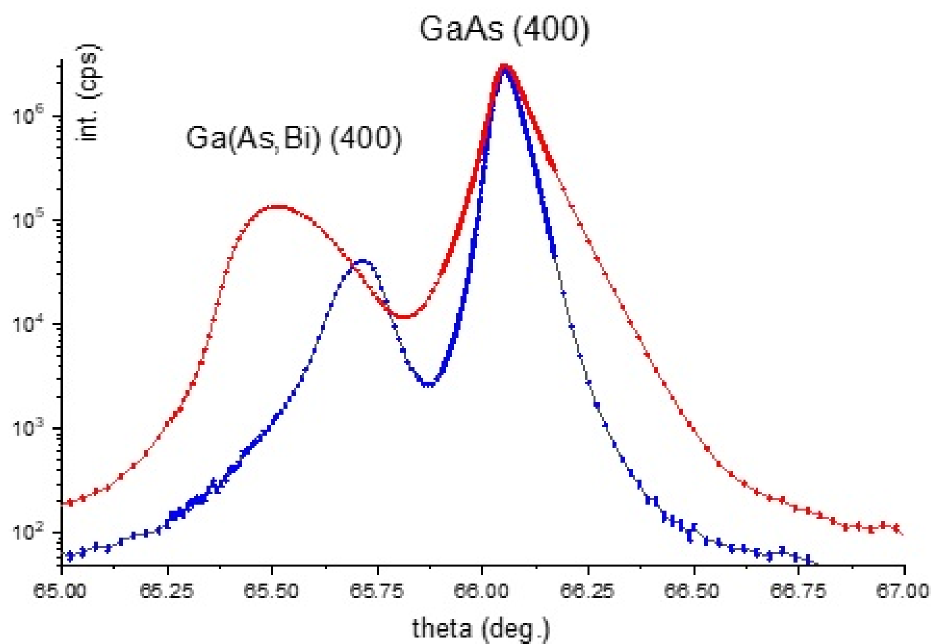

Figure S2.Asymmetrical (400) X-ray diffractions from GaAs/Ga(As,Bi) (311)B p-doped sample with small (red line) and large (blue line) incident angle of X-ray radiation. For clarity, plots of the intensity of the XRD signal obtained from the double angle of reflection for the considered reflection planes are shown.

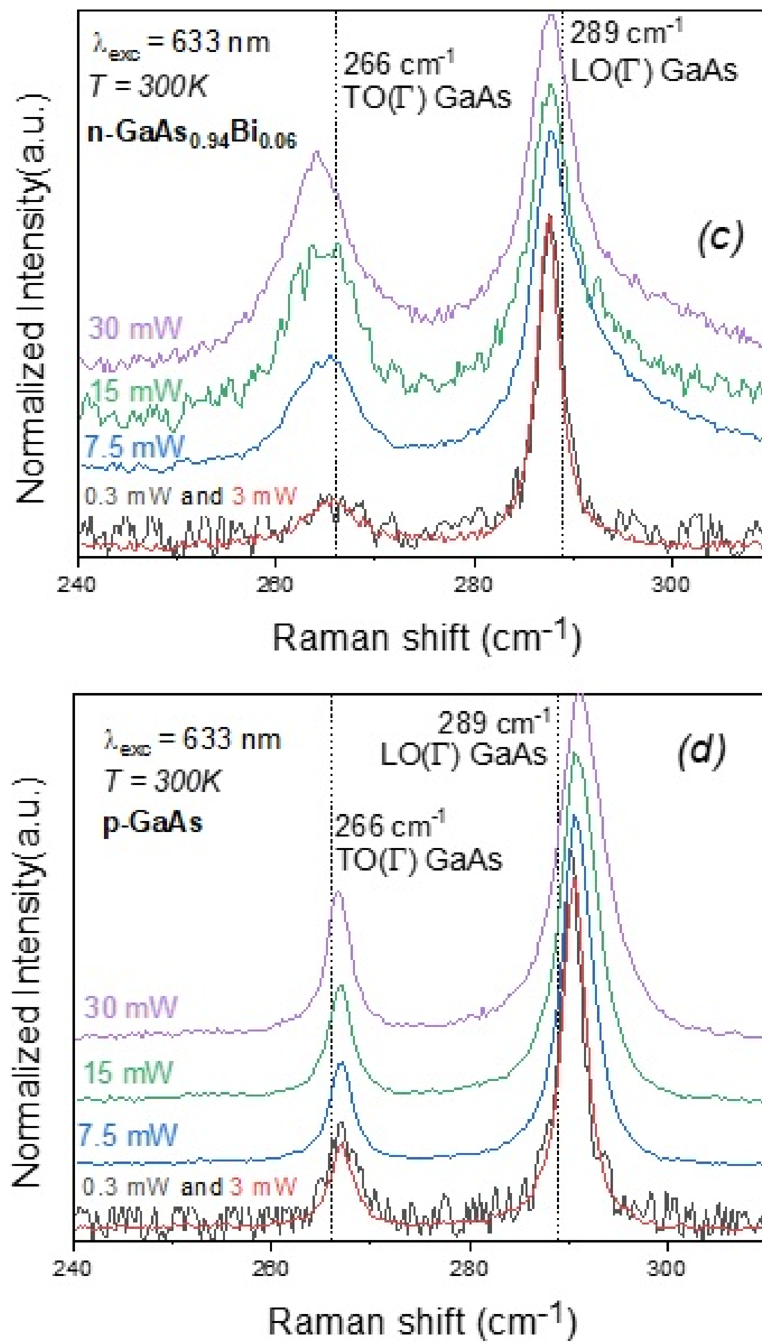

Figure S3. Laser power dependence of Raman spectra for (c) n-GaAs0.94Bi0.06 and (d) p-GaAs (311)B samples using a laser excitation of 633nm.

PUBLISHED ARTICLE

Journal of Alloys and Compounds

Investigation of the effect of substrate orientation on the structural, electrical and optical properties of n-type $GaAs_{(1-x)}Bi_x$ layers grown by Molecular Beam Epitaxy

Sultan Alhassan[a,b,1], Daniele de Souza[c,1], Amra Alhassni[a], Amjad Almunyif[a], Saud Alotaibi[a], Abdulaziz Almalki[a], Maryam Alhuwayz[a], Igor P. Kazakov[d], Alexey V. Klekovkin[d], Vladimir I. Tsekhosh[d], Igor A. Likhachev[e], Elkhan.M. Pashaev[e], Sergio Souto[f], Yara Galvão Gobato[c], Noor Al Saqri[g], Helder Vinicius Avanço Galeti[h], Faisal Al mashary[i], Hind Albalawi[j], Norah Alwadai[j], Mohamed Henini[a]

[a] School of Physics and Astronomy, University of Nottingham, Nottingham NG7 2RD, UK

[b] School of Physics, College of Science, Jouf University, 74631-7365 Sakaka, Saudi Arabia

[c] Physics Department, Federal University of São Carlos, São Carlos, SP, Brazil

[d] P.N.Lebedev Physical Institute, Russian Academy of Science, 119991, GSP-1, Moscow, Russia e National Research Center "Kurchatov Institute", 123182 Moscow, Russia

[f] FZEA/ZAB, University of São Paulo, Pirassununga, SP, Brazil

[g] Department of Physics, College of Science, Sultan Qaboos University, Oman

[h] Electrical Engineering Department, Federal University of São Carlos, São Carlos, SP, Brazil

[i] Department of Physics, College of Science, Qassim University, Buraydah 14452, Saudi Arabia

[j] Department of Physics, College of Science, Princess Nourah bint Abdulrahman University (PNU), Riyadh 11671, Saudi Arabia

Abstract

Current-Voltage (I-V), Capacitance-Voltage (C-V), Deep Level Transient Spectroscopy (DLTS), Laplace DLTS, Photoluminescence (PL) and Micro-Raman techniques have been employed to investigate the effect of the orientation of the substrates on the structural, electrically and optically active defects in dilute $GaAs_{(1-x)}Bi_x$ epilayers structures having a Bi composition x = ∼5.4%, grown by Molecular Beam Epitaxy (MBE) on (100) and (311)B

GaAs planes. X-ray diffraction results revealed that the in-plane strain in the Ga(As,Bi) layer of the samples grown on (100)-oriented substrate (-0.0484) is significantly larger than that of the samples grown on (311)B-oriented substrate. The substrate orientation is found to have a noticeable impact on the Bi incorporation and the electrical properties of dilute GaAsBi Schottky diodes. The I-V characteristics showed that (100) Schottky diodes exhibited a larger ideality factor and higher barrier height compared with (311)B samples. The DLTS measurements showed that the number of electrically active traps were different for the two GaAs substrate orientations. In particular, three and two electron traps are detected in samples grown on (100) and (311)B GaAs substrates, respectively, with activation energies ranging from 0.12 to 0.41 eV. Additionally, one hole trap was observed only in sample grown on (100) substrates with activation energy 0.24 eV. The observed traps with small activation energies are attributed to Bi pair defects. The photoluminescence (PL) and Raman spectra have evidenced different compressive strain which affects considerably the optical properties. Furthermore, the PL spectra were also affected by different contributions of Bi-related traps which are different for different substrate orientation in agreement with DLTS results.

1. Introduction

Dilute III-V bismide semiconductors materials such as GaAsBi alloys display strong reduction in the band gap when only a small percentage of bismuth atoms is incorporated into the lattice of the ost material like GaAs which has a band gap energy of 1.424 eV at 300 K. Particularly, a few percent of Bi incorporated into GaAs, i.e. $GaAs_{(1-x)}Bi_x$ with x being the Bi composition, leads to a giant bowing in the band gap energy (∼88 meV/%Bi) [1], as well as an increase in spin-orbit splitting energy [2,3]. These remarkable properties such as reduction of the band gap make GaAsBi a suitable material for several device applications such as multi-junction solar cells [4], photonic devices [1] and in long-wavelength optoelectronic devices [5].

It is well known that the growth temperature of III-V alloys can significantly influence their crystalline quality. In fact, substitutional incorporation of Bi into the host lattice of III-V compounds requires low temperature growth (< 400 °C). However, low growth temperature of GaAs causes an increased density of defects as well as leads to degradation of the optical quality of alloys [6]. For instance, growing GaAs at temperatures lower than the optimal growth temperatures (∼580-600 °C leads to the creation of many point defects, such as As-antisities (As_{Ga}), As-interstitials (A_{Si}) and Ga vacancies [7-9]. Additionally, it is found that as the growth temperature decreases deep level defects are generated in GaAs and their concentrations is enhanced [7,10]. Nevertheless, using Bi as a surfactant during the growth of GaAs at low temperatures has proven to enhance surface migration, to reduce the density of defects and to suppress the formation of traps in

GaAs. However, in GaAsBi epilayers where Bi is substituting an arsenic atom, Bi related defects are created. Recently, deep level transient spectroscopy (DLTS) and Laplace DLTS (LDLTS) studies of n-type $GaAs_{(1-x)}Bi_x$ layers grown by Molecular Beam Epitaxy (MBE) on n+ GaAs substrates with $0 \leq x \geq 0.012$ [11] have shown that a significant reduction of the total traps concentration by a factor of ~20, in contrast to GaAs layers grown at similar temperature (~330 $°C$). Furthermore, as anticipated for MBE growth at this temperature, the dominant deep level defect in these layers were proposed to be an As_{Ga}-related complex defect, with a deep level energy of about 0.65 eV [11]. More recently, Ł. Gelczuk et al. [7] employed DLTS to investigate the electron deep level defects in ntype $GaAs_{(1-x)}Bi_x$ alloys having $0 < x < 0.023$ grown by MBE on conventional (100) n+ GaAs substrates. They found that the incorporation of Bi into GaAs suppresses the formation of GaAs electron traps by reducing their total trap concentration to more than two order of magnitude compared to trap concentration in GaAs grown at similar conditions. Additionally, they reported that the two levels with activation energies ranging from 0.07 to 0.19 eV in GaAsBi with Bi compositions of 0.8–2.3%, are Bi- related traps. They suggested the origin of these defects to be related to Bi pair defects. [7].

Although most investigations of $GaAs_{(1-x)}Bi_x$ thin films and devices were performed using the conventional (100) GaAs substrates, there are few studies exploring the growth on high-index planes, which can considerably affect the Bi incorporation, and the structural, electrical and optical properties [12-16]. Remarkably, Henini et al. have shown that Bi incorporation in $GaAs_{(1-x)}Bi_x$ thin films can be more enhanced by using (311)B GaAs orientation [12]. In addition, there are relatively very few researches which addressed the doping process of only (100) $GaAs_{(1-x)}Bi_x$ [7,10,11,17-20]. Therefore, it isworth noting that the structural and optical properties of n-type $GaAs_{(1-x)}Bi_x$ alloys and devices using non-(100) GaAs substrates have not been investigated yet.

In this work the effects of substrate orientation on the structural, optical and the electrical properties of a n-type dilute $GaAs_{(1-x)}Bi_x$ epilayer structures grown at low temperature by MBE on conventional (100) and non-conventional (311)B n+ GaAs substrates were investigated using Current-Voltage (I-V), Capacitance-Voltage (C-V), deep level defects spectroscopy (DLTS), Laplace DLTS (LDLTS), Photoluminescence (PL) and Micro-Raman techniques.

2. Experimental details

The samples studied in this work were silicon-doped n-type $GaAs_{(1-x)}Bi_x$ epilayers grown on highly doped (100) and (311)B n+GaAs substrates by MBE at low temperature (~400 $°C$). Figure 1 shows the growth of the epitaxial layers which consisted of 0.1 μm thick GaAs buffer layer heavily doped with Si with a concentration 2×10^{18} cm^{-3}. This was followed by 1 μm thick Si doped GaAsBi layer with a Si concentration of 2×10^{16}

cm^{-3}. Additionally, similar structures (control samples) consisting of a 1 μm thick n-type GaAs layer (not containing Bi) were grown on (100) and (311)B GaAs substrates at similar conditions, for comparison purposes. Two n-type $GaAs_{(1-x)}Bi_x$ epitaxial layers with roughly 5.4% of Bi were examined (see Table 1). The compositions of the $GaAs_{(1-x)}Bi_x$ epilayer were measured by X-ray diffraction (XRD). For electrical characterization of these devices, all samples have been fabricated in form of circular mesas. Ge/Au/Ni/Au Ohmic contacts were thermally evaporated on the back side of the wafer, with thickness (10, 20, 20 and 150) nm, respectively. Then rapid thermal annealing (RTA) in an Ar atmosphere was performed at 380 $°C$ for 30 s. This was followed by Au deposition through a shadow mask to form circular mesas Schottky contacts with different diameters on the top side of the sample. PL spectra of (100) and (311)B $GaAs_{(1-x)}Bi_x$ samples were investigated as a function of laser power and temperature using a Janis closed-loop helium cryostat. The samples were excited with a 532 nm Nd:YAG solid state laser. The PL signal was collected in a 0.5 m Spex monochromator coupled with a nitrogen-cooled Ge detector. MicroRaman measurements were carried out with a 633 nm laser excitation. The Raman signal was measured in a Lab RAM HR Horiba Jobin Yvon system with 50× objective with spectral resolution of about 1 cm^{-1}.

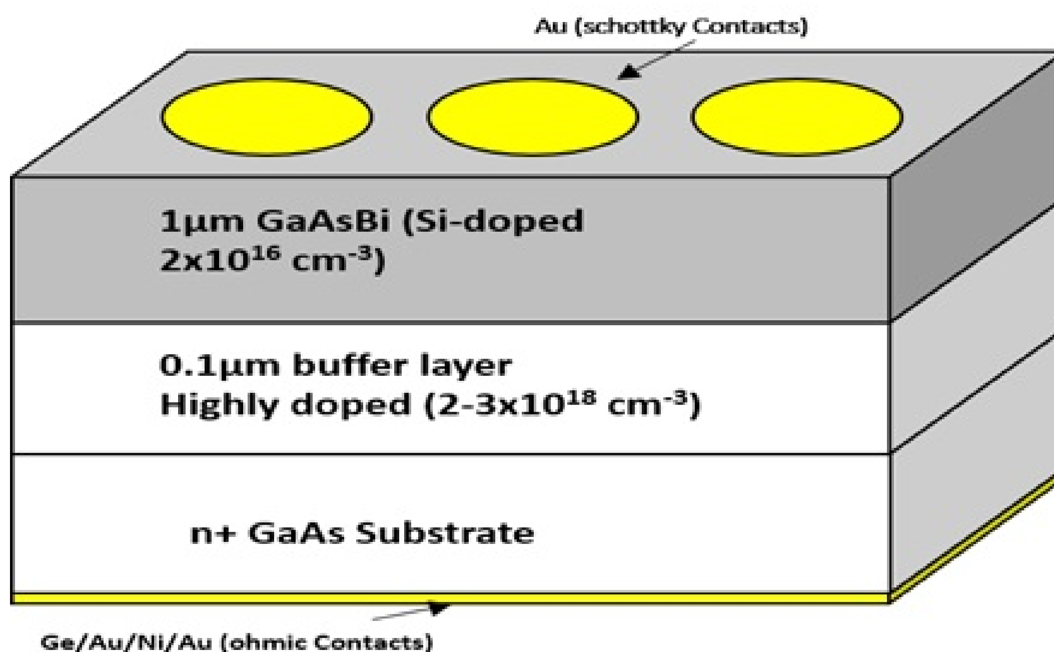

Figure 1. Schematic diagram of n-GaAsBi grown on (100) and (311)B n+ GaAs substrates.

Table 1 samples details: substrate orientation, Bi content obtained from XRD and doping concentration as determined from C-V measurements.

Sample	Substrate orientation	Bi contend (from XRD), %	Doping concentration N_d
n-GaAs	(100)	0	3.80x10^{17} cm^{-3}
n-GaAs	(311)B	0	3.40x10^{17} cm^{-3}
n-GaAs	(100)	5.4	1.03x10^{16} cm^{-3}
n-GaAs	(311)B	5.4	1.14x10^{17} cm^{-3}

3. Results and discussion

3.1. Structural characteristics

X-ray diffraction measurements were carried out on a Rigaku Smartlab laboratory diffractometer in the 2θ-ω mode using Cu-Kα1 radiation and a double-crystal Ge (220) monochromator with a horizontal slit positioned in front of the detector in order to reduce diffuse and background scattering. XRD curves were measured in θ-2θ scanning mode [21]. The X-ray spot on the sample's surface was about 5 mm $\times$ 0.4 mm. The structure parameters were determined from XRD curves using different (symmetrical and asymmetrical) experimental schemes. Typical XRD curves are shown in Figure 2 where symmetrical (311) and two asymmetrical (400) diffraction patterns are presented for the (311)B GaAsBi samples. Out-of-plane lattice parameter was obtained from the analysis of symmetrical XRD curves. For (100) GaAs and (311)B GaAs oriented surfaces, the asymmetric reflections (311) and (400) were measured, respectively. Asymmetrical reflexes were chosen based on the relative intensity (relationship between incident X-ray radiation and the reflected one). Asymmetrical reflections were measured from a set of planes with an angle less than the Bragg angle (θ_B) for these planes. The incidence angles θ_{asym} for these reflections are given by $\Theta_{asym} = \theta_B \pm \phi$, where ϕ is the angle between asymmetrical planes and surface of the sample. Knowing the out-of-plane lattice parameter and the angle between asymmetrical reflected plane and the planes parallel to the surface of the sample, the in-plane lattice parameter of epitaxial layer $a_{\|}$ can be calculated from simple geometric considerations [22].

Bi concentration was calculated from the lattice parameter of $GaAs_{(1-x)}Bi_x$ layer determined from symmetrical XRD using Vegard's law [23] with the assumption of diluted alloy of GaAs and GaBi. The drawback of such approach is that there are no reports of growth of bulk GaBi, and therefore one can only consider the theoretical calculation of GaBi lattice [24]. For the present work it was considered that GaBi has a zinc-blend cubic lattice with the lattice parameter a = 6.178 Å. It was found that Bi concentration is equal to 5.4% for both samples grown on (100) and (311)B-oriented surfaces. Residual strains (ϵ_{zz} and ϵ_{xx}) in $GaAs_{(1-x)}Bi_x$ layer were determined from the analysis of asymmetrical

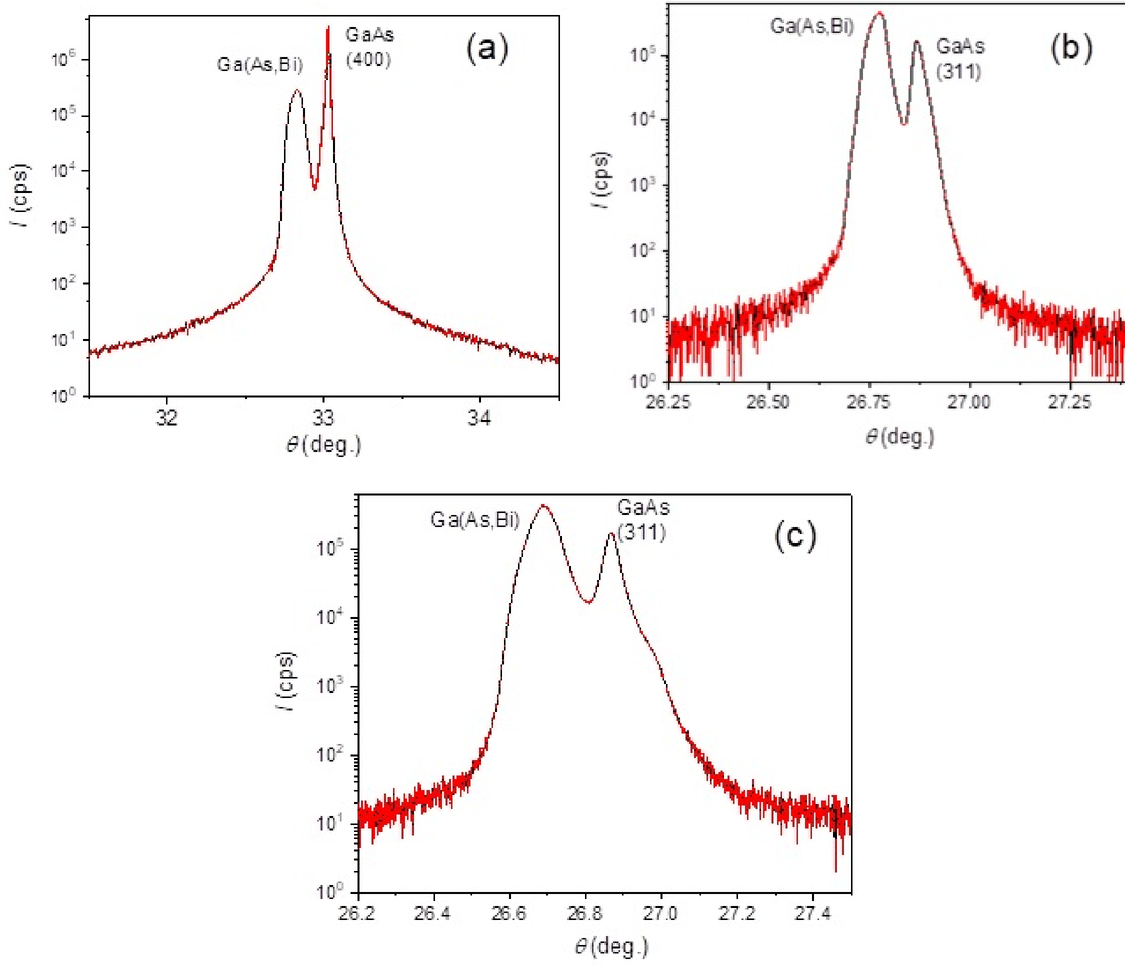

Figure 2. XRD curves of (311)B GaAsBi samples (a) symmetrical (311) diffraction pattern; (b) and (c) asymmetrical (400) diffraction patterns. Asymmetrical patterns were obtained with (b) θ_B - ϕ and (c) $\theta_B + \phi$ incidence angles, where θ_B is the Bragg angle for the given set of crystallographic planes, and ϕ is the angle between (100) planes and the (311)- oriented surface.

XRD. Out-of-plane $a_\perp$ and in-plane strain $a_\parallel$ were used to calculate the deformation of layer's lattice by using the following formulas for strains:

$$\epsilon_{zz} = \frac{a_\perp - a_{FR}}{a_{FR}} \tag{3.2}$$

$$\epsilon_{xx} = \frac{a_\parallel - a_{FR}}{a_{FR}}$$

where $a_\perp$ is the out-of-plane lattice parameter, $a_\parallel$ is the in-plane lattice parameter, and a_{FR} is lattice parameter of fully relaxed GaAs lattice. It was found that ϵ_{zz} is equal 0.00035 for both samples while ϵ_{xx} for the sample grown on (311)B-oriented surface is 2.64 times less than for (100)-oriented sample, namely -0.0484 and -0.0183 for (100) and (311)B-oriented samples, respectively.

3.2. Electrical properties

3.2.1. I- Current-voltage characteristics

In order to select suitable diodes for DLTS and LDLTS measurements for both samples, I-V characteristics were obtained at room temperature. The reverse bias current density (J) for all samples over the voltage bias range -1V to 0 is of the order of few μA/cm^2. Typical room temperature semi-logarithmic J-V characteristics are shown in Figure 3 for all samples. It can be seen from Fig. 3 that all samples display a relatively low leakage current density. In particular, the reverse current density for samples grown on (100) is larger than that grown on (311)B. The reverse current density at bias -1 V for (100) GaAs, (311)B GaAs, (100) GaAsBi and (311)B GaAsBi are 1.06 $\times$ 10^{-4} A/cm^{-2}, 8.26 $\times$ 10^{-8} A/cm^{-2}, 7.5 $\times$ 10^{-5} A/cm^{-2} and 6.2 $\times$ 10^{-6} A/cm^{-2}, respectively. The reason for the higher reverse current density in samples grown on (100) can be explained by the higher trap concentrations and more defects in (100) than (311)B [25]. Similar behaviour was observed in previous studies on n-type GaAs grown on conventional (100) and non-conventional substrate orientations (n11) [26] where the reverse current was found to decrease with increasing the index of the plane n.

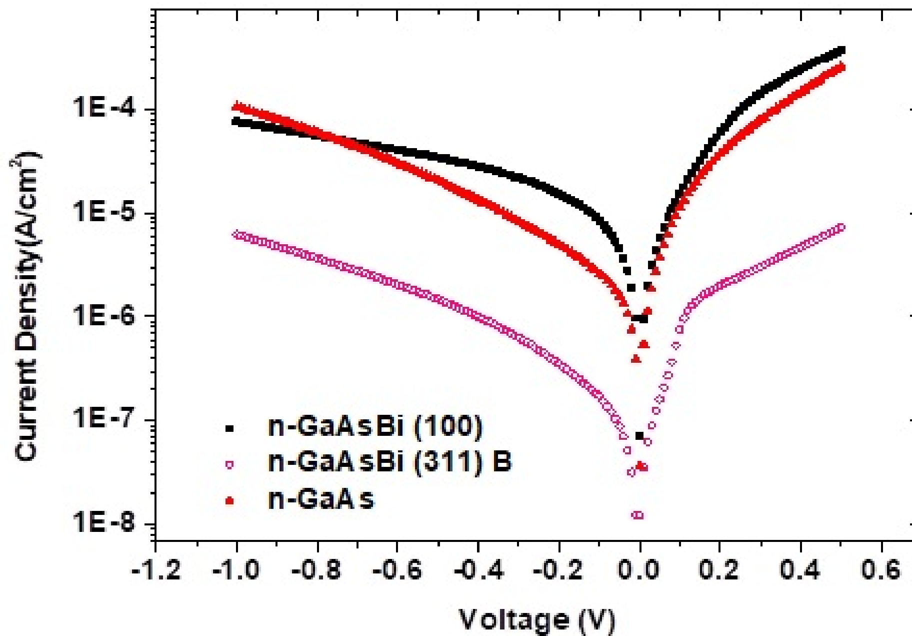

Figure 3. J-V plot for n-type (100) GaAs, (311)B GaAs, (100) GaAsBi and (311)B GaAsBi at room temperature.

Since these devices are Schottky diodes, the I-V characteristics of the diodes can be described by the thermionic emission model [27] as follows:

$$I = I_0[exp\left(\frac{q(V - IRs)}{nKT}\right) - 1] \tag{3.3}$$

where q is the electronic charge, V is the applied voltage, K is the Boltzmann's constant, n is the ideality factor of the diode, T is the absolute temperature in Kelvin, IRs is the series resistance of the effective diode, andI_0 is the saturation current which is given by:

$$I = AA^*T^2exp\left(\frac{-q\phi_b}{KT}\right) \tag{3.4}$$

where A is the diode area, A^* is the effective Richardson's constant (A^*= 8.16 Acm^{-2} K^{-2}), and b is the barrier height [28].

The characteristics parameters of these devices such as (n, R_s,b and I_0) were calculated by using the Werner's method [29].

Series resistance, ideality factors and barrier height for all the samples are obtained from the forward I-V characteristics at room temperature. These parameters are summarized in Table 2.

Table 2 Experimental data of ideality factor, barrier height and series resistance, obtained from I-V characteristics at room temperature for n-type (100) GaAs, (311)B GaAs, (100) (GaAsBi) and (311)B GaAsBi.

Sample	n	ϕ_B (eV)	kΩ
n-GaAs (100)	1.50±0.02	0.74±0.03	0.23±0.02
n-GaAs (311)B	1.49±0.02	0.69±0.02	1.32±0.03
n-GaAsBi (100)	2.33±0.01	0.67±0.01	36.30±0.01
n-GaAsBi (311)B	1.61±0.01	0.62±0.01	2.30±0.03

Figure 4 shows the temperature dependence of (a) the ideality factor (n) and (b) barrier height (B) of all samples over the temperature range 200-340 K.

As can be seen from Table 2, the ideality factor of all devices in forward bias deviates from unity, where n is nearly 2, which suggests that there is significant generation-recombination in depletion region, which is the dominant current mechanism [4,30]. It is worth noting that such deviation of the ideality factor from the thermionic emission can be attributed to several effects, such as inhomogeneity of Schottky barrier height, series resistance, interface states and nonuniformly of interfacial charges [31–33]. As shown in Figure 4(a) and (b) the values of n decrease with increasing temperature, where as the values of (ϕ_B) increase as temperature is increased. This behaviour is due to inhomogeneous metal/semiconductor (MS) contacts. At high temperatures, the current flows through the interface states in the regions with a lower barrier height and larger ideality factor, where as at low temperature the carriers are frozen, and therefore, the current does not follow the thermionic emission mechanism. Note that at low temperature, carriers can overcome the lower barriers, and the transmission mechanism will be dominated by the current flowing through the regions with the lower barrier height. As the temperature

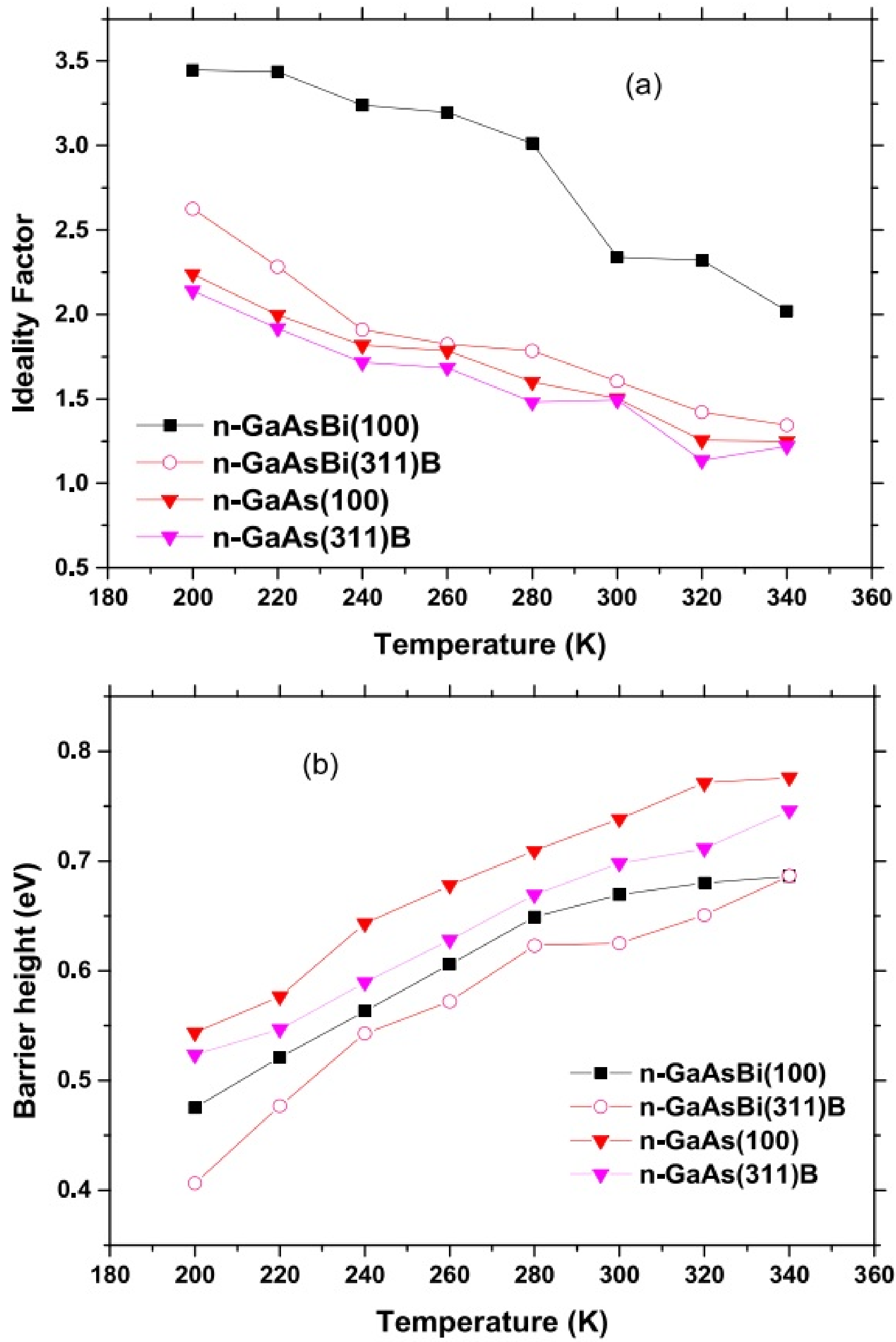

Figure 4. Temperature dependence of (a) ideality factor; (b) barrier height, obtained from I-V characterises for all n-type samples.

increases, the carriers gain enough energy to overcome the higher potential barrier, which causes the barrier height to increase with temperature. As a result, the barrier height will increase, while the ideality factor will decrease with increasing temperatures, due to barrier inhomogeneity in MS contacts [34]. However, (100) GaAsBi has larger ideality factors over all temperatures compared to other diodes, whereas the (311)B GaAs has the smallest values. It is worth noting that, and as to our knowledge, no previous reports have explained the Schottky diodes behaviour in GaAsBi grown on different substrate orientations in the literature. Therefore, the results will be discussed in context with dilute nitride GaAsN instead. Furthermore, from Table 2 it can also be seen that the barrier height at room temperature for (100) GaAsBi and (311)B GaAsBi are reduced compared with reference samples. In particular, (100) GaAs has relatively larger barrier height, while the (311)B GaAsBi diodes have the lowest values. This reduction in barrier height was observed also by Chen et al. [35] in their study using Cu Schottky contacts to n-type GaAsN grown on (100) and (311)A/B GaAs substrates grown by Chemical beam epitaxy (CBE). They found that samples grown on (311)B exhibited lower barrier height than (100). They attributed this reduction to the polarity of growth surface. On the other hand, Narayanamurti et al. [36] observed in their study using the ballistic electron emission microscopy (BEEM) technique, that the barrier height at room temperature decreases as the nitrogen content increases. They attributed the reduction in the barrier height to the reduction of the band gap, with increasing incorporation of nitrogen. It is well-known that Bi incorporation is more enhanced in (311)B than in (100) GaAs substrates. This results in an enhancement of the reduction of the energy band gap of (311)B with respect to the (100) samples, as reported previously [12,37]. This fact could explain the larger reduction of the barrier height observed in the (311)B samples.

3.2.2. II-Capacitance-voltage characteristics

The capacitance-voltage (C-V) measurements were carried out at room temperature with a frequency of 1 MHz in order to determine the free carrier concentration (N_d). Figure. 5(a) shows the experimental net carrier concentration N_d obtained from the slope of $1/C^2$ as a function of V (reverse voltage) for all samples. The free carrier concentration was found to be homogeneous for all samples. In particular, the free carrier concentrations of (100) GaAs, (311)B GaAs, (100) GaAsBi and (311)B GaAsBi, are $\sim 3.8 \times 10^{17}$ cm^{-3}, 3.4×10^{17} cm^{-3}, $\sim 1.03 \times 10^{16}$ cm^{-3} and $\sim 1.14 \times 10^{16}$ cm^{-3}, respectively. Figure. 5(b) shows Capacitance/Area (C/A) versus V plot for (100) and (311)B GaAsBi samples. As can be seen from Figure. 5(b), the value of the C/A of sample grown on (311)B has lower C/A than the one grown on (100). This reduction of C/A of (311)B sample could possibly be due to the growth orientation, which was found to affect the shallow donor concentration N_d, as confirmed previously by Hall measurement [35,38,39].

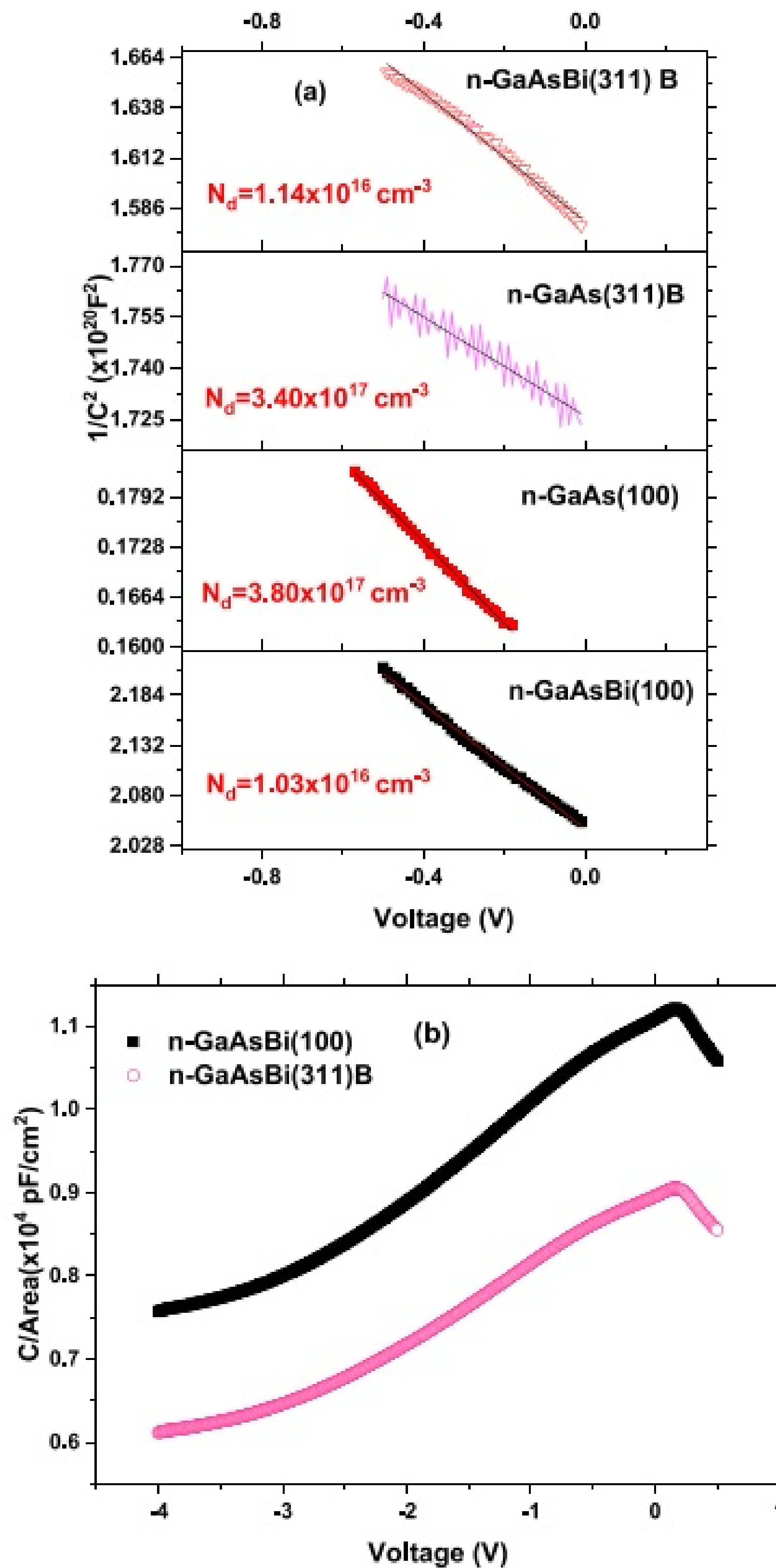

Figure 5. (a) Plot of $1/C^2$ versus reverse bias voltage for n-type (100) GaAs, (311)B GaAs, (100) GaAsBi and (311)B GaAsBi at room temperature. (b) The experimental C/Aversus V plot for (100) and (311)B GaAsBi samples at room temperature.

3.2.3. III- DLTS and Laplace (DLTS) measurements

In order to study the electrically active defects with energies within the forbidden band gap of these n-type (100) GaAs, (311)B GaAs, (100) GaAsBi and (311)B GaAsBi devices, DLTS technique has been employed [40]. As can be seen in Figure 6, the measurements were carried out over a temperature range from 100 K up to 450 K. The experimental parameters used are: reverse bias (V_R) of -1 V, filling pulse voltage (V_p) of 0 V with filling pulse time (tp) of 1 msec and rate window set to be at 200 s^{-1} for all investigated samples.

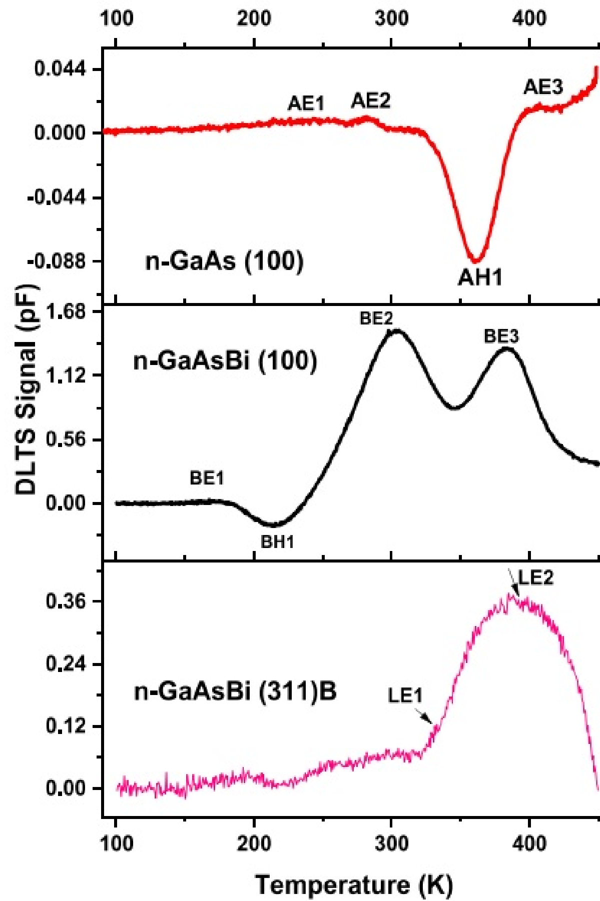

Figure 6. Typical DLTS spectra scans for n-type (100) GaAs, (100) GaAsBi and (311)B GaAsBi samples.

The standard DLTS spectra in Figure 6 of (100) GaAs and (100) GaAsBi samples show three positive peaks corresponding to three majority electron traps. In addition to the electron traps, a hole traps (negative peaks) were also observed in (100) GaAsBi and (100) GaAs, respectively. While for GaAsBi sample grown on (311)B (Figure 6), a very broad peak is detected over the temperature range ∼ 325 K to ∼450 K. For control sample (311)B GaAs no defects were detected by DLTS as their concentrations could be too low and are outside the detection limit of DLTS. In order to resolve the broad peaks obtained by DLTS measurements, as well for a better resolution of DLTS spectra observed in the investigated samples, Laplace DLTS (LDLTS) measurements were performed [41]

on all samples, under same conditions as those used in DLTS experiments. Laplace DLTS revealed the presence of the following traps: (i) (100) GaAs and (100) GaAsBi: three electron traps labelled as (AE1, AE2 and AE3) and (BE1, BE2 and BE3), one hole trap (AH1) and (BH1), respectively; (ii) (311)B GaAsBi: two electron traps namely (LE1 and LE2). The activation energies of each defect were determined from the Arrhenius plot of the emission rates as a function of inverse temperature as illustrated in Figures 7.

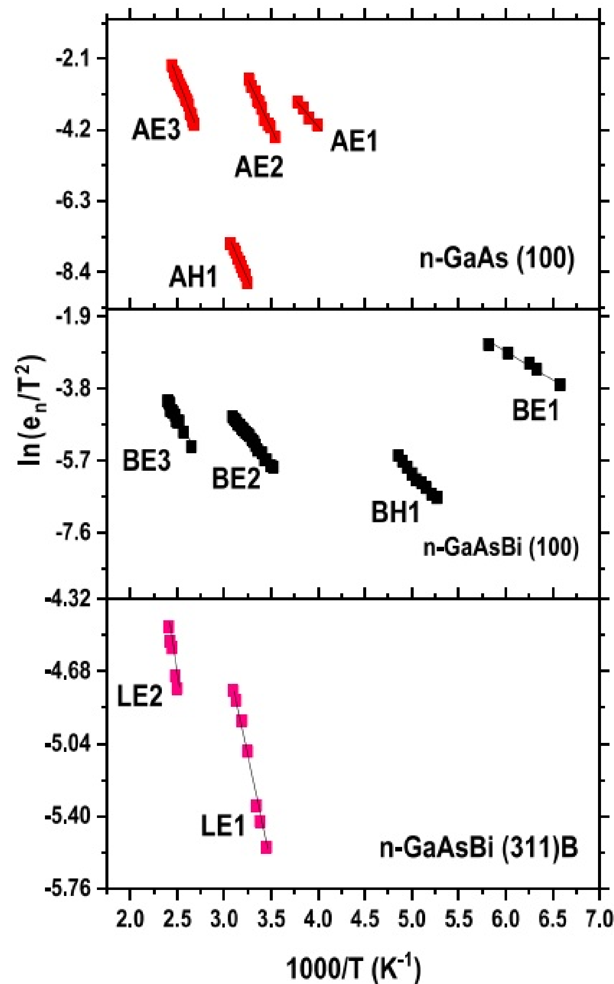

Figure 7. Arrhenius plots obtained from Laplace DLTS for n-GaAsBi grown oncrosssection (a) (100) and, (b) (311)B GaAs substrate, with reverse voltage V_R = -1, filling pulse height V_p= 0 V, and filling pulse time t_p = 1 msec.

The traps activation energies, apparent cross section and trap concentrations are calculated from the slope and intercept of the Arrhenius plot. The traps parameters are summarized in Table 3.

It can be seen from Table 3, that the number of traps detected in sample grown on (100) are higher than sample grown on (311)B. In fact, R. Mari [26] observed that the substrate orientations of GaAs have a significant impact on the incorporation of impurities and traps into the structure. It was reported that impurities are more susceptible to be incorporated in (100) plane than in other high index planes. This result correlated with

Table 3. Traps parameters for n-(100) GaAs and n- (100) GaAsBi and (311)B GaAsBi.

Sample	Trap Label	Activation energy (eV)	Apparent capture crosssection (cm^2)	Trap concentration (cm^3)
n-GaAs (100)	AE1	0.28 ± 0.03	4.3×10^{-17}	8.2×10^{15}
	AE2	0.54 ± 0.02	2.1×10^{-13}	7.2×10^{15}
	AH1	0.53 ± 0.02	4.8×10^{-16}	8.1×10^{15}
	AE3	0.61 ± 0.01	1.8×10^{-14}	5.1×10^{15}
n-GaAsBi (100)	BE1	0.12 ± 0.01	1.1×10^{-18}	1.2×10^{13}
	BH1	0.24 ± 0.01	9.8×10^{-18}	5.1×10^{13}
	BE2	0.27 ± 0.01	9.3×10^{-19}	7.7×10^{14}
	BE3	0.41 ± 0.04	6.3×10^{-18}	9.7×10^{14}
n-GaAsBi (311)B	LE1	0.19 ± 0.01	5.1×10^{-20}	1.4×10^{13}
	LE1	0.29 ± 0.01	1.8×10^{-19}	1.9×10^{14}

I-V characterization discussed above, where sample grown on (100) has higher reverse current than sample grown on (311)B due to higher number of traps.

It can be seen from Table 3, that the number of traps detected in sample grown on (100) are higher than sample grown on (311)B. In fact, R. Mari [26] observed that the substrate orientations of GaAs have a significant impact on the incorporation of impurities and traps into the structure. It was reported that impurities are more susceptible to be incorporated in (100) plane than in other high index planes. This result correlated with I-V characterization discussed above, where sample grown on (100) has higher reverse current than sample grown on (311)B due to higher number of traps.

The best way to identify these active traps created as a result of substrate orientations are to compare their activation energies to each other and/or their DLTS signals. The obtained results are also discussed and compared with previous works.

The traps BE1 (0.12 ± 0.01 eV) and LE1 (0.19 ± 0.01) observed in (100) GaAsBi and (311)B GaAsBi, respectively, are likely to correspond to the same traps ET_0 and ET_1 with activation energies ranging from 0.07 to 0.19 eV [7] and A with activation energy of 0.12 eV [11] reported previously. These were assigned to traps involving Bi as a constituent.

Traps AE1, BE2, and LE2 with similar activation energies in the range 0.27-0.29 eV could be of the same origin. This trap, labelled as ET_2 with an activation energy in the range 0.29-0.33 eV, was observed also in both GaAs and GaAsBi grown by MBE at low temperature by Gelczuk et al. [7]. This deep level can be attributed to the well-known M3 trap (E_c-0.34 eV) [42,43], which has same signature as EL6 trap reported in ref.[43]. The EL6 trap is generally related to complex pair defects involving arsenic antisite (As_{Ga}) and arsenic vacancy (V_{As}) [43] or to divacancy complex defect (V_{Ga} - V_{As}) [44]. On the other hand, using theoretical calculations by density functional theory (DFT method) [45] a trap with energy of 0.36 eV (similar to BE2) was found. The authors attributed its origin to a complex defect involving Bi.

Furthermore, the traps AE2 and BE3 with activation energies 0.54 ± 0.02 eV and 0.41 ± 0.04 eV and trap concentrations of 7.2 × 10^{15} cm^{-3} and 9.7 × 10^{14} cm^{-3}, were observed only in n-type (100) GaAs and GaAsBi samples, respectively. Similar deep defect was detected in n-type GaAsBi samples grown at temperatures 330 °C and 390 °C, respectively, labelled as trap C [11] and trap ET_3 [7] with activation energies varying in the range from 0.45 to 0.52 eV [7]. This trap most likely correspond to the trap level M4. The origin of this trap was attributed to an arsenic vacancy (V_{As}) complex involving an impurity [46].

In addition, the trap level AE3 with activation energy of 0.61 ± 0.01 eV and concentration 5.1 × 10^{15} cm^{-3} was detected only in the n-(100) GaAs control sample (without Bi). This trap was observed also in GaAs and GaAsBi as the dominant electron trap [7]. It was suggested that the origin of this deep level trap could possibly be attributed to trap M6, whose activation energy is (0.62 eV) [47]. It is interesting to note that M6 trap is a unique trap in GaAs layers grown by MBE [42]. The origin of this trap might be related to gallium and arsenic vacancies (V_{As}-V_{Ga}) or impurity related complexes (V_{As}-X-V_{Ga}), where X refers to the impurity or interstitial [47].

As seen in Table 3, hole traps were also observed in (100) GaAs and (100) GaAsBi labelled as (AH1) and (BH1), with activation energies (0.53 ± 0.02) eV, (0.24 ± 0.01) eV, respectively. Minority hole trap AH1 appears to have a similar activation energy as that of trap AH2 [48], and the trap with activation 0.54 ± 0.02 eV observed in ref. [49]. This trap was suggested to be likely attributed to donor level of the arsenic antisite As_{Ga} complexes defect [48]. Trap BH1 has similar DLTS spectra as those observed in p-type GaAsBi grown by MBE [50] and labelled as HT2 and HT3 with activation energies over a range (0.23-0.43 eV). These traps were assigned to AsGa or its relevant cluster.

3.3. Optical properties

3.3.1. IV- Raman spectroscopy

Figure. 8 shows the Raman spectra for all samples, i.e., (100) GaAs and (311)B GaAs (control samples) and (100) GaAsBi and (311)B GaAsBi, in the ranges (i) 150-245 cm^{-1} and (ii) 250-300 cm^{-1}.

Two intense peaks in the range of 260-300 cm^{-1} were observed in all samples. These Raman peaks are associated with the GaAs optical phonons at the Brillouin zone centre [51,52]. Particularly, the transverse optical mode (TO(Γ)) is observed at around 267 cm^{-1} and the longitudinal optical mode (LO(Γ)) at around 291 cm^{-1}. Furthermore, the GaAs TO (Γ) Raman peak is forbidden by Raman selection rules for the (100) samples, while for the (311)B samples this peak is allowed [53,54]. A broad TO (Γ) Raman peak was observed for the (100) GaAsBi sample, which can be explained by a breakdown of Raman

selection rules due to Bi-induced disorder.

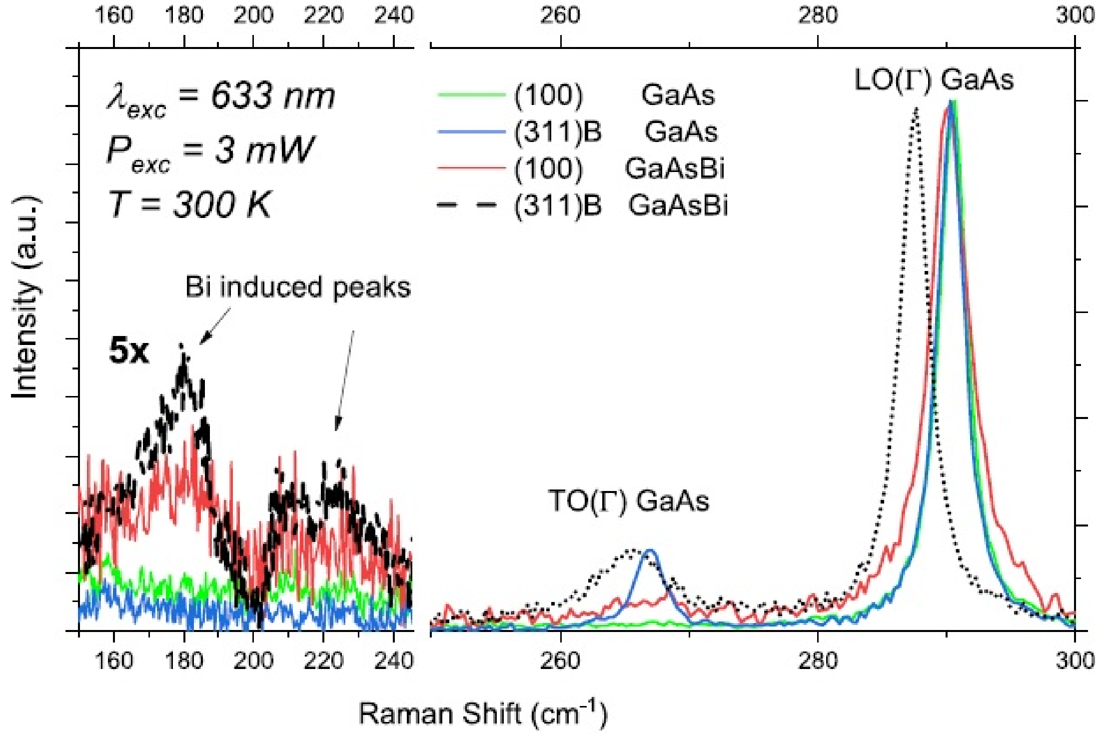

Figure 8. Raman spectra of GaAs and GaAsBi samples grown on GaAs (100) and GaAs (311)B substrates at 300 K.

For the GaAsBi samples, additional Raman peaks were detected in the range 150-240 cm^{-1}. The observation of these peaks was reported previously for GaAsBi samples [54-60]. Although the nature of the peaks is not well established, it is well known that these peaks are Bi-induced.

Our Raman spectra in the range 250-300 cm^{-1} were well fitted by two Lorentz functions (the fitting parameters are shown in Table 4). Although these samples are doped, we have observed no evidence of the presence of the peak due to plasmons-phonons coupling (LOCP). In general, our results show that the contribution of the LOCP is probably small and that this peak is not well resolved from GaAs LO (Γ) and TO (Γ) Raman modes. In addition, a red-shift of the LO (Γ) Raman peak for GaAsBi samples was observed as compared to the reference GaAs samples. It is expected that the incorporation of bismuth atoms will result in significant changes of the mechanical properties of $GaAs_{(1-x)}Bi_x$ alloys. Particularly, the Bi incorporation will change the frequency of phonon vibration modes of the crystalline matrix. It was previously observed that the GaAs LO(Γ) position changes linearly with the Bi concentration (x) [54,61]. On the other hand, the phonon frequencies can also be dependent on the presence of strain in the alloys [54,61]. Such stress-induced shifts can basically be described by the phonon deformation potentials (PDPs). Therefore, the total frequency shift could be associated with two different contributions: (i) the changes in the alloying composition (x) of the ternary material ($\Delta\omega_{alloy}$) and (ii) changes

of the strain field in the alloy ($\Delta\omega_{strain}$). The total shift of the optical phonon modes can then be quantitatively expressed as $\Delta\omega = \Delta\omega_{strain} + \Delta\omega_{alloy}$ [54,61]. As the Bi content is 5.4% for both (100) and (311)B samples, the different shifts observed for the Raman modes must be due to the strain effect. Particularly for the (311)B sample, the observed shift is - 60 cm^{-1}/xBi which is consistent with previous works [16,55,56,60,61]. On the other hand, for the (100) GaAsBi sample a lower shift was observed probably due to a blue-shift originated by compressive strain (-$\Delta\omega_{strain}$), in agreement with the shift reported by E. Tisbi et al. [55]. Furthermore, the HRXRD results have shown that the strain for the (100) GaAsBi sample is 2.7 times higher than that of (311)B sample. In addition, a broadening of the LO (Γ) Raman peak was observed for the GaAsBi samples, a disordering effect for these samples which is particularly higher in the (100) GaAsBi sample. Similar broadening was also observed for the TO (Γ) Raman mode, but more important the observation of this peak in (100) GaAsBi sample is probably due to Bi induced disorder. A smaller red-shift of the TO (Γ) Raman peak was observed as compared to the red-shift observed for the LO (Γ) Raman peak for GaAsBi samples, which were similarly reported previously in the literature. In general, our results indicate that the introduction of Bi in the (100) samples results in a higher compressive strain and higher crystal disorder as compared to the GaAsBi (311)B samples. These differences have an important impact on the optical emission of these samples as will be discussed below.

Table 4. Lorentzian fitting parameters.

	(100) GaAs	(100) GaAsBi	(311)B GaAs	(311)B GaAsBi
LO(Γ)				
ω_{peak} cm^{-1}	290.5±0.5†	290.2±0.5†	290.3±0.5†	287.5±0.5†
FWHM $-\Delta\omega(cm^{-1})$	2.6±0.5†	3.7±0.5†	2.5±0.5†	2.8±0.5†
Peak relative intensity TO(Γ)	1.00±0.01	0.98±0.01	1.00±0.01	0.97±0.01
ω_{peak} cm^{-1}	262.4±0.5†	266.7±0.5†	266.9±0.5†	265.5±0.5†
FWHM $-\Delta\omega(cm^{-1})$	22.9±0.5†	10.6±0.5†	2.7±0.5†	6.7±0.5†
Peak relative intensity	0.007*±0.01	0.04±0.01	0.16±0.01	0.13±0.01
Reduced chi-square	2.59 10^{-5}	1.77 10^{-4}	3.26 10^{-5}	9.14 10^{-5}
Residual Sum of Squares	0.00411	0.02807	0.00518	0.01453
R-Square	0.9992	0.9957	0.9990	0.9971

* Less than the noise level ≈ 0.01.
† The experimental error is bigger than the statistic error related to the fit processes. In these cases, we utilize the experimental error.

3.3.2. V- Photoluminescence

Figure 9 shows the photoluminescence spectra of GaAs (100), GaAs (311) B, GaAsBi (100) and GaAsBi (311)B layers. A sharp emission is clearly seen at around 1.52 eV for both GaAs layers as expected. In addition, other PL peaks were also observed: one

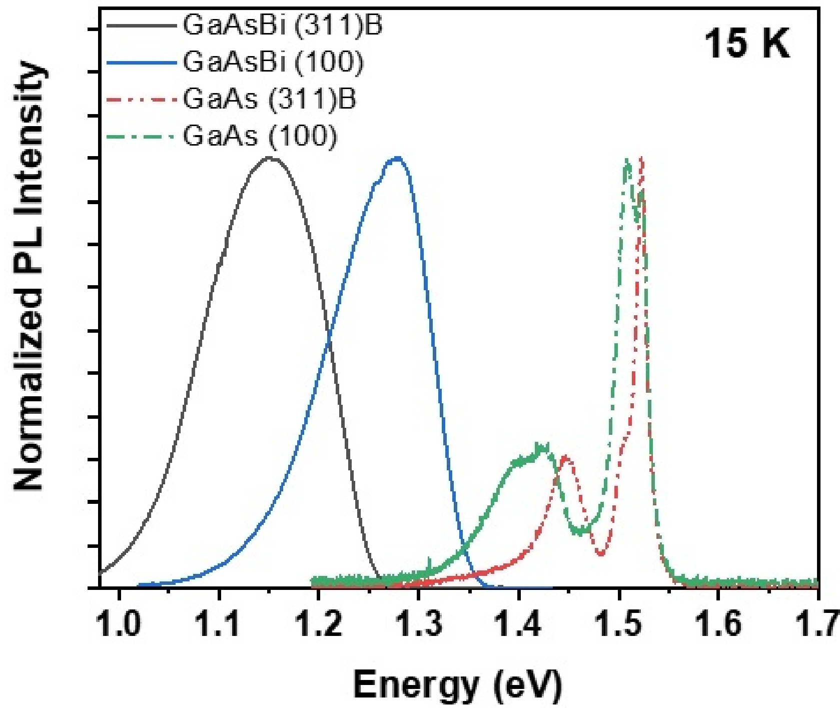

Figure 9. Normalized PL spectra of GaAs and GaAsBi layers at 15 K.

around 1.508 eV and a broad band in the range of 1.3-0.49 eV which were mainly associated to transitions related to GaAs-like traps/impurities due to the growth conditions. On the other hand, the PL spectra of both (100) and (311)B $GaAs_{0.94}Bi_{0.05}$ layers show a redshift as compared to GaAs samples, as expected [62-64]. The observed redshift of PL peak position was associated with Bi incorporation which induces a band gap reduction. Although both samples have the same Bi concentration, we have observed that the PL peak position of both samples are different and do not show the standard red shift of 89 meV/Bi% previously reported in the literature for GaAsBi layers [1,62,64]. Actually, for our samples this red shift is lower than previously reported. This effect is particularly more important for the (100) GaAsBi sample. It was previously shown a similar behavior for n-doped (100) GaAsBi samples [7] which was associated with the contribution of Bi induced donor traps next to the conduction band which could also induce an additional emission in the spectrum due to a donor traps (DT)-valence band (VB) transition and therefore could result in a reduced red shift. Particularly, our results show that the PL red shift of (100) GaAsBi layer is much lower than for (311)B GaAsBi sample although both samples have the same Bi concentration of 5.4%. The obtained values of PL peak position for the (100) and (311)B samples are different and could be due to the other contributions such as different Bi induced traps in these samples. However, the XRD results for these samples show that the samples also have different strain which could affect considerably their optical properties. Particularly, we notice that the DLTS results have shown higher number of carrier traps for the (100) GaAsBi sample as compared to the (311)B GaAsBi

sample which certainly could affect significantly its optical properties. However, the XRD results have also shown that the compressive strain for the (100) sample is 2.7 times higher than for the (311) B sample. An increase of compressive strain will certainly result in important changes in the band structure resulting in blue shift of PL peak position as shown previously [55].

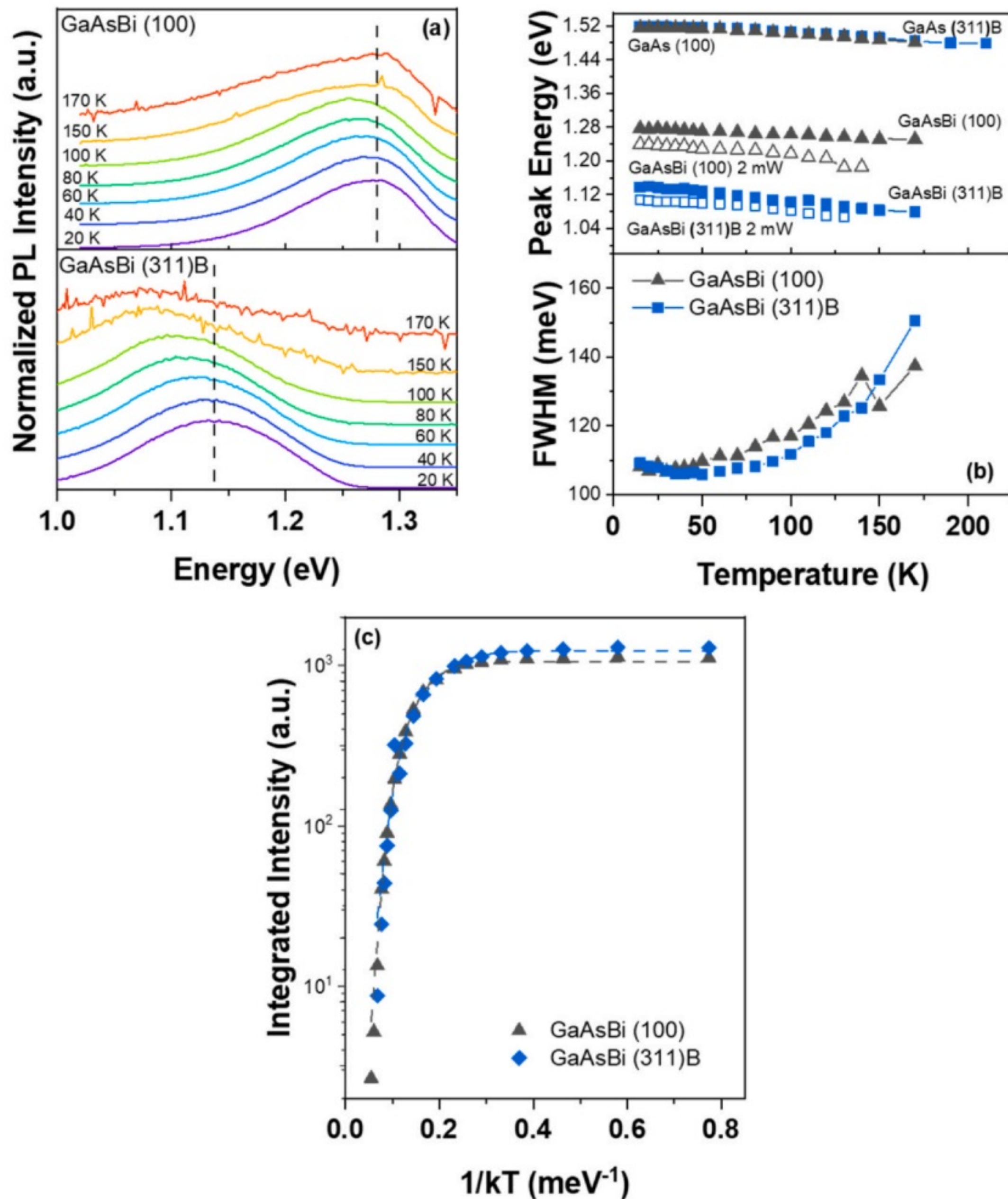

Figure 10. Temperature dependence of (a) PL spectra and of (b) PL peak position and linewidth (c) Arrhenius Plot and activation energies for (100) and (311)B GaAsBi samples.

Figure 10(a) shows the temperature dependence of the PL spectra, peak energy and FWHM of the doped $GaAs_{(1-x)}Bi_x$ samples. We observed that the PL energy peaks (Figure. 10(b)) exhibit a monotonic redshift with increasing temperature due to the decrease of

the band-gap energy with increasing temperature as expected. We have analyzed the temperature dependence of PL intensity with a modified Arrhenius equation [15]:

$$\frac{I_{PL}(T)}{I_0} = \frac{1}{1 + A_1 e^{\frac{-E_1}{\kappa_B T}} + A_2 e^{\frac{-E_2}{\kappa_B T}}} \tag{3.5}$$

where I_{PL} is the integrated PL intensity, A_1 and A_2 are constants related to the density of non-radiative recombination centers, E_1 and E_2 are activation energies, k_B is the Boltzmann constant, T the temperature and I_0 the approximate PL intensity when T→0. Figure. 10(c) shows the obtained results of Arrhenius fitting and the activation energy values for both GaAsBi (100) and (311)B samples. The obtained E_1 and E_2 values for (100) and (311)B samples are 20±3 meV and 95±4 meV, and 28±3 mV and 74±3 meV, respectively. These values evidence the presence of Bi clusters and alloy disorder in both samples. Actually, it was previously reported that the $GaAs_{(1-x)}Bi_x$ layers usually have localized Bi pairs and clusters, which have diferent configurations and binding energies, and also alloy disorder, and potential fluctuation [15]. Particularly, it was previously reported that the presence of defects/disorder results in two different activation energies: one in the range of 8-17 meV which is usually related to Bi clusters and Bi pairs and another around 50 meV which is usually related to GaAsBi alloy disorder [15,65]. Therefore our experimental values are fully consistent to this interpretation.

The laser power dependence of PL spectra for both samples was also investigated. Figure 11 (a), (b) and (c) shows the PL spectra versus laser power, the laser power dependence of PL peak position, and integrated PL, respectively at 10 K. We observed that there is a clear blue shift of PL peak energy with increasing laser power. However, this effect seems to be different for (311)B and (100) GaAsBi samples. Particularly, for the (100) samples we have observed a blue shift of about 25 meV with increasing laser power, while for the (311)B sample we have observed a blue shift of about 43 meV for a laser power of 50 mW (Figure 11(a) and (b)). Figure 11(c) shows the laser power dependence of integrated PL intensity also at 10 K. The laser power dependence was fitted by using the power law which is a standard procedure to investigate the nature of the PL band in semiconductor materials and is given by the following expression: $I = \alpha\ (P)^k$, where I is the integrated PL intensity, P is the laser power, α and k are fitting parameters [15,62]. It is well known for free exciton emission it is expected to obtain $k \approx 1$ [15,62]. However, for our samples we have obtained a value slightly lower than $k = 1$, i.e., $k \approx 0.8$ for the higher laser power range of 1-50 mW. Our results indicate some exciton localization which is similar to several previous results reported in the literature for GaAsBi layers [15,62,65]. Therefore, we have sociated our results with the emission of localized excitons by the presence of Bi clusters/ alloy disorder, which manifests in a clear blue shift of the PL peak with increasing laser power and is sistent with the obtained values for E_1 and E_2 activation energies [15,62,65]. We also remark that the DLTS results for the (100) sample have shown

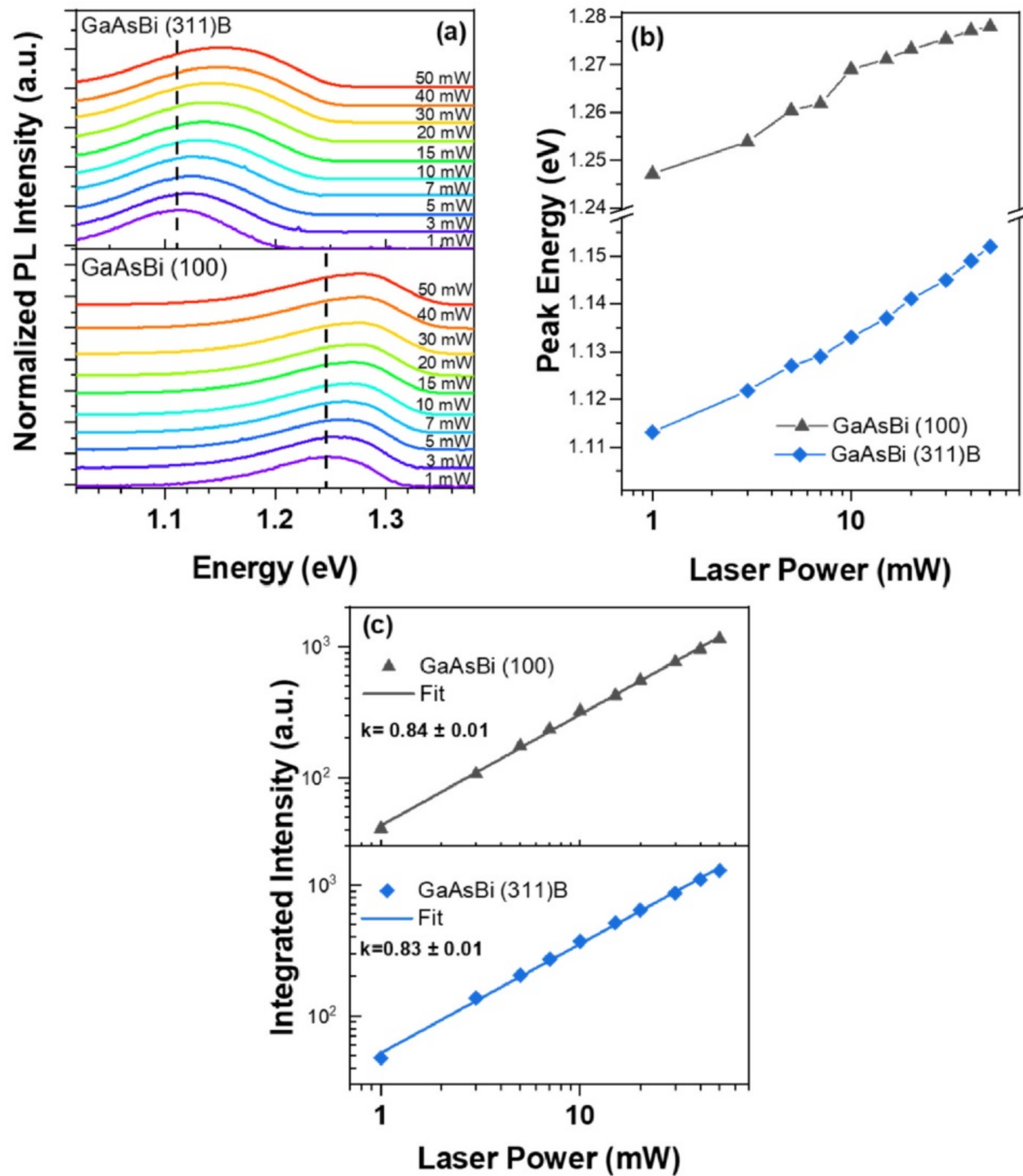

Figure 11. (a) PL spectra for different laser power (b) PL peak position and (c) Double logarithmic plot of the integrated intensity as function of laser power for GaAsBi (100) and (311) B samples at 10 K.

a larger number of traps as compared to the (311)B sample. As mention above, it was previously reported for n-doped (100) GaAsBi sample that the PL spectra have also a contribution of optical transition related to Bi induced traps close to the conduction band (donor band) which could also affect the laser power dependence and the PL peak position [7]. Therefore, our PL results are consistent with the DLTS results of these samples that have shown that the number of Bi induced traps are more important for (100) GaAsBi samples and therefore these traps affect more the PL of (100) samples as compared with the (311)B sample. On the other hand, as mentioned previously the higher compressive strain observed for (100) GaAsBi sample could also affect its optical properties resulting in the observation of PL peak position at higher energy as compared to GaAsBi (311)B sample with the same amount of Bi%.

Conclusion

We have investigated structural, electrical and optical properties of n-type GaBiAs layers grown under similar conditions on GaAs (100) and (311)B planes. It was found that although these samples have the same Bi concentration of 5.4%, they have shown different compressive strain which has important impact on their optical properties. Furthermore, it was observed that the introduction of Bi reduces the GaAs like electron traps but also induces Bi-related donor traps which are different for GaAsBi samples grown on (100) and (311)B planes. Particularly, the DLTS results have shown that Bi traps are reduced considerably for (311)B samples. Finally, the observed differences in the optical properties of (100) and (311)B GaAsBi samples can be explained by the presence of different compressive strain and by the presence of Bi-induced traps which affect considerably the optical properties of GaAsBi layers.

Reference

[1] S. Francoeur, M.J. Seong, A. Mascarenhas, S. Tixier, M. Adamcyk, T. Tiedje, Band gap of GaAs1-xBix, 0 < x < 3.6%, Appl. Phys. Lett. 82 (2003) 3874.

[2] B. Fluegel, S. Francoeur, A. Mascarenhas, S. Tixier, E.C. Young, T. Tiedje, Giant spin-orbit bowing in GaAs1-xBix, Phys. Rev. Lett. 97 (2006) 067205.

[3] Z. Batool, K. Hild, T.J.C. Hosea, X. Lu, T. Tiedje, S.J. Sweeney, The electronic band structure of GaBiAs/GaAs layers: influence of strain and band anti-crossing, J. Appl. Phys. 111 (2012) 11310.

[4] Z. Zhou, D.F. Mendes, R.D. Richards, F. Bastiman, J.P. David, Absorption properties of GaAsBi based p–i–n heterojunction diodes, Semicond. Sci. Technol. 30 (2015) 094004.

[5] V. Pačebutas, K. Bertulis, G. Aleksejenko, A. Krotkus, Molecular-beam-epitaxy grown GaBiAs for terahertz optoelectronic applications, J. Mater. Sci. Mater. Electron. 20 (2009)

363.

[6] X. Lu, D.A. Beaton, R.B. Lewis, T. Tiedje, M.B. Whitwick, Effect of molecular beam epitaxy growth conditions on the Bi content of GaAs1-xBix, Appl. Phys. Lett. 92 (2008) 192110.

[7] Ł, J. Gelczuk, T.B.O. Kopaczek, R.D. Rockett, R. Richards, R. Kudrawiec, Deep-level defects in n-type GaAsBi alloys grown by molecular beam epitaxy at low temperature and their influence on optical properties, Sci. Rep. 7 (2017) 12824.

[8] A.R. Mohmad, F. Bastiman, C.J. Hunter, J.S. Ng, S.J. Sweeney, J.P.R. David, The effect of Bi composition to the optical quality of GaAs1-x Bix, Appl. Phys. Lett. 99 (2011) 042107.

[9] J. Gebauer, R. Krause-Rehberg, S. Eichler, M. Luysberg, H. Sohn, E.R. Weber, Ga vacancies in low-temperature-grown GaAs identified by slow positrons, Appl. Phys. Lett. 71 (1997) 638.

[10] P.M. Mooney, M.C. Tarun, V. Bahrami-Yekta, T. Tiedje, R.B. Lewis, M. Masnadi- Shirazi, Defect energy levels in p-type GaAsBi and GaAs grown by MBE at low temperatures, Semicond. Sci. Technol. 31 (2016) 065007.

[11] P.M. Mooney, K.P. Watkins, Z. Jiang, A.F. Basile, R.B. Lewis, V. Bahrami-Yekta, M. Masnadi-Shirazi, D.A. Beaton, T. Tiedje, Deep level defects in n-type GaAsBi and GaAs grown at low temperatures, J. Appl. Phys. 113 (2013) 13370.

[12] M. Henini, J. Ibáñez, M. Schmidbauer, M. Shafi, S.V. Novikov, L. Turyanska, S.I. Molina, D.L. Sales, M.F. Chisholm, J. Misiewicz, Molecular beam epitaxy of GaBiAs on (311) B GaAs substrates, Appl. Phys. Lett. 91 (2007) 350.

[13] J.F. Rodrigo, D.L. Sales, M. Shafi, M. Henini, L. Turyanska, S. Novikov, S.I. Molina, Effect of annealing on the structural and optical properties of (3 1 1)B GaAsBi layers, Appl. Surf. Sci. 256 (2010) 5688.

[14] P.K. Patil, F. Ishikawa, S. Shimomura, GaAsBi/GaAs MQWs MBE growth on (411) GaAs substrate, Superlattices Micro 100 (2016) 1205.

[15] G.A. Prando, V. Orsi Gordo, J. Puustinen, J. Hilska, H.M. Alghamdi, G. Som, M. Gunes, M. Akyol, S. Souto, A.D. Rodrigues, H.V.A. Galeti, M. Henini, Y.G. Gobato, M. Guina, Exciton localization and structural disorder of GaAs1- xBix/GaAs quantum wells grown by molecular beam epitaxy on (311)B GaAs substrates, Semicond. Sci. Technol. 33 (2018) 084002. [16] J.A. Steele, R.A. Lewis, M. Henini, O.M. Lemine, A. Alkaoud, Raman scattering studies of strain effects in (100) and (311)B GaAs 1-xBix epitaxial layers, J. Appl. Phys. 114 (2013) 193516.

[17] R.N. Kini, L. Bhusal, A.J. Ptak, R. France, A. Mascarenhas, Electron Hall mobility in GaAsBi, J. Appl. Phys. 106 (2009) 04370.

[18] R.L. Field, J. Occena, T. Jen, D. Del Gaudio, B. Yarlagadda, C. Kurdak, R.S. Goldman, Influence of surface reconstruction on dopant incorporation and transport properties of GaAs(Bi) alloys, Appl. Phys. Lett. 109 (2016) 252105.

[19] M. Yoshimoto, M. Itoh, Y. Tominaga, K. Oe, Quantitative estimation of density of Bi-induced localized states in GaAs1-xBix grown by molecular beam epitaxy, J. Cryst. Growth 378 (2013) 73.

[20] M.A. Stevens, S. Lenney, J. McElearney, K.A. Grossklaus, T.E. Vandervelde, Characterization of tellurium and silicon as n-type dopants for GaAsBi, Semicond. Sci. Technol. 35 (2020) 105006.

[21] B.A. Aronzon, M.V. Kovalchuk, E.M. Pashaev, M.A. Chuev, V.V. Kvardakov, I.A. Subbotin, V.V. Rylkov, M.A. Pankov, I.A. Likhachev, B.N. Zvonkov, Y.A. Danilov, O.V. Vihrova, A.V. Lashkul, R. Laiho, Structural and transport properties of GaAs/δ-Mn/GaAs/In xGa_{1-x}As/GaAs quantum wells, J. Phys. Condens. Matter 20 (2008) 145207.

[22] D.K. Bowen, B.K. Tanner, High Resolution X-Ray Diffractometry And Topography, CRC Press, 2005.

[23] L. Vegard, Die Konstitution Der Mischkristalle Und Die Raumfüllung Der Atome, Z. Für Phys. 5 (1921) 17.

[24] M. Ferhat, A. Zaoui, Structural and electronic properties of III-V bismuth compounds, Phys. Rev. B. 73 (2006) 115107.

[25] R.H. Mari, M. Shafi, M. Henini, D. Taylor, Laplace DLTS of molecular beam epitaxy GaAs grown on (100) and (211)B substrates, Phys. Status Solidi 12 (2009) 2873.

[26] R.H. Mary, Electrical characterisation of defects in III-V compound semiconductors by DLTS, 2011.

[27] S.M. Sze, K.K. Ng, Physics of Semiconductor Devices, John Wiley & Sons, 2006.

[28] M. Biber, C. Coşkun, A. Türüt, Current-voltage-temperature analysis of inhomogeneous Au/n-GaAs Schottky contacts, Eur. Phys. J. Appl. Phys. 31 (2005) 79–86.

[29]J.H. Werner, Schottky barrier and pn-junctionI/V plots-Small signal evaluation, Appl. Phys. A. 47 (1988) 291.

[30] C.J. Hunter, F. Bastiman, A.R. Mohmad, R. Richards, J.S. Ng, S.J. Sweeney, J.P.R. David, Absorption characteristics of $GaAs_{1-x}Bi_x$/GaAs Diodes in the Near- Infrared, IEEE Photonics Technol. Lett. 24 (2012) 2191.

[31] B. Şahin, H. Çetin, E. Ayyildiz, The effect of series resistance on capacitance–voltage characteristics of Schottky barrier diodes, Solid State Commun. 135 (2000) 490.

[32] E.H. Rhoderick, Metal-semiconductor contacts, IEE Proc. I-Solid-State Electron Devices 129 (1982).

[33] N. Al Saqri, J.F. Felix, M. Aziz, D. Jameel, C.I.L. de Araujo, H. Albalawi, F. Al Mashary, H. Alghamdi, D. Taylor, M. Henini, Investigation of the effects of gamma radiation on the electrical properties of dilute GaAs1-xNx layers grown by Molecular Beam Epitaxy, Curr. Appl. Phys. 15 (2015).

[34] N. Yildirim, H. Korkut, A. Türüt, Temperature-dependent Schottky barrier inhomogeneity of Ni/n-GaAs diodes, Eur. Phys. J. Appl. Phys. 45 (2009) 10302.

[35] C. Dong, X. Han, X. Gao, Y. Ohshita, M. Yamaguchi, Electrical characterization of Cu Schottky contacts to n-type GaAsN grown on (311)A/B GaAs substrates, J. Alloy. Compd. 657 (2016).

[36] V. Narayanamurti, M. Kozhevnikov, H.P. Xin, C.W. Tu, A. Mascarenhas, Y. Zhang, Nitrogen-induced evolution of GaAs 1-x N x studied by ballistic electron emission spectroscopy, Natl. Renew. Energy Lab. (NREL). (2000).

[37] R. Kudrawiec, P. Poloczek, J. Misiewicz, M. Shafi, J. Ibáñez, R.H. Mari, M. Henini, M. Schmidbauer, S.V. Novikov, L. Turyanska, S.I. Molina, D.L. Sales, M.F. Chisholm, Photomodulated transmittance of GaBiAs layers grown on (001) and (311)B GaAs substrates, Microelectron. J. 40 (2009).

[38] J.V.V.N.K. Rao, S.V. Reddy, S.S. Naik, Electrical characteristics of rapid thermal annealing effects on co-polymer of Au / P (VDC-MA)/ n-type InP Schottky structures, Int. J. Res. Stud. Sci. Eng. Technol. 3 (2016).

[39] X. Han, C. Dong, Q. Feng, Y. Ohshita, M. Yamaguchi, Growth orientation dependence of Si doping in GaAsN, J. Appl. Phys. 117 (2015) 05570.

[40] D.V. Lang, Deep-level transient spectroscopy: a new method to characterize traps in semiconductors, J. Appl. Phys. 45 (1974) 3023.

[41] L. Dobaczewski, A.R. Peaker, K. Bonde Nielsen, Laplace-transform deep-level spectroscopy: the technique and its applications to the study of point defects in semiconductors, J. Appl. Phys. 96 (2004) 4689.

[42] D.V. Lang, A.Y. Cho, A.C. Gossard, M. Ilegems, W. Wiegmann, Study of electron traps in n -GaAs grown by molecular beam epitaxy, J. Appl. Phys. 47 (1976) 2558.

[43] K. Yokota, H. Kuchii, K. Nakamura, M. Sakaguchi, H. Takano, Y. Ando, EL2, EL3, and EL6 defects in GaAs highly implanted with sulfur, J. Appl. Phys. 88 (2000) 5017.

[44] Z.Q. Fang, T.E. Schlesinger, A.G. Milnes, Evidence for EL6 (Ec- 0.35 eV) acting as a dominant recombination center in n-type horizontal Bridgman GaAs, J. Appl. Phys. 61 (1987) 5047.

[45] G. Luo, S. Yang, G.R. Jenness, Z. Song, T.F. Kuech, D. Morgan, Understanding and reducing deleterious defects in the metastable alloy GaAsBi, NPG Asia Mater. 9 (2017).

[46] P. Blood, J.J. Harris, Deep states in GaAs grown by molecular beam epitaxy, J. Appl. Phys. 56 (1984) 993.

[47] A.Z. Li, H.K. Kim, J.C. Jeong, D. Wong, T.E. Schlesinger, A.G. Milnes, Trap suppression by isoelectronic In or Sb doping in Si-doped n -GaAs grown by molecular-beam epitaxy, J. Appl. Phys. 64 (1988) 3497.

[48] P.M. Mooney, M. Tarun, D.A. Beaton, A. Mascarenhas, K. Alberi, Deep level defects in dilute GaAsBi alloys grown under intense UV illumination, Semicond. Sci. Technol. 31 (2016) 085014.

[49] J. Lagowski, D.G. Lin, T. P. Chen, M. Skowronski, H.C. Gatos, Native hole trap in bulk GaAs and its association with the double-charge state of the arsenic antisite defect, Appl. Phys. Lett. 47 (1985) 929.

[50] T. Fuyuki, S. Kashiyama, Y. Tominaga, K. Oe, M. Yoshimoto, Deep-hole traps in p-type GaAs1-xBix grown by molecular beam epitaxy, Jpn, J. Appl. Phys. 50 (2011) 080203.

[51] R. Loudon, The Raman effect in crystals, Adv. Phys. 13 (1964) 423.

[52] R. Merlin, A. Pinczuk, W.H. Weber, Overview of phonon Raman scattering in solids, in: R. Merlin, W.H. Weber (Eds.), Raman Scattering in Materials Science, Springer, New York, 2000.

[53] J.A. Steele, P. Puech, R.A. Lewis, Polarized Raman backscattering selection rules for (hhl)-oriented diamond- and zincblende-type crystals, J. Appl. Phys. 120 (2016) 05570.

[54] J.A. Steele, Structural and Optical Studies of GaAs1-XBix and p-Bi203 for Optoelectronic Devices, University of Wollongong, 2015 (and references therein).

[55] E. Tisbi, E. Placidi, R. Magri, P. Prosposito, R. Francini, A. Zaganelli, S. Cecchi, E. Zallo, R. Calarco, E. Luna, J. Honolka, M. Vondráček, S. Colonna, F. Arciprete, Increasing optical efficiency in the telecommunication bands of strain-engineered Ga(As,Bi) alloys, Phys. Rev. Appl. 14 (2020) 014028.

4 Conclusion

We have investigated the optical and structural properties of films of III-V Bi-diluted alloys. Particularly, we have investigated GaSbBi alloys with different Bi concentrations grown by MBE on (100) GaSb substrates and n- and p-type GaAsBi alloys grown on (100) GaAs and (311)B substrates. The samples were investigated by HRXRD, Raman spectroscopy, AFM and low temperature photoluminescence.

For the the GaSbBi layers, we have observed several Raman modes, which were not observed for the GaSb films grown under similar conditions. In addition, we have observed a resonant Raman effect for a GaSbBi layer with 5.8%Bi using 633 nm excitation, which showed an enhancement of the Bi-induced Raman peaks. The resonant Raman effect and polarized Raman results were used to investigate in detail the nature of the Raman peaks. Specifically, the Raman mode observed at 185 cm^{-1} was associated with a convoluted LO(Γ) + TO(Γ) GaBi mode. The Raman modes observed at 136 cm^{-1}, 195 cm^{-1}, and 219 cm^{-1} were associated with DALA, atomic Bi_2 cluster, and TO(X)/TO(L) GaSb phonon modes, respectively. In general, we have observed that the GaSbBi samples present additional Raman peaks as compared to the GaSb reference sample. This is so because the bismuth atoms create a significant disorder in the (GaSb) matrix, relaxing the Raman selection rules, thus allowing the emergence of these additional peaks, which were mainly associated with the presence of Bi clusters.

For the n- and p-doped $GaAs_{(1-x)}Bi_x$ thin films grown by MBE on (311)B GaAs substrates, we have observed the same effective amount of Bi incorporation and strain in both types of doped $GaAs_{(1-x)}Bi_x$ samples. However, these samples have shown remarkable differences in terms of density of Bi-related defects. Particularly, these defects have important contributions in the presence of non-radiative centers, also contribute to different radiative recombination such as acceptor (donor) -to-band transition. Particularly, our results also indicate that the density of Bi related defects depend on the type of doping (n-or p-doping) of $GaAs_{(1-x)}Bi_x$ Bi-related defects on the PL properties of n- and p-doped GaBiAs layers grown on (311)B substrate orientation.

Furthermore, the n-doped samples grown on the crystalline planes (100) and (311) have the same concentration of Bi (5.4%), but have a different compressive strain, which has an important impact on the optical properties of these materials. Photoluminescence results of the n- and p-type doped samples in the (311)B crystalline plane have shown remarkable differences in terms of the density of defects associated with Bi. In particular, it was observed that the introduction of Bi reduces the GaAs-like electron traps but also induces Bi. The observed differences in the optical properties of (100) and (311)B

GaAsBi samples can be explained by the presence of different compressive strain and by the presence of Bi-induced traps, which affect considerably the optical properties of GaAsBi layer.

Bibliography

ALBERI, K. et al. Valence band anticrossing in ga bix as1-x. *Applied Physics Letters*, American Institute of Physics, v. 91, n. 5, p. 051909, 2007. Citado na página 21.

BASTIMAN, F. et al. Non-stoichiometric gaasbi/gaas (100) molecular beam epitaxy growth. *Journal of crystal growth*, Elsevier, v. 338, n. 1, p. 57–61, 2012. Citado na página 22.

BEAUDOIN, M. et al. Bandedge optical properties of mbe grown gaasbi films measured by photoluminescence and photothermal deflection spectroscopy. *Journal of Crystal Growth*, Elsevier, v. 425, p. 245–249, 2015. Citado na página 21.

BRODERICK, C. et al. Tight binding analysis of the electronic structure of dilute bismide and nitride alloys of gaas. In: IEEE. *2011 13th International Conference on Transparent Optical Networks*. [S.l.], 2011. p. 1–4. Citado na página 21.

CETINKAYA, C. et al. Optical properties of n-and p-type modulation doped gaasbi/algaas quantum well structures. *Journal of Alloys and Compounds*, Elsevier, v. 739, p. 987–996, 2018. Citado na página 21.

DELORME, O. et al. Molecular beam epitaxy and characterization of high bi content gasbbi alloys. *Journal of Crystal Growth*, Elsevier, v. 477, p. 144–148, 2017. Citado 2 vezes nas páginas 21 and 25.

EROL, A. et al. Raman and afm studies on nominally undoped, p-and n-type gaasbi alloys. *Journal of Alloys and Compounds*, Elsevier, v. 722, p. 339–343, 2017. Citado na página 21.

FITOURI, H. et al. Study of gaasbi movpe growth on (1 0 0) gaas substrate under high bi flow rate by high resolution x-ray diffraction. *Microelectronic engineering*, Elsevier, v. 88, n. 4, p. 476–479, 2011. Citado na página 22.

GELCZUK, Ł. et al. Deep-level defects in n-type gaasbi alloys grown by molecular beam epitaxy at low temperature and their influence on optical properties. *Scientific Reports*, Nature Publishing Group, v. 7, n. 1, p. 1–11, 2017. Citado na página 24.

HENINI, M. et al. Molecular beam epitaxy of gabias on (311) b gaas substrates. *Applied Physics Letters*, American Institute of Physics, v. 91, n. 25, p. 251909, 2007. Citado na página 24.

JUNG, D. et al. Next-generation mid-infrared sources. *Journal of Optics*, IOP Publishing, v. 19, n. 12, p. 123001, 2017. Citado na página 21.

KINI, R. et al. Effect of bi alloying on the hole transport in the dilute bismide alloy gaas 1- x bi x. *Physical Review B*, APS, v. 83, n. 7, p. 075307, 2011. Citado na página 21.

KUDRAWIEC, R. et al. Experimental investigation of the cmn matrix element in the band anticrossing model for gaasn and gainasn layers. *Solid state communications*, Elsevier, v. 129, n. 6, p. 353–357, 2004. Citado na página 22.

LINHART, W.; KUDRAWIEC, R. Temperature dependence of band gaps in dilute bismides. *Semiconductor Science and Technology*, IOP Publishing, v. 33, n. 7, p. 073001, 2018. Citado 3 vezes nas páginas 15, 22, and 23.

LONGENBACH, K.; WANG, W. Molecular beam epitaxy of gasb. *Applied physics letters*, American Institute of Physics, v. 59, n. 19, p. 2427–2429, 1991. Citado na página 25.

LUO, G. et al. Understanding and reducing deleterious defects in the metastable alloy gaasbi. *NPG Asia Materials*, Nature Publishing Group, v. 9, n. 1, p. e345–e345, 2017. Citado na página 21.

MARKO, I. P. et al. Optical gain in gaasbi/gaas quantum well diode lasers. *Scientific reports*, Nature Publishing Group, v. 6, n. 1, p. 1–10, 2016. Citado na página 21.

MAZZUCATO, S. et al. Low-temperature photoluminescence study of exciton recombination in bulk gaasbi. *Nanoscale Research Letters*, Springer, v. 9, n. 1, p. 1–5, 2014. Citado na página 21.

PAČEBUTAS, V. et al. Photoluminescence investigation of gaas1- xbix/gaas heterostructures. *Thin Solid Films*, Elsevier, v. 520, n. 20, p. 6415–6418, 2012. Citado na página 21.

PASHARTIS, C.; RUBEL, O. Localization of electronic states in iii-v semiconductor alloys: A comparative study. *Physical Review Applied*, APS, v. 7, n. 6, p. 064011, 2017. Citado na página 21.

POLAK, M.; SCHAROCH, P.; KUDRAWIEC, R. First-principles calculations of bismuth induced changes in the band structure of dilute ga–v–bi and in–v–bi alloys: chemical trends versus experimental data. *Semiconductor Science and Technology*, IOP Publishing, v. 30, n. 9, p. 094001, 2015. Citado na página 25.

PTAK, A. et al. Kinetically limited growth of gaasbi by molecular-beam epitaxy. *Journal of Crystal Growth*, Elsevier, v. 338, n. 1, p. 107–110, 2012. Citado na página 21.

PUUSTINEN, J. et al. Variation of lattice constant and cluster formation in gaasbi. *Journal of Applied Physics*, American Institute of Physics, v. 114, n. 24, p. 243504, 2013. Citado na página 22.

RAJPALKE, M. et al. Growth and properties of gasbbi alloys. *Applied Physics Letters*, American Institute of Physics, v. 103, n. 14, p. 142106, 2013. Citado na página 21.

RAJPALKE, M. et al. Bi flux-dependent mbe growth of gasbbi alloys. *Journal of Crystal Growth*, Elsevier, v. 425, p. 241–244, 2015. Citado na página 25.

SIMMONS, R. et al. Enhancement of rashba interaction in gaas/algaas quantum wells due to the incorporation of bismuth. *Applied Physics Letters*, AIP Publishing LLC, v. 107, n. 14, p. 142401, 2015. Citado na página 21.

TAIT, C. R.; YAN, L.; MILLUNCHICK, J. M. Droplet induced compositional inhomogeneities in gaasbi. *Applied Physics Letters*, AIP Publishing LLC, v. 111, n. 4, p. 042105, 2017. Citado na página 22.

USMAN, M. et al. Tight-binding analysis of the electronic structure of dilute bismide alloys of gap and gaas. *Physical Review B*, APS, v. 84, n. 24, p. 245202, 2011. Citado 3 vezes nas páginas 15, 23, and 24.

VARDAR, G. et al. Mechanisms of droplet formation and bi incorporation during molecular beam epitaxy of gaasbi. *Applied Physics Letters*, American Institute of Physics, v. 102, n. 4, p. 042106, 2013. Citado na página 22.

YOSHIMOTO, M. et al. Quantitative estimation of density of bi-induced localized states in gaas1-xbix grown by molecular beam epitaxy. *Journal of crystal growth*, Elsevier, v. 378, p. 73–76, 2013. Citado na página 24.